Zeitschrift: IABSE reports = Rapports AIPC = IVBH Berichte
Band: 67 (1993)

Rubrik: Session 2: Analytical evaluation of structures

SESSION 2

ANALYTICAL EVALUATION OF STRUCTURES

KEYNOTE SPEAKER

Evaluation of Reserve Capacity of Frames
Détermination de la réserve de capacité portante des cadres
Bestimmung der Tragreserve von Rahmen

Alan R KEMP
Prof. of Civil Eng.
Univ. of the Witwatersrand
Johannesburg, South Africa

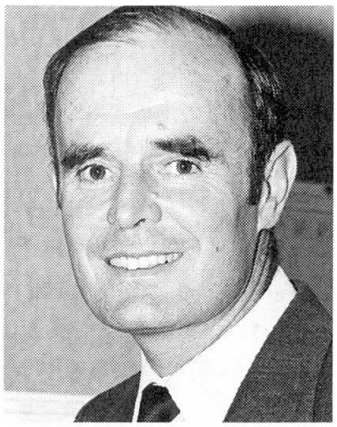

Alan Kemp obtained BSc & MSc degrees in civil engineering from the University of the Witwatersrand and PhD from Cambridge University. Before becoming Professor of Civil Engineering at the University of the Witwatersrand, he was Group Consulting Engineer of Dorman Long (Africa). He is a past President of the S A Institution of Civil Engineers.

SUMMARY

Twin algorithms are described for separating linear and nonlinear moment-curvature characteristics of submembers and then using these characteristics in elastic-plastic frame analysis with two submembers per frame member. Provision is made for complete stress-strain curves, residual stresses, shrinkage, plastic local and lateral buckling, interface slip and combinations of permanent and imposed load properties, as well as end connection flexibility. An example shows the enhanced ultimate load capacity that can be achieved in continuous structures and the required rotations of plastic hinges that are checked using a limit states criterion of ductility.

RÉSUMÉ

L'auteur expose des algorithmes doubles en vue de séparer les rapports courbures-moments de types linéaires et non linéaires dans les éléments porteurs secondaires, puis d'appliquer ces caractéristiques au calcul élastoplastique de cadres à deux éléments porteurs secondaires. Cette méthode prend en compte la totalité des diagrammes contrainte-déformation, les contraintes résiduelles, le retrait, le voilement et déversement local plastique, les surfaces de contact à glissement, la variation des propriétés sous charges permanente et utile, ainsi que la flexibilité des assemblages bout à bout. Un exemple met en valeur, d'une part l'augmentation de la charge portante ultime de structures hyperstatiques et, par ailleurs, les relations requises par les rotules plastiques qui sont vérifiées à l'aide d'un critère de ductilité à l'état ultime.

ZUSAMMENFASSUNG

Es werden Zwillingsalgorithmen zur Trennung der linearen und nichtlinearen Momenten-Krümmungsbeziehungen von Rahmenbauteilen mit zwei Untertraggliedern beschrieben. Sie berücksichtigen vollständige Spannungs-Dehnungskurven, Eigenspannungen, Schwinden, örtliches plastisches Beulen und Kippen, gleitende Kontaktflächen, Änderung der Eigenschaften unter Dauer- und Verkehrslast, sowie Nachgiebigkeit der Endverbindungen. Ein Beispiel belegt die gesteigerte Grenztragfähigkeit statisch unbestimmter Tragwerke und die benötigte Rotationsfähigkeit der plastischen Gelenke, die mit einem Duktilitätskriterium überprüft werden.

1. INTRODUCTION

Structural frames often possess load-resisting capacity above that assessed in the original design due to the following reasons:

- Semi-rigid end-connections that may provide continuity where simple-supports were assumed.
- Stress-strain properties of materials, including nonlinear effects, that differ from those originally assumed (conservative properties and partial material factors may be adjusted after in-situ testing).
- Partial composite action in structures where this was neglected.
- Benefits of limit states design codes allowing for redistribution of moments and ultimate (stress-block) resistances compared to older allowable stress codes, but also requiring more comprehensive analysis including non-linear P-Δ effects and ductility criteria.

If adequate analysis procedures are available, these factors will often lead to an assessed increase in load capacity. This may be improved further by strengthening procedures that enhance flexural resistance and stiffness, introduce additional continuity and load paths, or prevent secondary modes of strain-weakening behaviour.

The first two sections of this paper describe moment-curvature and frame analysis algorithms that link together to provide a computational method of allowing for all these nonlinear characteristics without the need for finite-element analysis involving numerous elements both across the sections and along the length. Features of this approach include:

1. In the frame analysis each "member" is represented by only two "sub-members", each reflecting the integrated non-linear behaviour between an end and the internal section of maximum moment (or the midspan if no maximum internal moment exists), without further discretization in inelastic regions.
2. The frame analysis identifies not only the ultimate load capacity, but also the plastic rotations at each critical section before loss of moment resistance, that are required to check the ductility, as described in the third section of the paper.
3. The behaviour of each element in positive and negative bending is determined in the moment-curvature algorithm allowing for nonlinear material behaviour, shrinkage, creep, interface slip, residual stresses and other effects.
4. This moment-curvature algorithm minimises the number of "elements" representing the cross-section because it is not necessary to subdivide for strain gradient through the depth.
5. Strain-hardening followed by strain-weakening behaviour beyond the elastic region is represented by an idealised elastic-perfectly-plastic moment-curvature relationship for frame analysis, together with expressions for determining the available plastic rotation prior to the moment falling below the design resistance.

The moment-curvature and frame analysis algorithms and the limit states criterion for ductility are illustrated by the example of a three-span composite beam in Fig. 1. Although this is a relatively simple structure, the approach has been applied to more complex sway structures involving frame instability [1,2]. This example is also used at the end of the paper to illustrate the reserve capacity that can be mobilised by allowing for nonlinear characteristics, including continuity in a previously simply-supported beam using the semi-rigid end detail reflected in Figs. 1b and c.

2. MOMENT/CURVATURE-ROTATION-DEFLECTION RELATIONSHIPS

2.1 Stress-strain models of material behaviour

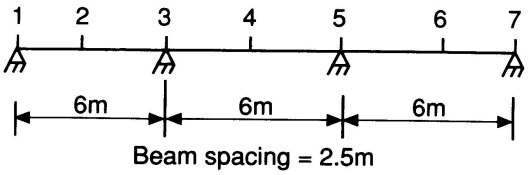

a) 3 - span beam : converted to continuous composite beam.

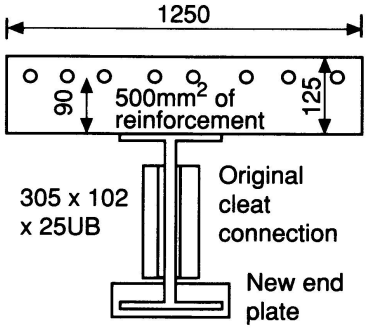

b) Section dimensions

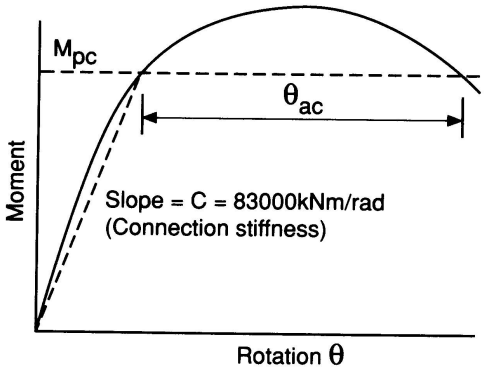

c) End connection M - θ curve

Fig.1 Composite beam example

The moment-curvature method described in this paper has its origins in some of the many stress-strain models that exist [3], but has been developed and tuned progressively over the last decade by the author to represent consistently the inelastic behaviour of a wide range of structural components. Importantly, the results may be integrated to determine the element properties required for nonlinear frame analysis, including the assessment of required ductility using a mixed method of analysis that is described in the next section.

Any stress-strain curve is subdivided into three regions as illustrated in Fig. 2. Each region is represented by a local curve with an origin at the start of the region and a relationship in region i of the following form:

$$\Delta\sigma_i = E_i\Delta\varepsilon_i + D_i(\Delta\varepsilon_i)^{n_i} \qquad (1a)$$

$$\Delta\varepsilon_i = \varepsilon - \varepsilon_{io} \qquad (1b)$$

which $\Delta\sigma_i$ and $\Delta\varepsilon_i$ are the changes of stress and strain at strain ε from the origin of the region, ε_{io} is the strain at the origin, E_i is the slope of the stress-strain curve at the origin and D_i and n_i model the observed characteristics of the material.

The general Eqns. 1a and 1b for each of the three regions are particularly useful in calculating the moment-curvature relationship because at any extreme fibre strain ε the average stress under the curve $\bar{\sigma}$, the location of the centroid of this area $c = \int\sigma\varepsilon d\varepsilon/\sigma\varepsilon^2$ and the tangental slope E_t may be expressed in simple algebraic form as follows:

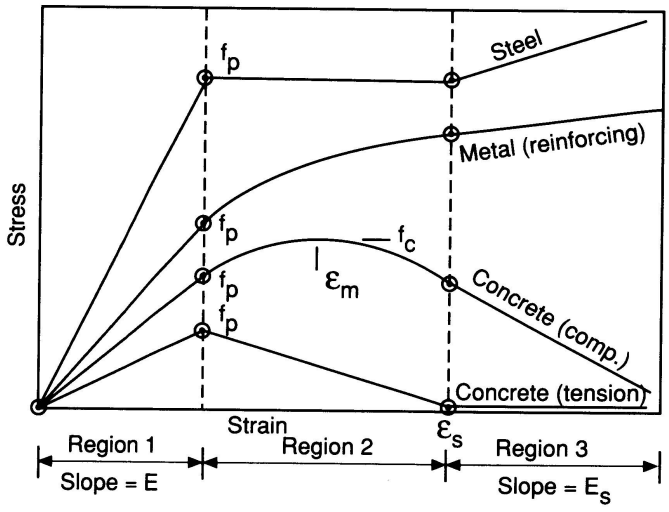

Fig.2 Stress-strain curves

$$\bar{\sigma} = \sum_i A_i/\varepsilon \qquad (2a)$$

$$A_i = \sigma_{io}\Delta\varepsilon_i + E_i\Delta\varepsilon_i^2/2 + D_i(\Delta\varepsilon_i)^{n_i+1}/(n_i+1) \qquad (2b)$$

$$c = \frac{\sum [A_i\varepsilon_{io} + \sigma_{io}\Delta\varepsilon_i^2/2 + E_i\Delta\varepsilon_i^3/3 + D_i(\Delta\varepsilon_i)^{n_i+2}/(n_i+2)]}{\bar{\sigma}\varepsilon^2} \qquad (2c)$$

$$E_t = E_i + n_iD_i(\Delta\varepsilon_i)^{n_i-1} \qquad (2d)$$

in which the summation extends over all regions i up to and including the region containing the strain ε, σ_{io} is the stress at the start of the region and A_i is the area under the stress-strain curve in any region given by Eqn. 2b. The index n_i is calculated from a known change of slope (E_t - E_i) over $\Delta\sigma_i$ and $\Delta\varepsilon_i$ from Eqns. 1a and 2d:

$$n_i = (E_i - E_t)\,\Delta\varepsilon_i / (E_i\Delta\varepsilon_i - \Delta\sigma_i) \qquad (2e)$$

The material properties that need to be specified to determine the unknowns E_i, D_i and n_i in the three regions of the curve apart from continuity are shown in Fig. 2 and Table 1. This table also includes in brackets typical design values, incorporating partial material factors, that are used in the example of Fig. 1.

2.2 Moment-curvature relationships

Any cross-section of a structural element comprising one or more materials and subjected to bending with or without coincident axial force, may be subdivided into an appropriate number of equivalent rectangular elements or concentrated areas to represent the geometry of the cross-section. This subdivision does not have to be sufficiently fine to neglect the strain gradient because of the availability of expressions for average stress and lever-arm of the resultant force vector given by Eqns. 2a to 2c. Thus a steel I-section may be represented by three equivalent rectangles and a reinforced concrete beam by one rectangle and one concentrated area, whereas a circular cross-section may require twelve rectangular elements.

A linear distribution of longitudinal strain is considered through the depth of the section and the strain gradient is assumed equal to the curvature. Considering any rectangular element j shown in Fig. 3 of breadth b, thickness t and depth of centroid y_c from an arbitrary reference level (the top surface), the axial force supported by the element and its moment of resistance may be determined directly from the stress-strain properties of the material described previously. The resistance of the rectangle under consideration ABCD may be represented by the difference in resistance of the rectangles ABEF and CDEF in this figure. For the strain distribution shown, representing a curvature or strain gradient ϕ:

Material (Fig.2)	Mod. of Elasticity E	Proportional limit f_p	Strain hardening/weakening	
			Onset	Slope
1. Structural Steel	(206 GPa)	$f_p=f_y$ (f_y=235MPa)	$\varepsilon_s=(5\text{-}15)\varepsilon_y$ ($\varepsilon_s=10\varepsilon_y$)	$E_s=E/(30\text{-}100)$ ($E_s=E/100$)
2. Metal (reinforcing)	(200 GPa)	$f_p=0.8f_y$ (f_y=390MPa)	$\varepsilon_s=(1.5\text{-}2)f_y/E$ ($\varepsilon_s=2f_y/E$)	$E_s=E/(30\text{-}200)$ ($E_s=E/200$)
3. Concrete (Compression)	E=20-35GPa (E=24GPa)	$f_p=(0.5\text{-}0.8)f_c$ f_c=15MPa f_p=9MPa	ε_m @ f_c = 0.002-0.0025 (ε_m =0.0022)	$E_s=-E/(3\text{-}50)^*$ ($E_s=-E/5$)
4. Concrete (tension)	E as for compression	$f_p=f_t=0.3(f_c)^{2/3}$ f_p=1.8MPa	$\varepsilon_s=(3\text{-}8)f_p/E$ ($\varepsilon_s=4f_p/E$)	E_s = 0

* Depends on extent of triaxial restraint provided by reinforcement

Table 1. Material properties for stress-strain curves in Fig. 2

$$\varepsilon_u = \phi y_u = \phi (y_c - 0{,}5t - y_n) \quad (3a)$$

$$\varepsilon_l = \phi y_l = (y_c + 0{,}5t - y_n) \quad (3b)$$

in which y_u and y_ℓ are the depths from the neutral axis to the upper and lower surfaces of the rectangle defined as positive below the neutral axis, ε_u and ε_ℓ are the corresponding strains and y_n is the depth of the neutral axis below the reference level.

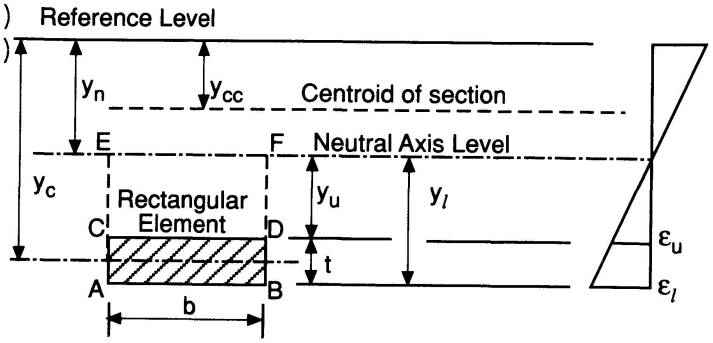

Fig.3 Assessment of element ABCD

The axial force F_j supported by element j is given by the difference in axial forces on the two rectangles ABEF and CDEF:

$$F_j = b (\bar{\sigma}_l y_l - \bar{\sigma}_u y_u) \quad (4)$$

in which $\bar{\sigma}_\ell$ and $\bar{\sigma}_u$ are the average stresses under the stress-strain curve given by Eqns. 2a and 2b at strains ε_ℓ and ε_u respectively.

The moment of resistance M_j of the element about the centroid of the complete section is given by the difference in moments of resistance of the two rectangles ABEF and CDEF:

$$M_j = b (\bar{\sigma}_l c_l y_l^2 - \bar{\sigma}_u c_u y_u^2) + F_j (y_n - y_{cc}) \quad (5)$$

in which c_ℓ and c_u are the centroidal ratios given by Eqn. 2c and y_{cc} is the depth of the centroid of the section from the reference level. Similar expressions may be derived for concentrated areas such as reinforcement [4].

In all of the above equations the assumed sign convention is stress, strain and force positive in tension, curvature and moment positive in sagging bending and depth y positive below the arbitrary reference level. The expressions apply whether the element is above or below or cut by the neutral axis. For materials such as concrete the form of these equations also enables different stress-strain curves to be adopted under compression and tension by referring $\bar{\sigma}_\ell$, c_ℓ and $\bar{\sigma}_u$, c_u to the properties of different materials if the neutral axis falls within the depth of the element.

In Eqns. 3 to 5 it is assumed that the depth of the neutral axis below the reference level y_n is known. At inelastic levels of stress and strain, y_n is determined iteratively to satisfy equilibrium between the net axial force resisted by the section, $\sum F_j$, and the external axial load N applied to the section.

The method has been applied [4] to a wide range of structures and elements of different materials at serviceability and ultimate load and has been adapted to model the following important aspects of structural behaviour:

- Prestressing and shrinkage in concrete elements, by introducing initial values of strain in the relevant elements.
- Residual rolling or welding stresses, by providing additional elements with different initial strains to reflect the residual stresses approximately, based on proposals such as Young [5].
- Interface slip in composite beams with partial shear connection, by introducing slip-strain increments at the interface that are a function of curvature and, when integrated over the half-

span of the beam, provide a total end slip that is consistent with measured behaviour in push-out or beam tests.

- A combination of differing section configurations and stress-strain properties under permanent and imposed loads.
- Strain-weakening due to interactive local and lateral buckling of yielded steel sections based on a semi-empirical model described by Kemp [6].

2.3 Idealisation for frame analysis

The moment-curvature relationships for the composite beam example shown in Fig. 1b, with material properties defined in brackets in Table 1, are illustrated by the solid lines in Fig.4 for positive and negative bending. The ultimate design resistance M_p is an important parameter that is determined from code rules in this case, or other considerations. These curves include the effects of residual rolling stresses, interface slip due to a 50% partial shear connection and interactive plastic local and lateral buckling at high moments in the negative moment region. The region of the beam adjacent to the semi-rigid end connection shown in Figs. 1b and c has been modelled by assuming that the steel section cannot resist tension.

In the three-span continuous beam of Fig 1a, the first regions to develop plastic hinges are adjacent to the internal supports. Uncertainty exists over the moment-curvature path followed by sections in the inelastic region adjacent to these supports (represented by portion PM in Fig. 4b) once the structure is loaded under displacement control beyond the maximum moment and experiences strain-weakening with the section of maximum moment following portion MM' in Fig. 4b. Based on a qualitative assessment of test behaviour it is proposed that the distribution of curvature in this inelastic region at the load level at which the maximum moment at the internal support falls to the design resistance M_p may be modelled simply and approximately by the line P'M'. This implies that curvature is a linear function of moment and the available inelastic rotation θ_{ap} is given by the shaded area in Fig. 4b as:

$$\theta_{ap} = 0.5M_p (m - 1) [\phi'_m - \phi_p (m + 1) / 2m]/mV_p \qquad (6)$$

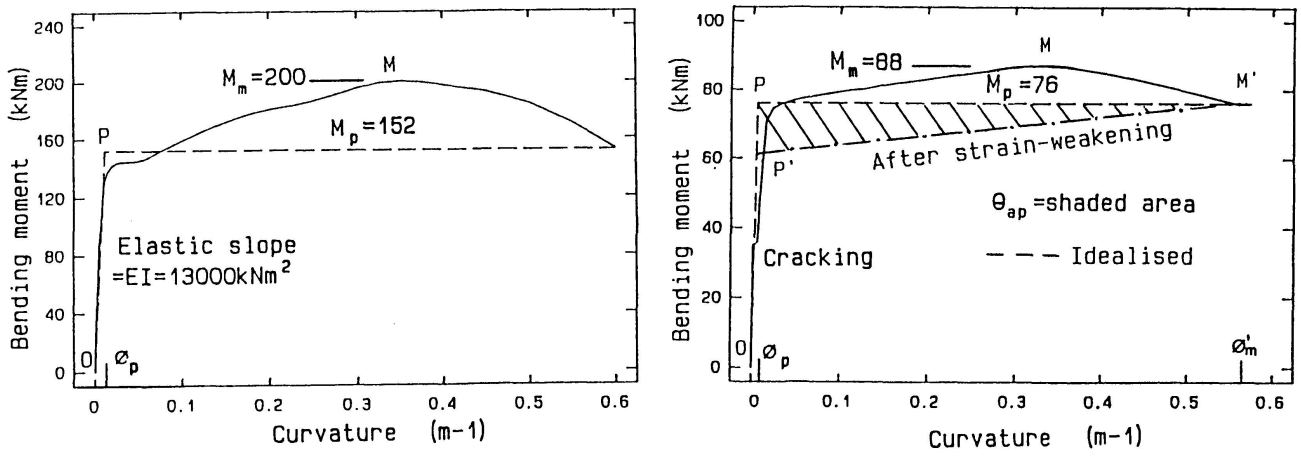

a) Positive (sagging) bending b) Negative (hogging) bending

Fig. 4 Moment-curvature relationships for example of Fig. 1

in which V_p is the shear force at the section of maximum moment and $m = M_m/M_p$ in Fig. 4b.

On this basis the behaviour of elements of the structure between sections of zero moment and adjacent sections of maximum positive or negative moment (or adjacent joints) may be modelled in the frame analysis described subsequently as the superposition of the following effects:

1. Elastic behaviour is represented by the slope of the dashed elastic region of the idealised moment-curvature relationship OP in positive bending $EI = M_p/\phi_p$.
2. Inelastic behaviour is modelled by the horizontal dashed line PM' representing a concentrated ideally-plastic hinge of moment capacity M_p with an available rotation capacity θ_{ap} equal to the shaded area in Fig. 4b and given by Eqn. 6.
3. Differences in stiffness between positive and negative moment regions including cracking of concrete adjacent to internal supports, is represented by an additional component of available plastic rotation θ_{acr} given approximately by the integration of a linear difference in flexural rigidity between the positive moment EI and the cracked negative moment EI', as follows:

$$\theta_{acr} = \theta_e [1 - (M_{cr} / M_p)^2] [(EI / EI') - 1] \qquad (7)$$

   in which θ_e is the calculated elastic rotation in the negative moment region and M_{cr} is the moment at which cracking occurs.
4. Semi-rigid end connections are represented by an idealised elastic stiffness C in Fig. 1c and, in cases where the connection rather than the adjacent member is the critical flexural element, by identifying the available plastic rotation θ_{ac} of the end connection prior to the moment falling below the design value M_p as shown in this figure.

3. FRAME ANALYSIS

3.1 Mixed flexibility/sway-deflection method

The selection and development of a mixed flexibility/sway-deflection method of analysis arose primarily from convenience in modelling elastic and inelastic behaviour, differences in negative and positive moment characteristics and semi-rigid connections, as outlined in the previous section [1,2]. By selecting end moments and independent sway-deflections as unknowns in frame analysis all of these properties including the development of plastic hinges can be considered on a consistent basis without changing the number or location of the unknowns. Additional benefits of this approach include:

- In nonlinear analysis the use of end moments as unknowns rather than joint displacements is likely to lead to more stable and sensitive solutions.
- Axial forces in members are determined from equilibrium considerations rather than as a stiffness function of axial distortions.
- The unknown independent sway-deflections are all directly related to the plastic and instability mode shapes of the structure and therefore relevant to inelastic P-Δ methods.

The method is described firstly in terms of the unknown end moments and then in terms of the additional unknown, independent sway-deflections.

3.2 Solution equations for unknown end moments

In the substructure shown in Fig. 5 that is used for illustrating this approach, ij is one of the two

sub-members representing member ijn between sections of maximum moment (or midspan if there is no internal section of maximum moment). The matrices relating end rotations θ to end moments M and relative end deflections due to sway δ_s (all positive anti-clockwise) in ij are:

$$\begin{pmatrix}\theta_{ij}\\ \theta_{ji}\end{pmatrix} = \frac{L}{EI}\begin{bmatrix}(b_1/3 + f) & -b_2/6\\ -b_2/6 & (b_1/3 + f)\end{bmatrix}\begin{pmatrix}M_{ij}\\ M_{ji}\end{pmatrix} + \begin{pmatrix}\delta_{sij}/L\\ \delta_{sij}/L\end{pmatrix} \qquad (8)$$

in which L and EI are the length and elastic flexural rigidity of the member, b_1 and b_2 are Berry stability functions [7] that allow for increased flexibility due to axial force and have values of unity when second-order P-Δ effects are neglected and f is the non-dimensional flexibility ratio of the end connection expressed in terms of the elastic stiffness of the connection, C in Fig. 1c :

$$f = EI / CL \qquad (9)$$

The following equations are used for solving the n unknown moments at the ends of the n members meeting at joint i in Fig. 5a (n = 4 in Fig. 5a) :

1. One equation representing equilibrium of the moments, M at the ends of the members meeting at joint i:

$$\sum_{1}^{m} M_i = M_{ij} + M_{ik} + M_{i\ell} + M_{im} = M'_i \qquad (10)$$

in which M'_i is the magnitude of any external moment applied to joint i.

2. (n-1) compatibility equations expressing the equality of rotations at the ends of each pair of members meeting a joint i (three compatibility equations for joint i in Fig. 5a representing equal rotations at end i of members ij and ik, ij and iℓ, and ij and im), as follows:

$$\bar{\theta}_{ij} = \bar{\theta}_{ik} \; ; \; \bar{\theta}_{ij} = \bar{\theta}_{i\ell} \text{ and } \bar{\theta}_{ij} = \bar{\theta}_{im} \qquad (11)$$

in which, for example in sub-member ij, $\bar{\theta}_{ij} = \theta_{ij} + \theta'_{ij} + \theta_{rij}$ and $\bar{\theta}_{ij}$ is the superposition of θ_{ij} (the end rotation due to unknown end moments given by Eqn. 8), θ'_{ij} (the end rotation due to member loads with end moments equal to zero - i.e. simply-supported) and θ_{rij} (the required plastic rotation of a hinge if it develops at this section, as discussed subsequently). In considering P-Δ effects the end rotations θ' may be amplified due to axial force using Berry functions [7].

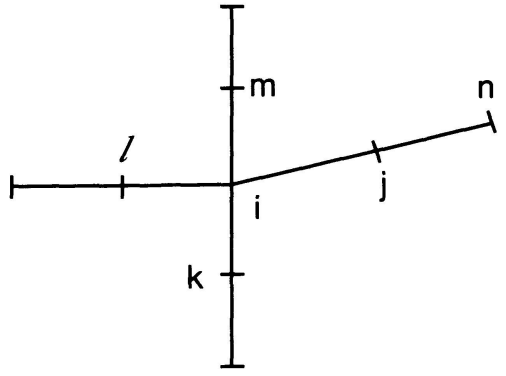

a) Substructure and sub - members

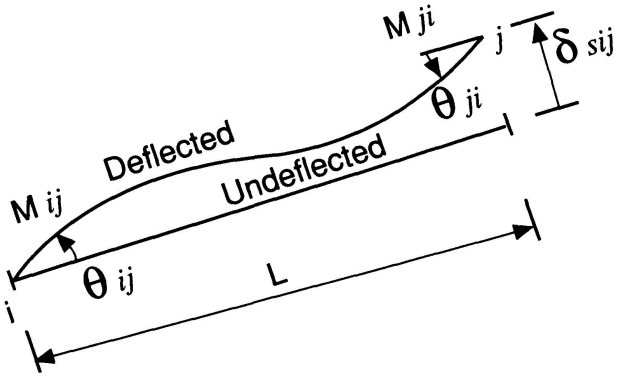

b) Sub - member *ij*

Fig.5 Sub-member ij at joint i

The only exception to this subdivision of equilibrium and compatibility equations occurs at a fixed support where all n equations will be compatibility equations.

3.3 Solution equations for unknown sway deflections

The independent modes of sway are treated as additional unknowns and the approach therefore becomes a mixed method combining unknown end moments with unknown independent sway deflections.

In a structure with j joints, m members and r constraints to global translation at support joints (horizontal and vertical components), there are s independent components of sway deflection given by:

$$s = 2j - m - r \qquad (12)$$

A systematic approach has been developed by the author [1] for identifying the most appropriate unknown joint translations to represent these s unknown modes of sway and their relationship to the other joint translations. Typically there is one mode of sway representing plastic collapse of each member and one representing each mode of sway instability. In this algorithm conventional sway-equilibrium equations are used to solve for each unknown sway deflection and are derived by the Principle of Virtual Displacements applied to a virtual free body displacement of the structure in the mode of sway. These sway equilibrium equations are expressed in terms of:

- the unknown end moments in the sub-members,
- P-Δ terms for elastic or inelastic stability analysis in which P are the axial forces extrapolated from the previous iteration and Δ are the unknown sway deflections normal to P.

3.4 Application of this frame analysis method

This mixed flexibility/sway-deflection method may be used in the same form for elastic, elastic-plastic and elastic-plastic-instability (P-Δ) analyses as follows:

1. Elastic analysis (including elastic connection flexibility) : The unknown end moments are solved using the idealised (dashed) elastic properties in Fig. 4a and the joint equilibrium and compatibility Eqns. 10 & 11 and the unknown sway deflections using conventional sway-equilibrium equations.
2. Elastic-plastic analysis : After the elastic analysis, plastic hinges may be introduced at critical sections either by defining the ultimate design resistance M_p or by identifying a specified ratio between the moment capacities at two sections and the location at which a hinge is expected to develop. In either case the moment at the plastic hinge is then known and is replaced as unknown by the required plastic hinge rotation θ_r (forming part of Eqn.11) to accommodate the necessary redistribution of moments, as discussed subsequently.
3. Elastic-plastic-instability and P-Δ analyses : The elastic-plastic analysis approach is extended to include the Berry stability functions in Eqns. 8 & 11 and the P-Δ term in the sway-equilibrium equations. The member axial force is extrapolated from the previous analysis step introducing a limited iterative procedure.

4. REMAINING CAPACITY ASSOCIATED WITH REDUNDANCY

A significant source of reserve or remaining capacity may exist in redundant structures if they possess sufficient ductility to redistribute moments from heavily stressed sections, at which the

ultimate stress-block moment M_p is achieved, to less heavily stressed sections as the load is increased. The two preceding parts of this paper have described relatively simple algorithms for determining results that are directly relevant to assessing ductility, namely:

1. The available inelastic rotation θ_a at plastic hinges prior to the moment falling below the ultimate resistance M_p and made up of components due to plastic behaviour θ_{ap} (Eqn. 6), inelastic rotation of end connections θ_{ac} (Fig. 1c) and reduced stiffness due to cracking of negative moment regions, θ_{acr} (Eqn.7).
2. The required inelastic rotation θ_r at the same plastic hinges from the frame analysis of the redundant structure for specified loads and ultimate resistances M_p.

A general limit states criterion of ductility has been proposed [2] for determining how much capacity exists in indeterminate structures to redistribute moments. This requires that the available inelastic rotation θ_a at each plastic hinge should be greater than the plastic rotation θ_r required to achieve the specified level of moment redistribution or hinge development:

$$\text{i.e. LIMIT STATE OF DUCTILITY : } (\theta_a / \gamma_{md}) > \theta_r \qquad (13)$$

in which γ_{md} is a partial material factor to allow for the considerable uncertainties in assessing θ_a and θ_r, in the range 1.5 to 3 depending on whether it is a ductile or brittle mode of failure. This criterion may be expressed non-dimensionally in terms of rotation capacity by dividing both sides by the elastic rotation at M_p between the plastic hinge and the adjacent section of zero moment. The criterion conforms to limit-states terminology by having a resistance on the left hand side and an action effect on the right hand side, and may be applied to any mode of failure inhibiting ductility for all types of structural materials.

5. EXAMPLE

Consider the three-span steel beam illustrated in Fig.1 that was originally designed as non-composite and simply supported with cleat connections only resisting shear, but is to be considered for upgrading into a continuous composite beam. The slab contained 0.4% longitudinal reinforcement over the internal supports for crack control and this will be utilised. The spans are about 2/3rds of a typical full-scale beam, but reflect the dimensions of a similar specimen tested by the author for available plastic rotation [8]. The nominal load carrying capacity of the existing beam is 6kN/m of permanent and 2 kN/m^2 of imposed load on the basis of an existing allowable stress code for steel, assuming the compression flange is restrained against lateral buckling.

Upgrading will be achieved by cutting out slots in the concrete above the steel beam to accomodate a partial shear connection capable of mobilising 50% of the ultimate slab force in sagging bending and the full effective area of reinforcement over the internal supports (500 mm^2). Each beam will be propped at midspan during casting of the grout around the shear connectors and welding of the end plate to the bottom flange of the steel beam and adjacent web as shown in Fig. 1b. This end plate provides a semi-rigid end connection with moment resistance made up of the reinforcement in tension and the bottom flange in compression when the prop is released [8].

The evaluation of the enhanced load-carrying capacity at the ultimate flexural limit state is undertaken as follows:

- The properties of rows 1 to 4 of Table 2 are determined using the moment-curvature results in Fig. 4 allowing for interactive plastic local and lateral buckling in negative bending and concrete crushing in positive bending.

- The properties in rows 5 and 6 of this table are calculated from these values using Eqns. 7 and 6 respectively.
- The elastic flexibility ratio f of the end connection (row 7) is determined from experimental results (Fig. 1c) using Eqn.9 : no significant nonlinear component of connection rotation was apparent at the level of moment developed in the adjacent member, so $\theta_{ac} = 0$ in this case.
- An ultimate load capacity of the three-span beam of 41.8 kN/m associated with plastic hinges at the internal supports and midspan region of the outside spans, is determined from the frame analysis, in two steps (elastic and plastic) using 6 sub-members (Fig. 1a) and 12 unknown end moments and 3 unknown sway deflections. This represents a more than three-fold increase in the existing imposed load capacity of this beam.
- Required plastic hinge rotations in the outside spans adjacent to the internal supports θ_r = 0.0135 rad. are obtained from the frame analysis and are used as the action effect in Eqn. 13 to check the ductility involved in plastic moment redistribution. A partial material factor of $\gamma_{md} = 1.5$ is adopted for ductile failure due to local and lateral buckling and the resistance effect is the available plastic rotation $\theta_a = 0.0216$ rad. made up of θ_{ac} (equal to zero), θ_{acr} and θ_{ap} (from Table 2, rows 5 and 6).

Limit States Criterion (Eqn.13) : (0.0216 / 1.5 > 0.0135)

The available plastic rotation θ_a compares favourably with tests on composite beams with similar semi-rigid end connections [8]. This excellent ductility is explained in this reference by the location of the plastic neutral axis being close to the compression flange which severely inhibits local and lateral buckling.

Moment-curvature properties (Fig.4) :	+ve Moment Region	-ve Moment Region
1. Elastic flexural rigidity EI (kNm^2)	13000	13000 (+ve moment)
2. Ultimate design resistance M_p (kNm)	152	76 (semi-rigid)
3. Maximum moment M_m (kNm)	200	88
4. Falling branch curvature ϕ'_m (m^{-1})		0.56
Assessed properties:		
5. Plastic rotation (Concrete cracking) θ_{acr} Eqn.7 (rad.)	N/A	0.0017
6. Plastic rotation (yielding) θ_{ap} Eqn. 6 (rad.)	N/A	0.0199
Experimentally measured properties:		
7. Elastic flexibility ratio of end connection f = EI/CL (Eqn.9)	N/A	0.05

Table 2. Properties required for frame analysis

6. CONCLUSIONS

A significant source of reserve capacity exists in many structures if the implications of inelastic material behaviour, continuity and plastic redistribution of moments as well as the ductility requirements, can be assessed analytically without resorting to finite elements models that require

numerous elements both across the section of the members and along their length. A twin algorithm is illustrated in this paper for assessing firstly the inelastic section properties of two sub-members per frame member, and secondly the elastic-plastic-instability analysis of frames comprised of these sub-members. These analyses also identify the available and required plastic rotations that are used to check adequate ductility using a simple limit states criterion involving material plasticity, inelastic properties of end connections and differing flexural rigidities in positive and negative bending.

7. REFERENCES

1. KEMP A.R., A Consistent Mixed Approach to Computer Analysis of Frames. Civil Engineer in South Africa, 30(7), 317-322, July 1988.
2. KEMP A.R., Quantifying Limit States of Rotation Capacity in Flexural members. Proc. Institution of Civil Engineers, 89(2), 387-406, Sept. 1990.
3. DESAI C.S. and SIRIWARDANE H.J., Constitutive Laws for Engineering Materials. Prentice-Hall, New York, 1984.
4. KEMP A.R., Simplified Modelling of Material Non-Linearity in Structural Frames. Civil Engineer in South Africa, 30(9), 425-432, Sept. 1988.
5. YOUNG B.W., Residual Stresses in Hot-Rolled Sections. Dept. of Engin., Technical Report No. CUED/C - Struc/TR8, University of Cambridge, 1971.
6. KEMP A.R. and DEKKER N., Available Rotation Capacity in Steel and Composite Beams. The Structural Engineer, 69(5), 88-97, March 1991.
7. PIPPARD A.J.S. and BAKER J.F., The Analysis of Engineering Structures. 3rd Edition, Edward Arnold, London, 550-555, 1957.
8. KEMP A.R., TRINCHERO P. and DEKKER N., Ductility Effects of End Details in Composite Beams. Engineering Foundation Conference on Composite Construction, Potosi, Missouri, June 1992.

SELECTED PAPERS

Is there still Life after the Lifetime of Sheetpiling?
Est-il possible de prolonger la durée de vie des rideaux de palplanches?
Gibt es lebensverlängernde Massnahmen für Spundwände?

Ad van der TOORN
Civil Engineer
State Public Works
Utrecht, The Netherlands

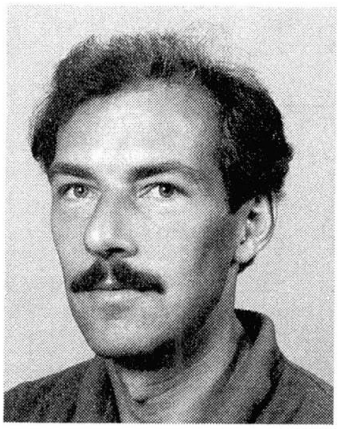

Ad van der Toorn, born in 1951, got his degree at the Technical University Delft. For two years he was working on the Royal Military Academy as a teacher, followed by a five year as project leader on large infrastructural works. Now he is working as researcher partly on the State Public Works and the University of Twente.

SUMMARY

This paper deals with the way in which an existing and so deteriorated structure of sheetpiling can be evaluated. Applying more advanced structural methods than the ones used in the design stage will uncover hidden structural reserves and together with the once more adjusted safety margin it may give a new residual lifetime. To stretch this 'life after death' a range of possible maintenance actions, inclusive 'doing nothing', should be weighted against cost and ectended lifetime.

RÉSUMÉ

Cet article traite de la vérification de structures existantes comportant des réseaux de palplanches dégradés. Il est possible de mobiliser des réserves latentes de résistance, donnant ainsi à ces constructions une longévité supplémentaire, par l'utilisation de méthodes de calcul plus affinées, contrairement aux hypothèses de calcul et aux coefficients de sécurité admis à l'origine. Cette prolongation de durée de vie devrait résulter de la comparaison de mesures d'entretien possibles, y compris de ne rien faire, avec les coûts correspondants et le supplément le longévité ainsi acquis.

ZUSAMMENFASSUNG

Der Beitrag behandelt die Überprüfung bestehender, verfallener Spundwandskonstruktionen. Werden gegenüber den ursprünglichen Berechnungsannahmen und Sicherheitsbeiwerten verfeinerte Nachweisverfahren angewendet, können versteckte Tragreserven für eine neue Restlebensdauer mobilisiert werden. Um sie zu verlängern, sollten mögliche Unterhaltsmassnahmen (entschliesslich der Option der Untätigkeit) gegen die Kosten und die verlängerte Lebensdauer abgewogen werden.

1. INTRODUCTION

All civil engineering structures deteriorate, so don't trust the one who tries to sell you a 'maintenance-free' structure.
Only the scale of time in which the ageing-processes takes place can vary and so can save or foolish us.
The ancient pyramides, though still in function if we have not robbed them, suffer from a substantial surface-damage when given a nearby view.
For the more ordinairy structures of our times we don't have to wait so long.

Civil engineering structures like roads have the shortest lifecycle (15 - 25 year), primairy caused by the wear and tear of the traffic, but speeded up by the ever growing intensity and a bad quality of subsoil.

Sheetpiling-structures, allthough designed for a fifty years or more, often appeares to have a much shorter lifetime (10 - 25 year), because of the much more aggressive environment.
Corrosion-velocities of 0.25 mm per year with maxima in the order of 0.5 mm are measured, not only along the seashore but also for inland polluted canals.
When design or building-failures makes airsupply to the backside of the sheetpiling possible, these velocities will nearly double.
So even heavy walls with a steel thickness of 10 mm or more are in that case of 'a short breath'.

Most of our civil engineering structures have a protection layer on the actual bearing construction. For example a paint-coating on a steel bridge, a concrete cover on buildings or the armour-blocks on the slope of a dike.
So degradation is from a so called 'two-stage-mechanism', in which the damage of the first stage is a warning-bell for the starting attack of the second underlaying structural more essential part.

In contrary a sheet-piling structure most of the time is from the type 'one-stage-mechanism', that is degradation (corrosion) allmost starts from the very early beginning.

It's a lucky circumstance that in contrast with others, this degradation (corrosion) is rather easy to measure by way of ultrasonic waves or more destructive by drilling or oxygen burning followed by a normal thickness measurement.
So on the side of 'the assessment of the condition-parameters' there are less problems than on the side of 'the assessment of structural (reserve) capacity' but above all 'the adjustment of acceptable risk'!

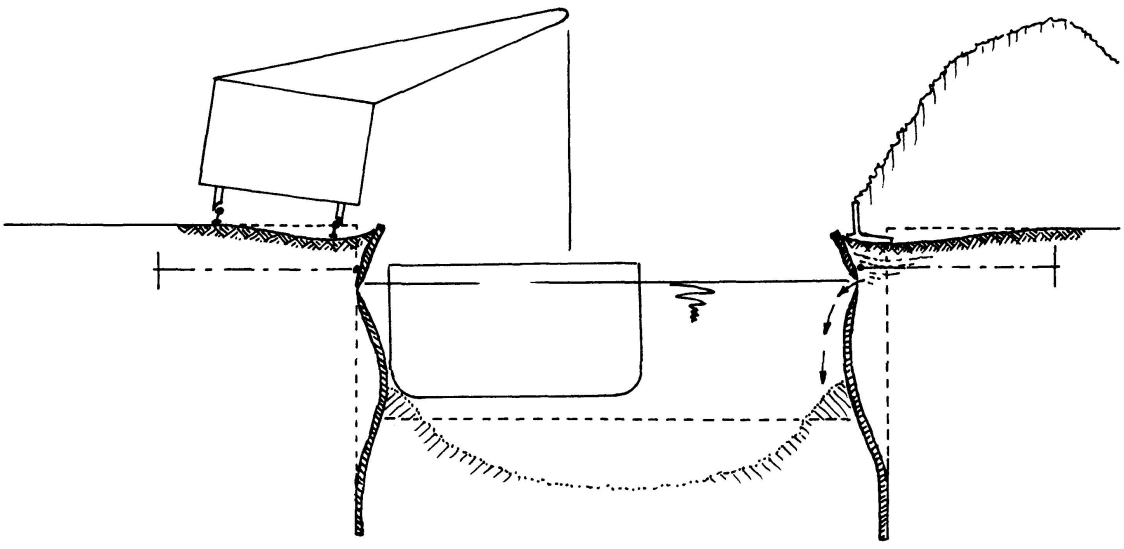

Fig.1 Structural reserve and acceptable risk

2. THE STANDARD DESIGN METHODS

In normal practice a sheetpiling wall is at best designed as a two-dimensional structure, which has an infinite extent in the third dimension.
The variation in this third dimension, with respect to loads, geometry, soil and construction properties is considered to be small or to be brought into account in the variation of the other two dimensions.
Even local loads or anchors are translated in a kind of equivalent line-loads, so the third dimension can be neglected.

For the two-dimensional computation of sheetpiling walls there are a few analytical or grafical methods available, like Rowe, Brinch Hansen, Blum.
Because the mechanical problem is in fact staticaly indetermined, these methods give approximate solutions under certain assumptions like infinite rigid piling and only hydrostatic active or passive earth pressure.

More recently developed computer programs (like the dutch programs MSHEET or DAMWAND/3) do take into account the stiffness of the sheetpiling and the stiffness of the soil by bi-linear springs (dependent on the horizontal displacement they come at last in the active or passive plastic stage).

The input for these computations is in general as follows:

Given or assumed by experience: - GEOMETRY (H,h,α,β)
- SOIL PROPERTIES (ϕ,c,γ,δ)
- LOADINGS (q,F)

Estimated by rules of thumb : - SHEETPILING (l,I)

Than computation results in : - BENDING MOMENTS M(z)
- SHEERFORCES D(z)

With the admissible stresses : - MODULUS OF RESISTANCE (W min.)
- THICKNESS OF BODY (t min.)

If the estimated profile doesn't fit, design is repeated with a better one.

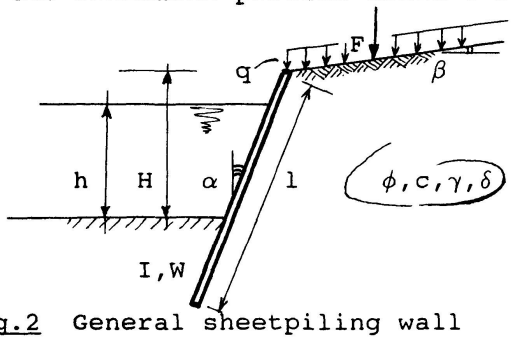

Fig.2 General sheetpiling wall

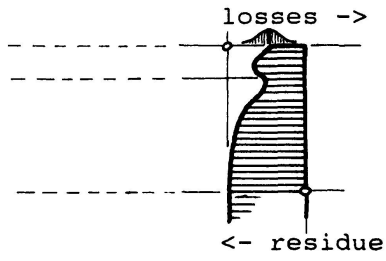

Fig.3 General corrosion profile

The actual sheetpiling profiles are mostly heavier than strictly needed with respect to the computation.
If extensive corrosion is expected the designer will take a few millimeters more (if he is aware of the phenomenon and in the possition to do so!).
But in fact at that moment he has first to answer the difficult question:

> What could and should be the minimum thickness of flange and body at the end of the designlife in relation to the function of the sheetpiling, so the consequencies of failure, the influence of inspection on this, the ability of a new (more plastic) equilibrium, etc.

If ram-ability of the sheetpiling in that specific soil is expected to be a problem, this can result in a heavier profile too.

The sheetpiling that finally will be found at location still can differ from the one selected above, because of delivery problems, sheetpiles in stock of the contractor, problems with achieving the right depth etc.
This 'as build' data should be saved well in a kind of birth-register because it is of great importance for the reassesment of the structure!

3. THE DEGENERATION PROCES

In the case of sheetpiling composed of steel profiles like Larssen, Hoesch etc. the degeneration process is mainly ordinairy corrosion. Besides steel there are two elements needed for the initiation and the continuation of this corrosion process, namely oxygin and water.

So in general a vertical corrosion profile is found with two maxima, one just beneath the low water level and one in the splash zone (Fig.3).
The first is limited by the amount of oxygin, and the other by the amount of water.

Also in horizontal direction there will be found a wide spread in loss of material.
The first fluctuation is measured within one single plane of a sheetpile and may be in the order of 100 mm due to local steel properties.
The next fluctuation is found between flanges, bodies and edges. Especially for cold-rolled profiles at the deformed outward corners, the grid is 'open for corrosion', so warm-rolled profiles are prefered in cases of extensive attack.
Over the sheetpiling wall there may be spots working like anodes and others like cathodes, caused by the metal composition, deformations and soil properties. The addition of copper and other more precious metals ment to prevent or to decrease corrosion, after some times proves to intensify this anodic and cathodic spots perhaps due to unequal alloys.
The largest fluctuation in horizontal direction may have its origin in the location or use of the sheetpiling wall. Tidal streams in combination with fresh water tonques, manoeuvring ships, etc. may cause a tendensy to vary over distances in the order of a 100 meters.

It will be clear that there is a discision problem. On the one hand in the case of too little information (thickness measurements) it is impossible to make distiction between the sources of above mentioned fluctuations.
So this 'all on one heap' approach will lead to an overestimated loss of thickness and so to an underestimation of the remaining strength.
At the other side more information will ask for money, but may lead to a better understanding and probable to a longer residual service life.
The smallest fluctuations over one plane are just of interest for the moment that minimum thickness will become zero and so loss of soil material may start, because strength will depend on the mean value.
The largest fluctuation in the order of the construction length, sometimes will lead to a seperate consideration and perhaps measurements for parts of the wall.
So in that case only the spread in the midrange-variations remains of direct interest for the reassesment of sufficient strength.

Besides the decreasing thickness (that influences strength), the geometry and the loads may change in time too.

Geometry may differ from design because of dredging, scouring, additions, so in case of doubt measurements like sounding the bottum can give insight. Keep in mind taht the computation and so the behaviour of sheetpiling is more sensitive to the retaining height H than to the thickness t!

Loads may differ from design because the destination of the adjacent site may be different (gravel storage is not covered by the often arbitrairy chosen one ton per square meter!).

Allthough soil properties will hardly change, original design assumptions may be of an arbitrary or global level. Supplementary measurements may give a better insight in the present situation.

After the state of the sheetpiling wall is well mapped, the evaluation will finally start.

4. THE REASSESMENT OF SHEETPILING WALLS

4.1 The general concept

In principal during the design stage of a structure there ought to be made a weighing between the initial investment plus expected maintenance cost of this new structure on the one hand versus the risc involved with the loss of functions on the other hand and so looking for the total cost optimum in the life-cycle.
Allthough this is a sound economic concept it is hardly been done.

As in most of the cases there are design codes or at least practical rules that relieves the designer of this difficult economic approach.
These codes of practice prescribes certain safety-margins that covers the above mentioned balance 'on the safe side', that is a rather low risc gained by a little bit more investment (Fig.4).
The consequencies of this practical concept is that during lifetime the risc won't dominate so fast and we may say 'nature is mild'!
These safety-margins are historically grown and reflects the level of prosperity and the aversion of society against structural failure, because this risc is extremely low in comparison with others [1].

For existing structures things have changed even without deterioration!

Design values for geometry, loads, soil and material properties may be known better by measurements, deteriorated construction properties are more scattered than before, consequencies of failure can be better estimated but in comparison with design, cost of adjustment are now of higher order.

Yet for existing structures the engineer still tries to hide behind design codes, because that is the easiest and common way but unfortunately in many cases no more practicable.
As special codes or rules for existing structures are hardly available at this moment, every engineer has to do this unknown exercition himself.

First he tries to uncover all hidden structural reserves. Material reserves like differences between 'as build' and 'as needed' profiles or mechanical reserves applying more advanced models. But if deterioration is extensive this won't be enough.
Then trying to exploit reliability-reserves, he will be confrontated with the basic questions about safety-margins and acceptable reliability-levels for existing structures in relation with design-values.
The considerations may be:

- Well known loads and resistance by way of measurements may lead to less variation so to a smaller safety-margin with equal probability of failure (Fig.6)
- A shorter residual lifetime may lead to lower extreme loads (if time dependend) and less loss of material so to smaller safety-margins, ending up with a margin for temporary sheetpilings (if known!).
- More costly maintenance measures together with better known failure consequencies may lead to a higher probability of failure (Fig.5) so to a smaller safety-margin but should not exceed other social riscs.

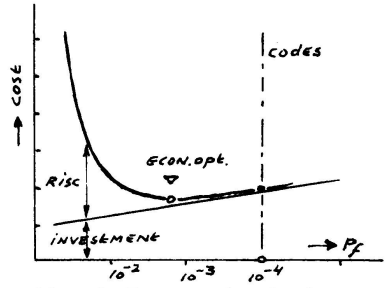

Fig.4 Economic balance in design stage

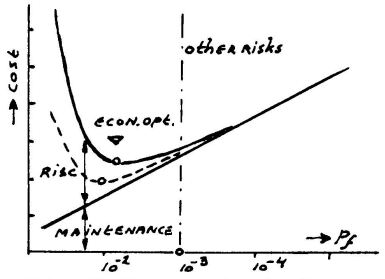

Fig.5 Economic balance for maintenance

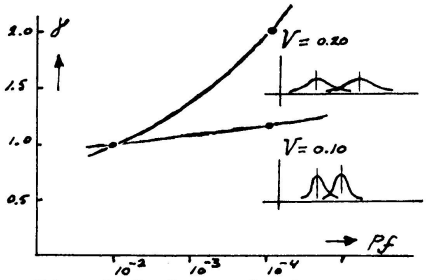

Fig.6 Safety-factor vs. failure probability

4.2 The evaluation of a sheetpiling wall

The reassesment of a sheetpiling wall follows the above given concept.

First the engineer tries to interprete all the thickness measurements in terms of a 'representative value' at the different levels. For instance using the 5%-value of the normal probability function. So overthickness given in design or construction stage will be included. With this new adjusted values and all others like in design he tries to passes through the 'design-loop' with the ordinairy two-dimensional computation.

If this still doesn't satisfy the present-day design rules, the more hidden and so less computable structural reserves will be taken into account.

In vertical direction there may be a certain redistribution of moments, if a more plastic behaviour of the sheetpiling in the computation is possible. There are computer programs written for the design of concrete retaining walls, that can handle yielding moments (for example the dutch program DIEPWAND/1). Yet reduction of the fieldmoment leads to increasing (acceptable?) moments and forces about tie level and the fixed end (Fig.7).

Also in horizontal direction there is a possibility of a certain redistribution between the individual sheetpiles.
Less corroded piles will take over a part of the load on heavy attacked sheetpiles. In fact in the third dimension the wall can be seen as a structure with a certain amount of parallel elements. What exactly will be the zone to be mobilized by a weak pile depends on the given local situation.
The stiffness of the wale, the geometry and the soilproperties play an important role in this.
A three dimensional computation (with the dutch program DIANA) has proved that in particular for the case of an anchored sheetpiling this horizontal redistribution may be considarable (Fig.8) [2].
Though this mobilized zone is in the order of the retaining height of the sheetpiling it has not been possible yet to derive a general rule of thumb.

The expectation is that within this zone short and midrange fluctuations may be ignored and only the mean value of the thickness have to be taken into account.

So in opposite if combined measurements are always done for such a to be mobilized zone, the mean value of that thickness may be of direct use in the normal two-dimensional computation.

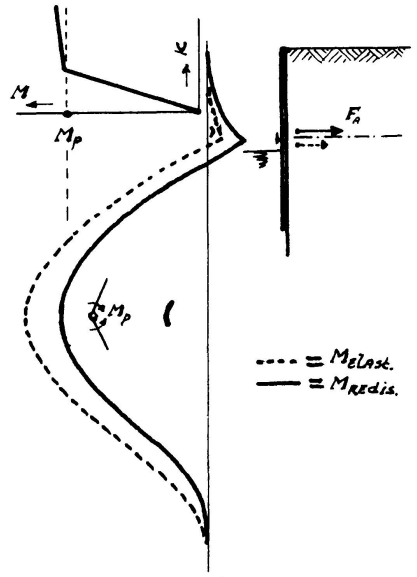

Fig.7 Redistribution of bending moments

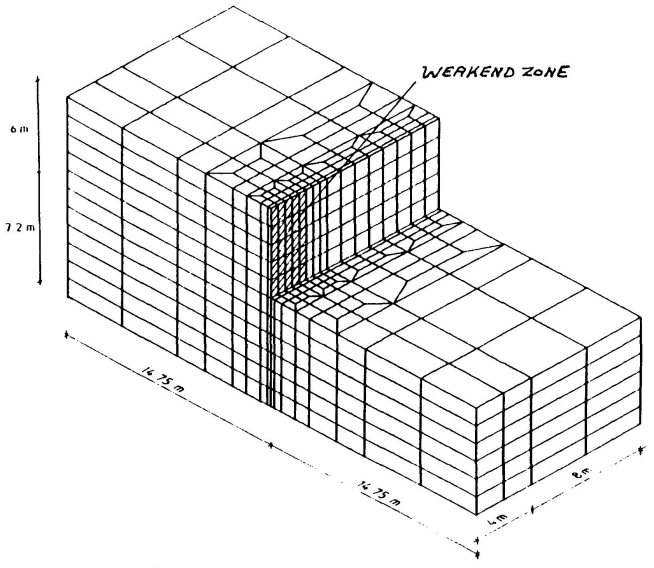

Fig.8 A 3-dimensional FEM-model of a sheetpiling wall.

Now a lot more hidden structural capacity is brought into sight it is possible that the sheetpiling wall satisfies the present-day (!) design rules.

If not it has been argued that for existing structures and time passes by safety-margins may decrease with relation to the original design-values. The arguments already given above are shortly:

1. A better knowledge about strength and loads so less uncertainty.
2. A shorter residual lifetime so less extreme loads and losses.
3. More costly (maintenance) measures i.r.t. design changes.
4. Better known failure consequencies i.r.t. design starting-points.

Quantifying these arguments leads to:

ad.1 Main contributions to the failure of a sheetpiling are given by the soil properties (ϕ,c), the retaining height (H), the thickness of the sheetpiles (t) and if applied the anchors.
Measurements may give the actual coëfficient of variation (0.1-0.2), so with reliability theory it may be possible to check if an other safety-margin may be applied (Fig.6). But since design was based on traditional building codes, first a calibration is needed to know the hidden starting-points in terms of coëfficients of variation.

ad.2 As sheetpilings usually are not designed for time varying loads, the only benefit could be the time dependend loss of material. But again in the traditional design it is not clear which part of the total safety margin was reserved for this.

ad.3 In general maintenance measures are from a higher order (factor 10) in relation with design measures having the same effect on risc.
So the new cost optimum will result in an higher probability of failure (factor 5) and so in a reduced safety-margin (factor 1.1).

ad.4 If failure consequencies are from a lower order (factor 10), the probability of failure may rise with the same magnitude for constant risk. This may lead to a reduced safety-margin (factor 1.2). But again the original starting-points are not known.

Although tendencies are clear, the traditional safety-margin used like a 'dust-bin' makes it hard to pay the individual aspects.
Only calibration of traditional designs based on probabilistic methods taking into account al relevant parameters and used mechanical model may give better insight! In Holland this study is now underway [3,4].

So in the meantime a more arbitrairy reduction factor up till 1.3 is used now in practice, mainly affected by the consequencies of failure [5].

5. STRETCHING THE REMAINING LIFETIME

Now it has been proven by measurements and calculations that there is still any 'life after death', the responsible authority should be informed about the best way to manage that structure in the future. So the next step is the weighing of alternative scenarios.

There are a few technical possibilities to stretch the residual lifetime of sheetpiling by applying a (combination of) preventive maintenance action(s) like the wellding of plates or beams to seal and strengthen the sheetpiles, painting and cathodic protection to slow down the corrosion proces, ground-injection to stop losses of soil etc.

Each alternative has his own cost and expected stretch of lifetime.

Cost may be the direct cost of the maintenance action plus cost ahead to sustain or maintain this action.
Cost also contains the risk involved with this solution, by which risk is the probability times the consequences of function loss (inserviceability or failure). On its turn this probability is dependent on the frequency of inspection, which again represents cost.
On the other hand the expected lifetime is inflenced by these inspection and maintenance actions too.

It is up to the engineer to bring all this in the right weighing within one scenario and next to balance these scenarios against the zero option 'doing nothing', so replacement after certain time [6].
Now this complex desicion may be sustained by some analytical or Markovian models which brings into account cost, lifetime and interactions [7,8].

Nevertheless this rational approach there are often practical restrictions like budget-shortage and traditional philosophies that dictates the real life, especially when no one is responsible for the total life-cycle cost!

REFERENCES

1. CIRIA Report 63. Rationalisation of safety and serviceability factors in structural codes. July 1977.

2. BIJNAGTE J. e.a., The consequencies of corrosion for the computation of a sheetpiling wall (in dutch). Grondmechanica Delft. May 1992.

3. CALLE E., Safety of cantilever sheetpiling structures (in dutch). A probabilistic method for the determination of partial safety factors. Grondmechanica Delft. May 1987.

4. SPIERENBURG S., Safety of anchord sheetpiling structures (in dutch). A probabilistic method for the determination of partial safety factors. Grondmechanica Delft. June 1988.

5. TOORN van der A., The evaluation of existing sheetpiling walls (in dutch). Rijkswaterstaat-Bouwspeurwerk. June 1989.

6. TOORN van der A., Management and maintenance of sheetpiling walls (in dutch). CUR-Rijkswaterstaat. Jan.1992.

7. WIJNMALEN D. e.a., Minimisation of maintenance cost by flexible strategies (in dutch). TNO-FEL. Dec.1990.

8. WALTMANS M. e.a., Computation of an optimal maintenance strategy for a sheetpiling wall (in dutch). ICIM. July 1991.

Retrieval of System Properties of Existing Structures
Détermination des caractéristiques de systèmes de structures existantes
Ermittlung der Systemeigenschaften bestehender Tragwerke

Amin HELOU
Prof. of Struct. Eng.
AN-Najah University
West Bank - via Israel

Amin Helou, born 1949, got his Civil Engineering degree from Roberts College, Turkey. He got his Ph.D. from North Carolina State University, Raleigh, NC, USA. Amin Helou has a long consulting experience in the United States and in the Middle East, and now is a Professor of Structural Engineering.

SUMMARY
Existing older structures are sometimes hard to evaluate, due to certain limitations in identifying their physical properties. It is shown, however, that the application of known forces at the nodes, together with the measurement of the associated displacements, leads to the retrieval of the physical characteristics of the structure, namely the stiffness matrix.

RÉSUMÉ
Il est parfois difficile d'évaluer les anciennes structures, en raison de certaines restrictions à identifier leurs caractéristiques physiques. Il apparait toutefois que l'utilisation de forces connues aux noeuds, combinée à la mesure des déplacements correspondants, permet de de déterminer les caractéristiques physiques de la structure, notamment la matrice de raidissement.

ZUSAMMENFASSUNG
Die Möglichkeiten zur Eruierung der physikalischen Eigenschaften bestehender alter Tragwerke sind naturgemäss beschränkt. Wie jedoch gezeigt wird, kann aus der Applikation bekannter Kräfte an den Knoten und Messung der zugehörigen Verschiebungen die Steifigkeitsmatrix des Tragwerks gewonnen werden.

1. INTRODUCTION

Environmental attacks, corrosion and prolonged use of existing structures make their structural evaluation rather limited because their members' properties may not conform to the design values. Hence, classical methods of structural analysis become inadequate to tackle and overcome the difficulty involved. Therefore, it is both necessary and prudent to improve such methods. In this study, system identification techniques are introduced. In such techniques, the structural stiffness is recovered from known forces and known associated displacements. Once the stiffness matrix of a structure is determined, the internal design forces due to any loading condition can readily be obtained.

2. STATEMENT OF THE PROBLEM AND THE SOLUTION

Present methods of structural analysis are primarily based upon the stiffness methods of analysis in which the input is a family of stiffness coefficients presented in a matrix form and the loading conditions entered in a vector form. The unknowns are displacements and subsequently internal forces. The standard mathematical representation of these three variables is:

$$\{F\} = [K]\{x\} \tag{1}$$

in which

F is an Nx1 loading vector
K is an NxN stiffness matrix
x is an Nx1 system displacement vector
N is the number of degrees of freedom

In the traditional approach to structural analysis, $\{x\}$ is the unknown, whereas in this study the unknowns are the elements of K, which in some sense represent the characteristics of the structure. A process that has been developed for other engineering disciplines, but which is being introduced in structural engineering, is generically referred to as "System Identification". It is an attractive procedure to formulate and improve mathematical models.

To illustrate the derivation of the stiffness of the structure in terms of the applied force vector and the associated and measured displacements, the following situation is used:

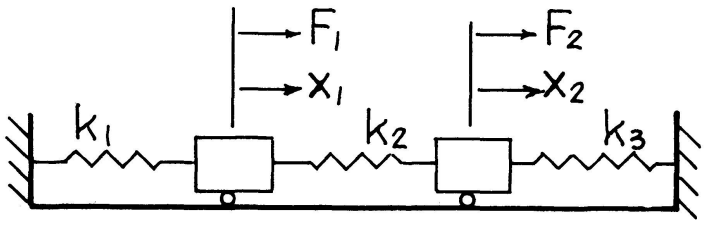

Figure 1

Figure 1 shows a two-degree of freedom system in which two lumped masses are attached to three linear springs with stiffnesses k_1, k_2, k_3 .

The force displacement relation for this situation is written in the following form:

$$\begin{Bmatrix} F_1 \\ F_2 \end{Bmatrix} = \begin{bmatrix} k_1+k_2 & -k_2 \\ -k_2 & k_2+k_3 \end{bmatrix} \begin{Bmatrix} x_1 \\ x_2 \end{Bmatrix} \tag{2}$$

For an exact solution, the following statement holds true, i.e.

$$\begin{Bmatrix} F_1 \\ F_2 \end{Bmatrix} - \begin{bmatrix} k_1+k_2 & -k_2 \\ -k_2 & k_2+k_3 \end{bmatrix} \begin{Bmatrix} x_1 \\ x_2 \end{Bmatrix} = \begin{Bmatrix} 0 \\ 0 \end{Bmatrix} \tag{3}$$

However, when this is not the case equation error vectors can be defined as:

$$\begin{Bmatrix} E_1 \\ E_2 \end{Bmatrix} = \begin{Bmatrix} F_1 \\ F_2 \end{Bmatrix} - \begin{bmatrix} k_1+k_2 & -k_2 \\ -k_2 & k_2+k_3 \end{bmatrix} \begin{Bmatrix} x_1 \\ x_2 \end{Bmatrix} \tag{4}$$

To obtain an error function the right hand side of equation (4) is squared and the result is then summed over the number of degrees of freedom. For the present case, the squared error function becomes

$$E^2 = E_1^2 + E_2^2 \tag{5}$$

The problem now is reduced to that of minimizing the error function with respect to the unknown stiffnesses. This is achieved by taking the derivative of E^2 with respect to each unknown element stiffness and setting it equal to zero. This leads to a set of linear equations equal in number to the number of elements.

Taking the first derivative of equation (5) with respect to k_1, k_2 and k_3 yields the following set of equations written in matrix form

$$\begin{bmatrix} x_1 & 0 \\ x_1-x_2 & -x_1+x_2 \\ 0 & x_2 \end{bmatrix} \begin{Bmatrix} F_1-(k_1+k_2)x_1+k_2x_2 \\ F_2+k_2x_2-(k_2+k_3)x_2 \end{Bmatrix} = \begin{Bmatrix} 0 \\ 0 \end{Bmatrix} \tag{6}$$

which may be further reduced to

$$\begin{bmatrix} x_1 & 0 \\ x_1-x_2 & -x_1+x_2 \\ 0 & x_2 \end{bmatrix} \begin{bmatrix} x_1 & x_1-x_2 & 0 \\ 0 & -x_1+x_2 & x_2 \end{bmatrix} \begin{Bmatrix} k_1 \\ k_2 \\ k_3 \end{Bmatrix} = \begin{bmatrix} x_1 & 0 \\ x_1-x_2 & -x_1+x_2 \\ 0 & x_2 \end{bmatrix} \begin{Bmatrix} F_1 \\ F_2 \end{Bmatrix} \tag{7}$$

Defining a Jacobian matrix $[J]$ as follows

$$[J] = \begin{bmatrix} \frac{\partial E_1}{\partial k_1} & \frac{\partial E_1}{\partial k_2} & \frac{\partial E_1}{\partial k_3} \\ \frac{\partial E_2}{\partial k_1} & \frac{\partial E_2}{\partial k_2} & \frac{\partial E_2}{\partial k_3} \end{bmatrix} \tag{8}$$

It is readily noticed that equation (7) can be written in the following form

$$[J]^T[J]\{k\} = [J]^T\{F\} \tag{9}$$

From which $\{k\}$ can be solved for directly

$$\{k\} = [[J]^T[J]]^{-1}[J]^T\{F\} \tag{10}$$

The following example illustrates the solution. In this example a determinate truss configuration is chosen for simplicity in which displacements were actually computed using the standard Direct Stiffness Method. This is a numerical experiment meant to test the proposed method for the retrieval of the structure's unknown element stiffnesses. It must be mentioned, however, that for a determinate truss no such elaborate procedure is necessary because the problem in such a case is reduced to the solution of a system of linear equation.

For an indeterminate truss the inverse of $[J]^T[J]$ upon which the solution hinges is not guaranteed. To circumvent such a situation and to assure the existence of a solution two or more loading cases must be used and the squared error function given in equation (5) can be formally written as

$$E^2 = \sum_{n=1}^{NLC} \sum_{i=1}^{N} \left[F_i^n - \sum_{\ell=1}^{N} K_{i\ell} \chi_\ell^n \right]^2 \tag{11}$$

in which N is the number of degrees of freedom and NLC is the number of loading conditions.

From which the solution for the element stiffness may be written as

$$\{k\} = \sum_{n=1}^{NLC} \left[[J]_n^T [J]_n \right]^{-1} \sum_{n=1}^{NLC} [J]_n^T \{F\}_n \tag{12}$$

3. EXAMPLE

The determinate truss shown in figure 2 is used to test the procedure. The truss is composed of 3 elements of cross sectional area equal to 25 cm^2. The modulus of elasticity is $200 \times 10^6 \frac{kN}{m^2}$. The truss has 3 unrestrained degrees

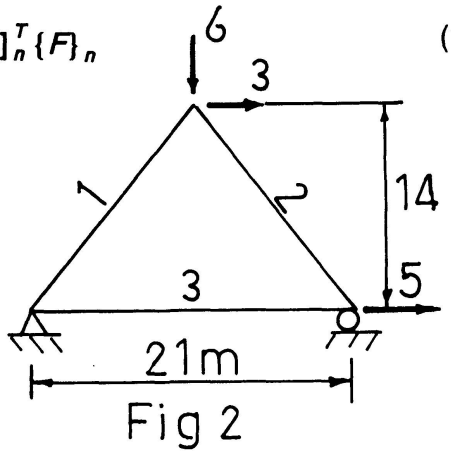

Fig 2

of freedom with the following reduced stiffness matrix derived with the standard Direct Stiffness Method for pin jointed trusses and written in terms of the unknown element stiffnesses.

$$[K] = \begin{bmatrix} 0.36k_1 + 0.36k_2 & 0.48k_1 - 0.48k_2 & -0.36k_1 \\ 0.48k_1 - 0.48k_2 & 0.64k_1 + 0.64k_2 & 0.48k_2 \\ -0.36k_2 & 0.48k_2 & k_3 + 0.36k_2 \end{bmatrix}$$

The applied loads are written in the following standard load vector

$$F = \begin{Bmatrix} 3 \\ -6 \\ 5 \end{Bmatrix} kN$$

Therefore the error vector of equation can be written as

$$\begin{Bmatrix} E_1 \\ E_2 \\ E_3 \end{Bmatrix} = \begin{Bmatrix} F_1 \\ F_2 \\ F_3 \end{Bmatrix} - \begin{bmatrix} 0.36k_1 + 0.36k_2 & 0.48k_1 - 0.48k_2 & -0.36k_1 \\ 0.48k_1 - 0.48k_2 & 0.64k_1 + 0.64k_2 & 0.48k_2 \\ -0.36k_2 & 0.48k_2 & k_3 + 0.36k_2 \end{bmatrix} \begin{Bmatrix} x_1 \\ x_2 \\ x_3 \end{Bmatrix}$$

From which the following Jacobian matrix can readily be deduced

$$[J] = \begin{bmatrix} 0.36x_1 + 0.48x_2 & 0.36x_1 - 0.48x_2 - 0.36x_3 & 0 \\ 0.48x_1 + 0.64x_2 & -0.48x_1 + 0.64x_2 + 0.48x_3 & 0 \\ 0 & -0.36x_1 + 0.48x_2 + 0.36x_3 & x_3 \end{bmatrix}$$

Upon performing the operation as defined by the derived formula (10) the element stiffness are retrieved i.e. $k_1 = k_2 = 28571.4 \frac{kN}{m}$ and $k_3 = 23809.5 \frac{kN}{m}$ which are exactly the same as can be computed using EA/L . It must be reiterated that the displacements x_1, x_2 and x_3 supposed to measured, were in this numerical experiment computed using standard computer programs.

4. REFERENCES

Matzen, V.C. and McNiven, H.D., Investigation of the Inclastic Characteristics of the Single Story Steel Structure Using System Identification and Shaking Table Experiments, *Report No. EERC 76-20*, Earthquake Engineering Research Center, University of California, Berkeley, August 1974.

Shield, P.C., *Elementary Linear Algebra*, Worth Publishers Inc.

Touqan, A.R., Najah 91, *An Engineering Analysis Program for Framed Structures*, November 1990.

White, R.N., Gergely, P., Sexsmith, R.C., *Structural Engineering*, Combined Edition, John Wiley and Sons.

Strength Evaluation of Existing Masonry Structures
Evaluation de la résistance de constructions en brique
Festigkeitsermittlung für bestehende Mauerwerksbauten

Xinggang ZHOU
Research Assist.
Yantai University
Yantai, China

Zhou Xinggang, born in 1963, received his engineering master's degree from Tsinghua University, China in 1989. Now he is a research assistant in Civil Engineering.

SUMMARY
According to experimental data and theoretical analysis, the relationship between strength and rigidity, rigidity deterioration, accumulated deformation energy in earthquake damage of masonry structures are studied. Methods are suggested that show how to evaluate the strength of masonry structures in serviceability state, and how to predict and evaluate the damage degree of masonry structures by earthquakes.

RÉSUMÉ
Sur la base de données d'essai et d'analyses théoriques, l'article étudie la relation entre la résistance de constructions en brique et la rigidité, la détérioration de rigidité, l'énergie de déformation accumulée lors de séismes. Des méthodes sont proposées pour l'évaluation de la résistance et de l'aptitude au service de constructions en briques, ainsi que pour l'évaluation de dommages possibles lors de séismes.

ZUSAMMENFASSUNG
Anhand experimenteller Ergebnisse und theoretischer Überlegungen, wird der Zusammenhang zwischen Festigkeit und Steifigkeit sowie des Steifigkeitsabfalls mit der kumulierten Verformungsenergie bei Erdbebenschäden an Mauerwerksbauten studiert. Es werden Verfahren vorgeschlagen, wie aus dem Gebrauchsverhalten von Mauerwerk auf seine Robustheit geschlossen und wie der Schädigungsgrad im Erdbebenfall vorhergesagt und evaluiert werden kann.

1. INTRODUCTION

As for existing masonry structures, it is known that many of them are in illness state in their serviceability life time, slightly or seriously. In fact, suffering various unfavourable factors in construction and application, such as dispersity of masonry material, temperature cracks etc. , masonry structures are in insufficient strength or strength deterioration state which is one of illness state concerned seriously. But the problem how to precisely examine the real serviceability state of masonry structures have not been solved for a long time. In this paper, mothod solving this problem was investigated, and the mothod developed from experimental information and theoretical analysis.

2. STRENGTH AND RIGIDITY

2. 1 Compressive strength and rigidity

Compressive stress—strain curve of masonry envalope can be expressed[1][2]:

$$\sigma = f_m(1 - e^{-\alpha f_m^{1/2}\varepsilon}) \qquad (2-1)$$

where, σ and ε are compressive stress and strain respectively. f_m is the compressive strength of masonry envalope, α is a coefficient. Therefore, elastic modulus of masonry envalope can be obtained:

$$E = \frac{d\sigma}{d\varepsilon}\Big|_{\varepsilon=0} = \alpha f_m^{3/2} \qquad (2-2)$$

Based on experimental information[1], the statistical value of α is 370. As we know, the (lateral)rigidity K is equal to the ratio of lateral load to displacement:

$$K = \frac{1}{\delta} = \frac{1}{\frac{h^3}{12EI} + \frac{h\xi}{GA}} = \frac{1}{\frac{h^3}{Etb^3} + \frac{1.2h}{0.3Etb}} = \frac{Et}{(\frac{h}{b})^3 + 4(\frac{h}{b})} \qquad (2-3)$$

Substituting equation (2 — 2) into formula (2 — 3), the ralation bettween rigidity and compressive strength can be got:

$$K = \frac{\alpha f_m^{3/2} t}{(\frac{h}{b})[(\frac{h}{b})^2 + 4]} \qquad (2-4)$$

in which, t, h and b are the thickness, height and width of masonry wall respectively.

2. 2 Shear strength and rigidity

Researching the hysteresis characteristic of masonry wall[1][2][3], the statistical skeleton curve of hysteresis loops are shown in Figure 1, it is indicated that in the initial stage the load—displacement relationship is linear and after cracking the displacement increases significantly with appeared and developed cross cracks. Defined P_u as the ultimate load, $\triangle u$ as the displacement in regard to p_u, and σ_c is the normal stress of masonry wall. The skeleton curve can be expressed as follow:

$$(1)\ P/P_u = 2.6\frac{\triangle}{\triangle u} \qquad (0 < P/P_u \leqslant 0.78, 0 < \frac{\triangle}{\triangle u} \leqslant 0.3) \qquad (2-5)$$

$$(2)\ P/P_u = 0.69 + 0.31\frac{\triangle}{\triangle u} \qquad (0.78 < P/P_u \leqslant 1;\ 0.3 < \frac{\triangle}{\triangle u} \leqslant 1) \tag{2-6}$$

$$(3)\ P/P_u = 1 + 0.44(1 - 0.085\sigma_c) - 0.44(1 - 0.085\sigma_c)\frac{\triangle}{\triangle u} \tag{2-7}$$

$$(P/P_u < 1;\ 1 \leqslant \frac{\triangle}{\triangle u} \leqslant 0.3)$$

$$(4)\ P/P_u = 0.55 + 0.04\sigma_c \tag{2-8}$$

From formula(2—5),the rigidify K can be written as follow also:

$$K = \frac{P}{\triangle} = 2.6\frac{P_u}{\triangle u} = 2.6\frac{f_v tb}{\triangle u} \tag{2-9}$$

where, f_v is the shear strength of masonry wall. According statistical analysis, the ralationship bettween f_v and $\triangle u$ is:

$$\triangle u = (3 + 4.5f_v)^{1/2}/(0.45 + 0.05\sigma_c) \tag{2-10}$$

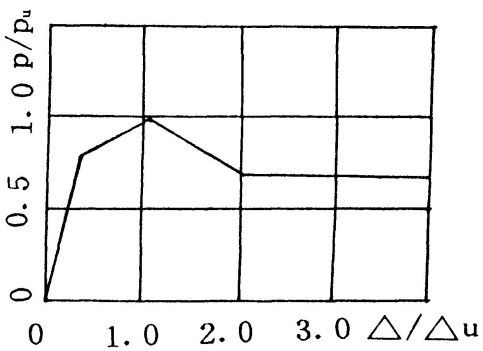

Fig. 1 Skeleton curve of masonry wall

Thus,

$$K = \frac{(1.17 + 0.13\sigma_c)f_v tb}{(3 + 4.5f_v)^{1/2}} \tag{2-11}$$

Equation (2 — 11) illustrates the ralationship bettween the rigidity K and the shear strength f_v.

2.3 Rigidity deterioration

Looking Fig. 1 again, it can be found that as increasing of displacement the stiffness of masonry wall decrease obviously. The stiffness K' at any displacement many be calculated from the following empirical formula:

$$K' = 0.0017(\triangle/H)^{-0.91}K \qquad (\triangle/H > 1/1000) \tag{2-12}$$

In other word, formula(2—12)show the deteriration of rigidity as increasing of displacement $\triangle$ under later load.

3. ACCUMMLATED DEFORMATION ENERGY AND DAMAGE INDEX

3.1 Input energy of perunit mass

The problem related to the strength and stiffness of masonry wall in serviceability state are discussed above. In order to predict the damage degree of masonry structure, accumulated deformation energy should be stuided, because any damage by earthquake is the result of accumulated deformation in vabration process Assume that w is the accumulated deformation energy[4,5]. As for one—freedom system, in general,

$$W = \frac{1}{2}m\dot{X}^2_{emax} \tag{3-1}$$

where, $\dot{X}_{emax}$ is the maximum value of elastic vabration velocity of system, and,

$$\dot{X}_{emax} = \dot{y}_{max}/2^{1/2} \qquad (3-2)$$

$\dot{y}_{max}$ is the maxiumum velocity of earth's surface vabration. Substitute formula (3—2) into formula (3—1), then,

$$W = \frac{1}{4}m\dot{y}_{max}^2 = mE_0 \qquad (3-4)$$

E_0 can be defined as the input energy of perunit mass. From statitical analysis, E_0 can be formulated as follow:

$$E_0 = \frac{1}{4}\dot{y}_{max}^2 = exp(1.385I - 6.39) \qquad (3-5)$$

Where, I is the earthquake intensity.

3.2 Damage index of masonry structure

The vabration equilibrium equation of ith storey for multistorey masonry structures can be expressed (damp is neglected):

$$m_n(\sum_{j=1}^{n}\ddot{x}_j + \ddot{y}) + m_{n-1}(\sum_{j=1}^{n-1}\ddot{x}_j + \ddot{y}) + \cdots\cdots + m_i(\sum_{j=1}^{i}\ddot{x}_j + \ddot{y}) = f_i(x_i) \qquad (3-6)$$

Multiplying the equation by $\dot{x}_i dt = dx_i$, and integralling the equation in the whole vabration time, thus

$$\int(\sum_{k=1}^{n}m_k\sum_{j=1}^{k}\ddot{x}_j)dx_i + \int\dot{x}_i\sum_{k=i}^{n}m_k\ddot{y}dt = \int f_i(x_i)\dot{x}_i dt \qquad (3-7)$$

It is noted that:

$$\int\ddot{x}_j dx_i = \int\ddot{x}_i dx_j = \int\dot{x}_j d\dot{x}_i = \int\dot{x}_i d\dot{x}_j = 0$$

$$\int\ddot{y}\dot{x}_1 dt = \int\dot{x}_1 d\dot{x}_1$$

$$x_i = h_i x_1/h_1$$

therefore,

$$w_i = \int f_i(x_i)dx_i = \sum_{k=i}^{n}m_k\int\ddot{y}dx_i = \sum_{k=i}^{n}m_k\int\frac{h_i}{h_1}\dot{x}_1 d\dot{x}_i = \sum_{k=i}^{n}m_k\frac{h_i}{h_1}E_0 \qquad (3-8)$$

h_i, h is the height of storey.

Assume that η_p and η are the ratio of ultimate deformation energy to elastic deformation energy and the ratio of deformation energy to elastic deformation energy respectively. According to experimental date, η_p is about 12 refer to masonry structures. η_i can be wrote as follow:

$$\eta_i = W_i/W_{iy} = 2\sum_{k=i}^{n} m_k \frac{h_i}{h_1} E_0/P_{cr}\triangle cr = 2K_r \sum_{k=i}^{n} m_k \frac{h_i}{h_1} E_0/(\gamma f_v tb)^2 \qquad (3-9)$$

γ is a statitical factor which is equal to 0. 78. Let β express the damage index of masonry structures by earthquake, then,

$$\beta = \frac{W - W_y}{W_r - W_y} = \frac{\eta - 1}{\eta_r - 1} \qquad (3-10)$$

From experimental and earthquake damage information[2,3,6], it can be defined that:

$\beta \geqslant 1.0$	*partly collapse*
$0.90 \leqslant \beta < 1.0$	*serious damage*
$0.50 \leqslant \beta < 0.90$	*moderate damage*
$0.15 \leqslant \beta < 0.50$	*slight damage*
$0 \leqslant \beta < 0.15$	*intact state*

4. APPLICATION

4.1 Application

Up to now, we discussed the strength, rigidity and accumulated deformation energy. In this section, we will discuss how to evalute the strength of masonry structures in service. Serviceability state and how to predict the damage of masonry structure by earthquake. As we know that structure's natrual frequency and mode of vabration can be measured and analyzed from ambient vabration. So the rigidity of structures can be identified using the date of natrual frequency, mode of vabration and equibibrium equation of vabration. Since the rigidity can be indentified, substituting the rigidity into formulae (2—4)and(2—11). Using formulae (2—1)and(2—3), the compressive and shear strength of masonry structures can be evaluted. On the basis of these results, it can be found that which storey is the weak part in serviceabilty state or under earthquake circumstance. Applying (3—9)and(3—10), it can be pridicted that which degree of damage will be caused under grant earthquake intensity.

4.2 Example

A multistorey masonry structure. Seven storey, the height of storey is 2800mm. it's plane figure refering to Fig2. The thickness of outer horizatal wall is 490mm, inter horizatal wall are 370mm(the first floor) and 240mm (from the second to the seventh). The thickness of outer transerve wall is 370mm. The results of measured date from ambient vabration are show in table 1. Using the date of table 1 and the method discussed above. The distribution of rigidity, strength and damage index under seven degree of earthquake intersity etc are caculated and shown in table 2.

Table 1. The results of ambient vabration

Floor	weight(kg)	Ai(mm)	K_i(KN/m)
1	6.928×10^5	0.019	8.75×10^6
2	6.566×10^5	0.038	8.53×10^6
3	6.566×10^5	0.061	6.74×10^6
4	6.566×10^5	0.16	1.42×10^6
5	6.566×10^5	0.18	55.43×10^6
6	6.566×10^5	0.20	33.50×10^6
7	4.156×10^5	0.26	1.49×10^6
note	frenquence $f_1=2.832$HZ		

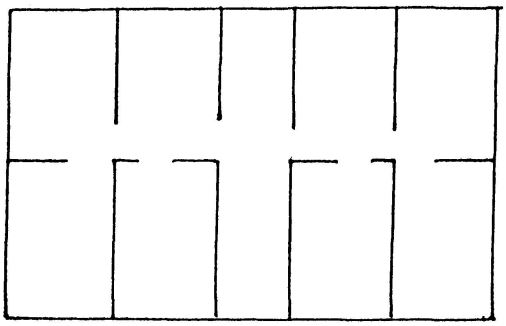

Fig. 2 Plane figure of example

Table 2 The results of evalution

Floor	K_i(KN/m)	Compressive strength(MP_a)	shear strength(MP_a)	compressive stress(MP_a)	earthquake shear stress	Damage index
1	8.75×10^6	2.80	0.47	0.47	0.15	0
2	8.53×10^6	3.62	0.599	0.55	0.29	0.44
3	6.74×10^6	3.10	0.440	0.46	0.26	0.13
4	1.42×10^6	1.10	0.076	0.36	0.23	7.10
5	5.43×10^6	2.68	0.332	0.27	0.18	0.20
6	3.50×10^6	2.00	0.200	0.19	0.122	0.30
7	1.44×10^6	1.13	0.092	0.09	0.05	0.26

note: 1. earthquake intensity is seven degree.
2. earthquake shear stress caculated by equivalent base shear method.

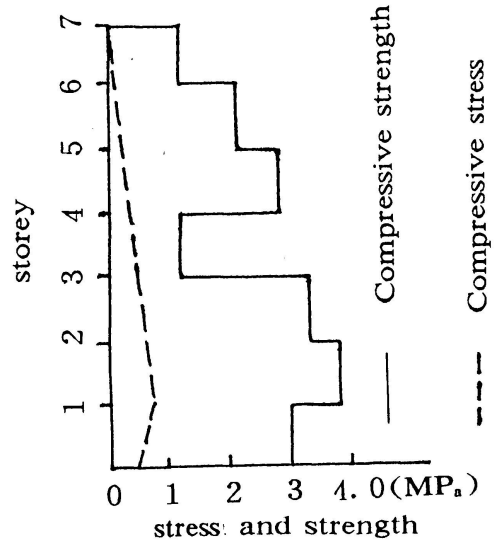

Fig. 3 Distribution of compressive strength and stress

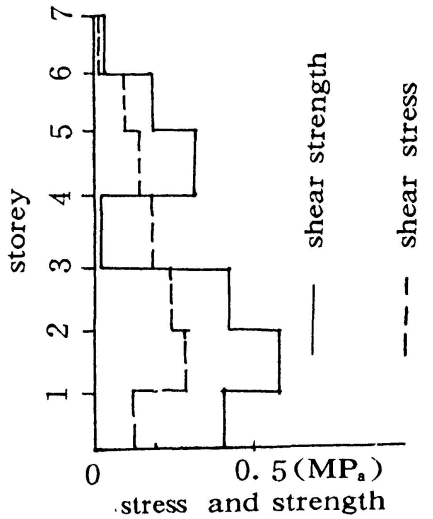

Fig. 4 Distribution of shear strength and stress

6. CONCLUSION AND DISCUSSION

① Above, the strength, the rigidity, the deformation energy and the damage index of masonry structure are studied. Ralationship bettween them are given also.

② Using the ralationship and date from ambient vabration, the serviceiability state of existing masonry structures can be asserted, and the damage index by earthquake can be predict also.

③ Based on experimental statisfical information and structural dynamic analysis. The method reflect every aspect involved in masonry structure and suggest a way to examine the existing masonry structure comprehensively.

④ Example show that the compressive strength, the shear strength and the damage index evaluted by the mathod are in good agreement.

⑤ Examples show that the mathod are feasible. The assertment results of existing masonry structure are reliability.

⑥ Further investigation should be carried and make the mothod more perfecter.

REFERENCES

1. YiLiang Q. The paper slection of masonry structures, Huonan university publish house, 1989.

2. Jing qin, X. Some problem about seismic Resistance of Brick Masonry walls. The proceding of Seismic Risistance Vol2. 1986.

3. Jumin S, Xinggong Z, Shiping F, Seismic Behavior of Reinforced Brick Masonry Cavity walls, IABSE SYMPOSIUM BRUSSELS 1990,

4. G. W. Houser, Limit Design of Structures to Risist Earthquakes, Pros, ist. W, c. E. E. Berkeleg 1986.

5. Haodong L, The evalution of Brick Masonry Structures after Earthquakes, The proceeding of Seismic Resistance vol 1. 1986

6. Yucheng, Y. The Analysis of Damage to Multistorey Brick Buildings During the Tangshang Earthquake, Congress Earthquake Protection of Construction in Sersmic Area Ramania, 1978. 11

7. Bao zhiwen. etal. Ambient Vibration Survey of Some High Building in Hongkong. Tsinghua Publish House, 1985

Stress Assessment of Reinforced Concrete Structures with Cracks

Estimation des contraintes des constructions en béton armé fissurées

Spannungsermittlung in gerissenen Stahlbetontragwerken

Petras PUKELIS
Associate Professor
Vilnius Technical University
Vilnius, Lithuania

Petras Pukelis, born 1932, received his diploma of civil engineer and candidate of science degree at Kaunas Technological University, Kaunas, Lithuania. His scientific interests are shear strength of reinforced concrete, evaluation and strengthening of structures of existing buildings.

Vidmantas JOKUBAITIS
Associate Professor
Vilnius Technical University
Vilnius, Lithuania

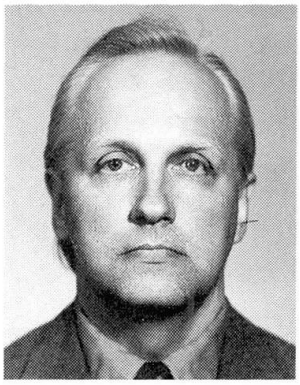

Vidmantas Jokubaitis, born 1938, received his diploma of civil engineer and candidate of technical science degree at Kaunas Technological University, Kaunas, Lithuania. Main area of his research activity is evaluation of reinforced concrete structures with cracks of existing buildings.

Kazys Algirdas KAMINSKAS
Associate Professor
Vilnius Technical University
Vilnius, Lithuania

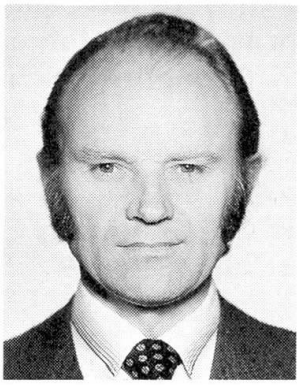

Kazus Algirdas Kaminskas, born 1940, received his diploma of civil engineer and candidate of technical science degree at Kaunas Technological University, Kaunas, Lithuania. For twenty years he was involved in prestressed concrete and strengthening of reinforced concrete structures.

SUMMARY

A new method to evaluate stress in tensile reinforcement and compressed concrete of reinforced concrete members is proposed. The method is based on principles of crack propagation theory in brittle bodies. The stresses are estimated by taking into account external force action and the parameters of cracks.

RÉSUMÉ

L'article propose une méthode précise de calcul des contraintes d'armature longitudinale tendue et du béton comprimé dans des éléments en béton armé. On détermine les contraintes sur la base des efforts externes et des paramètres de la fissure normale. La méthode de calcul se base sur la théorie linéaire de rupture mécanique dans un corps fragile.

ZUSAMMENFASSUNG

Es wird eine relativ genaue Methode vorgeschlagen, um bei bestehenden Stahlbetontragwerken die Zugs- und Druckspannungen in gerissenen Querschnitten zu ermitteln. Basierend auf der linearen Bruchmechanik für spröde Körper werden die einwirkenden Kräfte und Kenngrössen der Biegerisse berücksichtigt.

1. INTRODUCTION

Evaluation of existing reinforced concrete structures is very important for maintenance, renovation and reconstruction of industrial and other in-service buildings. There are several methods to evaluate stress and strains in structures using their examination data. In the case of reinforced concrete structures with normal cracks in tensile zone it is possible to evaluate stress by the crack parameters measured during the examination of these structures. The degree of crack development is considered as a result of existing stress - strain state in the member [1]. In this paper a posibility to employ classical theory of crack propagation in a brittle body for calculation of tensile reinforcement stresses at the cross section through crack is investigated.

2. REINFORCEMENT AND CONCRETE STRESSES IN CROSS SECTION THROUGH CRACK

Within the limits of assumed model of a brittle body in the case of macroscopic cracks the following equation is valid [2]:

$$\lim_{s\to 0} \{\sqrt{s}\ \sigma_{y(s,p)}\} = \frac{K}{\pi} \tag{1}$$

where s is the distance of body points situated in the crack plane from the top of the crack; $\sigma_{y(s,p)}$ is breaking stress for a member with macroscopic crack of $2l_0$ length and K is modulus of bond. It is shown in [2] that stresses in body outside the crack $(x>l)$ due to any normal pressure acting in the banks of this crack may be expressed by formula, see Fig.1(a):

$$\sigma_{y(x,0)} = \frac{1}{\pi\sqrt{x^2-l^2}} \int_{-l}^{l} \frac{p_n(\xi)\sqrt{l^2-\xi^2}}{x-\xi}\, d\xi \tag{2}$$

Due to limitation of stress $\sigma_{y(x,0)}$ in the body for the case of $x\to l$ the following equation must be observed:

$$\lim_{x\to l} \int_{-l}^{l} \frac{p_n(\xi)\sqrt{l^2-\xi^2}}{x-\xi}\, d\xi = 0 \tag{3}$$

Boundary conditions for the function of the normal pressure $p_n(\xi)$ in the tensile zone of a reinforced concrete member, see Fig.1(a), may be written as follows:

$$p_n(\xi) = \begin{cases} p_0(\xi) & |\xi| \le c \\ 0 & |\xi| \le l_0 - c \\ -f_{ct} & l_0 < -x \le 1 \\ -\dfrac{\sigma_s \beta}{\alpha} & l_0 < x \le 1 \end{cases} \tag{4}$$

where $p_0(\xi)$ is arbitrary function of pressure applied on banks of the crack and estimated as a resultant of stresses acting in

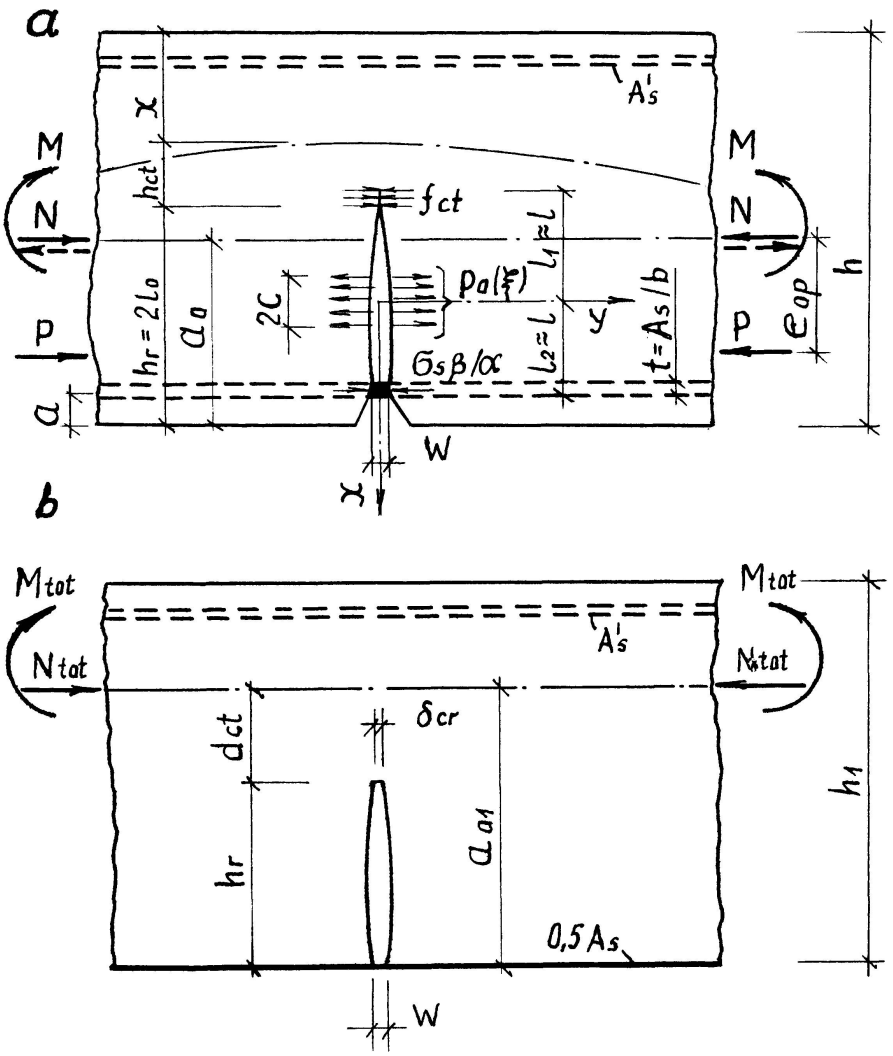

Fig.1 Models of normal crack in tensile zone of reinforced concrete member: a - for evaluation of reinforcement stress intensity coefficient; b - for assesment of tensile reinforcement stress in crack

continuous concrete of the crack zone $|x| \leq l$; f_{ct} is tensile strength of concrete; $\sigma_s\beta/\alpha$ is stress at the level of tensile reinforcement; $\alpha = E_s/E_c$; $\beta = 125\,\rho$ and is used when longitudinal reinforcement ratio $\rho = A_s/(bd)$ is small when $\rho \geq 0.008$, $\beta = 1$.

Using equation (4) and considering that $s = x - l_0$, $\sqrt{x^2 - l_0^2} = \sqrt{s}\,\sqrt{l_0 + s}$, equation (3) may be rearranged into the following form

$$\lim_{s\to 0} \{\sqrt{s}\,\sigma_{y(s,p)}\} \approx \frac{2\sigma_s\beta}{\alpha\pi}\,\sqrt{t} \tag{5}$$

From equations (1) and (5) tensile reinforcement stress

$$\sigma_s = \frac{K\alpha}{2\beta\sqrt{t}} \tag{6}$$

and critical steel stress intensity factor

$$K_{cr} = 1.6\ f_s \sqrt{t}\frac{\beta}{\alpha} \tag{7}$$

where f_s is strenght (yield limit) of reinforcement steel. Values greater than critical K_{cr} values leads to the fracture of not overreinforced concrete member with tensile steel.

By similar method as in [2] assuming bodies as isotripic expression of the modulus of bond K for reinforced concrete member has been deduced. A fictitious cross section of the depth h_1 was assumed, see Fig.1(b), the centroid of which coincides with the central axis of the member. The depth h_1 is obtained from the following expression:

$$h_r + h_{ct} = \frac{S_1}{A_1} \tag{8}$$

where S_1 is statical moment of ficticious cross - sectional area A_1 in respect to the centroid of longitudinal tensile reinforcement.

Modulus

$$K = \left(\frac{M_{tot} - \Delta M}{W_1} - \frac{N_{tot}}{A_1}\right)\sqrt{h_r}\ \frac{\pi}{2} \tag{9}$$

where $M_{tot} = M - Pe_{op}$ and is the total moment in relation to the centroid of the real cross section of the member, see Fig.1; P is longitudinal reinforcement prestressing force; e_{op} is the eccentricity of P; $\Delta M = N_{tot}\ (a_{01}-a_0\ )$ and is the increase in bending moment due to deviation of centroid of fictitious cross section from the centroid of the real cross section of the member; $N_{tot} = P \pm N$ and is the total longitudinal force acting in the centroid of the real cross section. Compressive N force is positive; $W_1 = I_1/(0.75h_r + h_{ct}\ )$ and is modulus of cross section ; I_1 is inertia moment of fictious cross section in relation to the neutral axis situated at distance $h_r + h_{ct}$ from the tensile face of fictitious cross section; $h_{ct} = \delta_{cr} h_r / w$ and is the depth of concrete tensile zone above the crack, see [1].

The critical width of the crack end

$$\delta_{cr} = 0.00012\ a\ \sqrt[3]{\phi}\ \eta\ \frac{3.5 - 100\ \rho_1}{3.5 - 100\ \rho_2} \tag{10}$$

where ϕ is bar diameter of tensile reinforcement in mm; η is factor for consideration of bond between concrete and reinforcing steel; $\rho_1 = A_s / [bh+(b_f - b)h_f\ ] \leq 0.02$ and $\rho_2 = A_s / (bh) \leq 0.02$ and they are longitudinal reinforcing factors; b_f and h_f are width and the thickness of the flange in the tensile zone of the member.

Substitution of modulus K value by (9) into formule (6) gives the final expresion of tensile reinforcement stress value

$$\sigma_s = [\frac{(M_{tot} + \Delta M)(0.75h_r + h_{ct})}{I_1} - \frac{N_{tot}}{A_1}]\frac{\pi\alpha}{4\beta}\sqrt{\frac{h_r}{t}} \quad (11)$$

If the neutral axis is located extreme compressed concrete fiber stress σ_c may be calculated by the equation:

$$\sigma_c = \frac{M\ (h - h_r - h_{ct})}{I_{red}} \quad (12)$$

where I_{red} is inertia moment about neutral axis of transformed cross section by reducing its area by $A_{ct} = h_r b$.

For concrete coefficient

$$K_{cr} = \sqrt{\delta_{cr} E_c f_{ct}} \quad (13)$$

where E_c and f_{ct} are modulus at elasticity and tensile strength of concrete respectively.

3. RESULTS OF EXPERIMENTAL INVESTIGATION

Special test specimens, beams and eccentrically compressed reinforced concrete members, were investigated. Prestressed concrete beams of rectangular cross section $b \times h = 100 \times 180$ *mm*, span $l = 1800$ *mm*, longitudinal prestressing steel ratio $\rho = 0.8 - 0.95$ %, prestressing force $P = 41.2 - 132.5$ *kN* were subjected to two concentrated forces at 1/3 distances from supports. Electrical resistance gauges were used to measure steel strain in the cross section through crack. The parameters h_r and w of crack in pure bending zone of beams were measured by 24 times magnifying microscope and concroled by electrical resistance strain gauges closely spaced on beam face along its height.

Results of special tests on beams reported in [3] also are employed to evaluate theoretical proposotions of this paper. Reinforced concrete beams of rectangular crosis section $b \times h = 120 \times 300$ *mm*, span length $l = 2000$ *mm*, longitudinal tensile reinforcement ratio $\rho = 0.48 - 3.83\%$, without prestress were loaded by two concentrated forces at 1/3 distances from supports. Special notches were formed in the test beams to locate the main cracks. Steel strain in the main crack and parameters h_r and w of this crack were measured.

Eccentrically compressed members of rectantgular cross section $b \times h = 100 \times 150$ *mm*, length $l = 1000$ *mm*, tensile reinforcement rat io $\rho = 0.46 - 1.26\%$ were tested by the authors of this paper. Notches in the middle of the member length from tensile face up to longitudinal reinforcing bars deep were formed. Crack parameters were measured by a microscope magnifying 24 times and by a dial gauge at the level of tensile reinforcement.

The values of tensile reinforcement stresses obtained by tests $\sigma_{s,obs}$ and calculated by equation (11) σ_s are compared, see Fig.2. In the case of eccentrically compressed

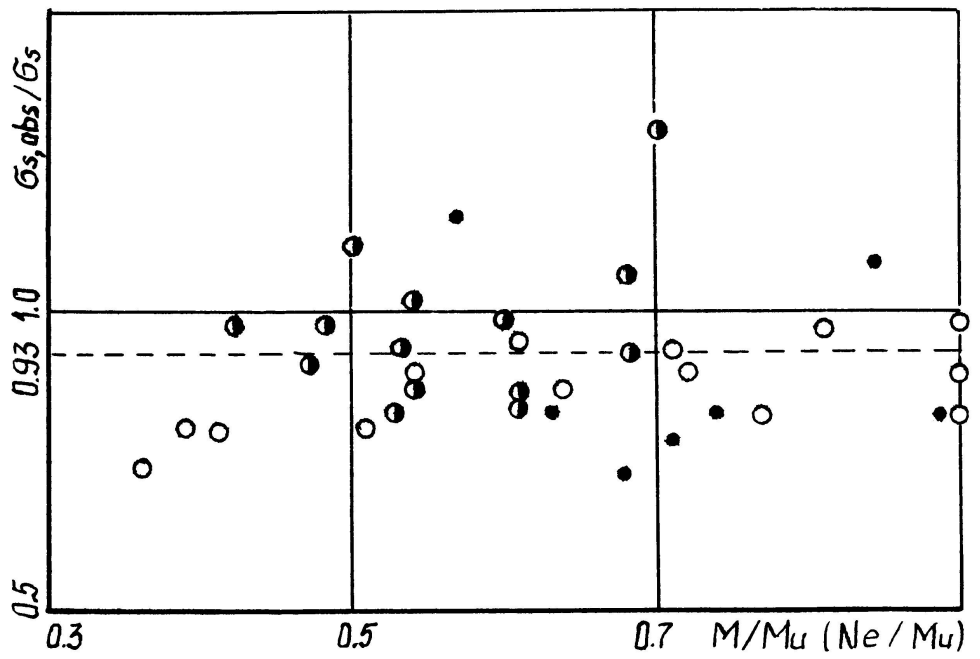

Fig.2 Comparison of measured in tests $\sigma_{s,obs}$ and theoretical σ_s calculated by formula (11) tensile reinforcement stress values: • - prestressed concrete beams; o - reinforced concrete beams; ◑ - eccentrically compressed members

members ratio $\sigma_{s,obs} / \sigma_s$ is plotted in respect to quantity Ne / M_u where N is external force acting at distance e from centroid of tensile reinforcement and M_u is the ultimate bending moment of the cross section.

Theoretical values σ_s calculated by (11) are on the average 7% higher than $\sigma_{s,obs}$ measured in tests. The variation coefficient of the ratio $\sigma_{s,obs} / \sigma_s$ is equal to 0.15.

Experimental values of concrete extreme fiber stress $\sigma_{c,obs}$ obtained from tests [3] were compared with theoretical values σ_c of this stress calculated by equation (12). Theoretical values σ_c on the average are 3% higher than experimental values $\sigma_{c,obs}$ of this stress. Coefficient of variation of the ratio $\sigma_{c,obs} / \sigma_c$ is equal to 0.11.

4.CONCLUSIONS

Contour of through normal crack in tension zone of a reinforced concrete member always is continguous to tensile concrete and to reinforcement. The latter has substantial influence on rupture strength of tensile concrete. Parameters of this strength K_{cr} and δ_{cr} expressed by (7), (10) and (13) define correctly character of stable crack propagation observed in tested samples.

Calculation of stresses in tensile reinforcement by (11) and in extreme fiber of compressed concrete by (12) makes it possible to assess stress state of reinforced concrete structures in service with sufficient accuracy.

REFERENCES

1. JOKUBAITIS V., PUKELIS P., Stress - strain state estimation in existing reinforced concrete structures subjected to bending (in russian). Transactions of Lithuanian universities. Reinforced concrete structures No.12, Vilnius,1983.

2. PANASIUK V., Ultimate equilibrium of brittle bodies with cracks (in russian). Kijev, 1968.

3. CHUBRIKOV V., Criteria of fracture mechanics for stress assesment in reinforced concrete bending member section with crack (in russian). Lvov, 1989.

Detection of Local Stiffness Changes of Buildings
Mesure des variations locales de rigidité dans des bâtiments
Messung örtlicher Steifigkeitsänderungen in Hochbauten

Ghee Koh CHAN
Senior Lecturer
National Univ. of Singapore
Singapore

Ming See LIN
Research Assistant
National Univ. of Singapore
Singapore

Thambirajah BALENDRA
Associate Professor
National Univ. of Singapore
Singapore

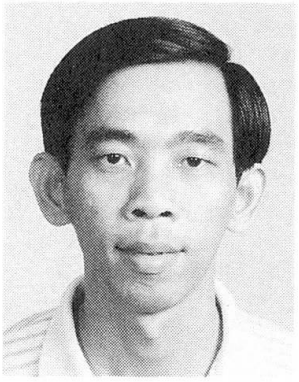

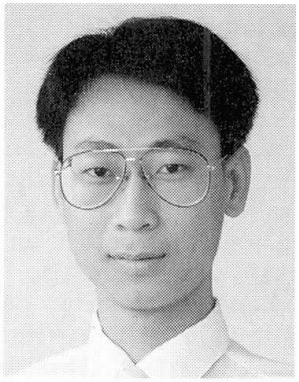

Chan Ghee Koh, born in 1956, got his Ph.D in Civil Engineering at the University of California Berkeley. He taught at the National University of Singapore since 1986. His current research area is structural dynamics with emphasis on vibration control, system identification and offshore structures.

SUMMARY

A method for identification of local structural changes in terms of storey stiffnesses of buildings is proposed here. Static condensation is applied to reduce the size of system for identification, while stiffness changes are determined recursively in a remedial model by the extended Kalman filter. The efficacy of this "improved condensation" method under various noise levels is illustrated numerically by an example of a twelve-storey plane frame building.

RÉSUMÉ

L'auteur présente ici une méthode pour identifier les faiblesses structurales locales des bâtiments. Il se base pour cela sur la détermination de la rigidité des étages par identification du système, appliquée à un modèle réduit par compression statique, en procédant par la méthode itérative de Kalman de filtrage non linéaire. Il démontre ainsi l'efficience de cette méthode de compression améliorée en l'appliquant à un bâtiment de douze étages à ossature plane en portique, sous niveaux différentiels de perturbations.

ZUSAMMENFASSUNG

Es wird eine Methode zur Auffindung örtlicher Tragwerksschwächungen in Hochbauten vorgestellt. Sie basiert auf Ermittlung der Stockwerkssteifigkeit durch Systemidentifikation an einem durch statische Kondensation reduzierten Modell, wobei iteraktiv mit einem erweiterten Kalman-Filter vorgegangen wird. Die Effizienz dieses verbesserten Kondensationsverfahrens wird an einem zwölfgeschlossigen ebenen Rahmentragwerk für unterschiedliche Störsignalpegel demonstriert.

INTRODUCTION

In recent years, application of system identification (SI) to damage assessment and safety evaluation of civil engineering structures has received considerable attention (e.g. Natke and Yao 1987; Agbabian et al. 1991). Based on input and output measurements of dynamically excited structures, structural parameters such as stiffnesses are determined and then compared with intended design values. In this manner, periodic monitoring of state of structures can be performed for detection of structural changes due to damage or deterioration. However, several problems have yet to be resolved before this methodology can become viable for actual structures.

One of the problems reported by some researchers is that current SI techniques have not been satisfactory in detecting local damages. Modal parameters as determined by frequency domain analysis are not sensitive to local damages, except for small structural systems or unless high modes are taken into account. The accuracy of high modes is, however, often difficult to achieve because of measurement noise. Hence, there is apparently a trend that researchers prefer time-domain SI approaches, among which the extended Kalman filtering (EKF) originally developed by Kalman and Bucy (1961) is perhaps most widely used. Nevertheless, it has been found that the change in stiffness matrix due to member stiffness changes in the locality tends to "spread out" or "diffuse" into adjacent structural members (herein referred to as "stiffness diffusion"), thereby making local damage identification difficult (Natke and Yao 1987).

In addition, from the viewpoint of structural safety evaluation, it is important to estimate the confidence level (or reliability) of identified parameters taking into consideration measurement noise as well as modeling errors. In this aspect, Agbabian et al. (1991) has applied least-squares approximation methods to successive time windows of input and output (I/O) time histories. In their numerical studies, the effects of I/O noise have been taken into account. However, to the authors' knowledge, modeling errors have thus far not been considered in the confidence estimate of identified parameters.

IMPROVED CONDENSATION METHOD

The problem of local damage detection is aggravated by the large number of degrees of freedom (DOFs) in modeling an actual structure. When applied to a complete structural model involving all DOFs, the EKF and other time-domain SI approaches alike are often found to be numerically inefficient in terms of accuracy, convergence and computation speed. Alternatively, a "reduced" model with a smaller number of DOFs can be considered. For instance, if quantification of storey stiffness changes of a building suffice for the purpose of damage detection, a simple lumped mass model can be used to reduce DOFs. Unfortunately, as a result of considerable modeling errors, diffusion problem of storey stiffness into adjacent storeys would render local damage detection ineffective.

As an attempt to detect the location of damage and quantify the magnitude of damage in terms of stiffness reduction of a building, an improved condensation method (ICM) is proposed here. For illustration purpose, a single-bay n-storey plane frame building as shown in Fig. 1(a) is considered. Axial and shear deformations are assumed to be negligible. Static condensation is first conducted, reducing the complete structural model to a "condensed" model with a significantly smaller number of DOFs [Fig. 1(b)]. In this study, columns are considered to be the critical elements where damages are likely to occur and affect the overall performance of the building.

Non-critical elements (beams) are assumed to be undamaged and any difference in storey stiffness is solely due to changes in column flexural rigidities (EI). In order to narrow the gap between the condensed model and the actual structure (upon which I/O measurements are taken), a "remedial" (or correction) stiffness matrix $\mathbf{K}_R$ is derived based on a lumped mass model as shown in Fig. 1(c). By applying the EKF on a time window of data, the stiffnesses of this remedial model are identified and then used to update the condensed model. This process is repeated for a specified number of time windows (or until convergence).

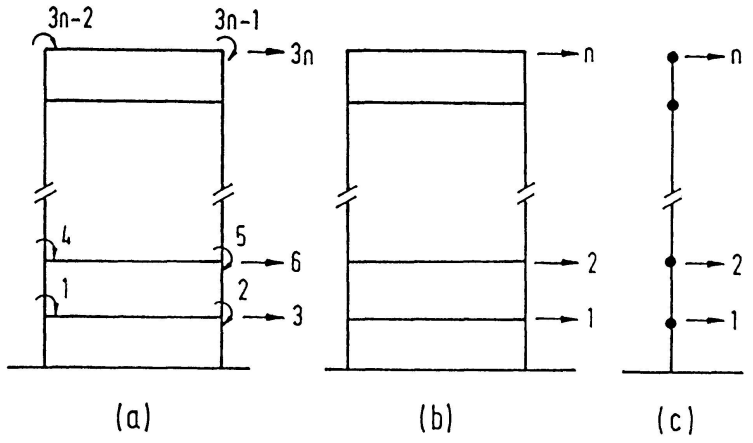

FIG. 1. (a) Complete Model; (b) Condensed Model; (c) Remedial model. (Numbers indicate DOFs).

The procedure of the ICM for damage detection of the building considered is described below.

(1) Divide the excitation and response time histories into time windows.

(2) Form mass matrix $\mathbf{M}$ ($3n \times 3n$) for the complete model based on known mass distribution. Given flexural rigidities of the "undamaged" building, form complete stiffness matrix $\mathbf{K}$ ($3n \times 3n$) encompassing all DOFs, i.e. two joint rotations and one horizontal translation per floor [Fig. 1(a)].

(3) Damping matrix $\mathbf{C}$ ($3n \times 3n$) is constituted by adopting Rayleigh damping , assuming that damping ratios of two vibration modes are known. (This assumption can be relaxed by including damping ratios as additional unknown parameters to be identified.)

(4) Perform static condensation to obtain condensed mass matrix $\mathbf{M}_C$, damping matrix $\mathbf{C}_C$ and stiffness matrix $\mathbf{K}_C$, all of size $n \times n$ [Fig. 1(b)].

(5) The improved condensation model is derived by adding the remedial stiffness matrix $\mathbf{K}_R$ (as explained earlier) to the condensed stiffness matrix $\mathbf{K}_C$. Elements in $\mathbf{K}_R$ are the unknown parameters to be identified by the EKF, while $\mathbf{K}_C$ remains unchanged.

(6) Compute stiffness correction factor η_j for the j-th storey as follows:

$$\eta_j = \sum_{k=1}^{N_W} (EI_R)_j^{(k)} / (EI_U)_j \qquad (1)$$

where U denotes the undamaged quantity, R denotes the remedial quantity and N_W is the current time window number. Since the remedial model is derived from a shear building, the remedial flexural rigidity is given by $(EI_R)_j = (K_R)_j \, l_j^3 / 12$, where $(K_R)_j$ is the corresponding storey stiffness in $\mathbf{K}_R$, and l_j is the column length. The updated flexural rigidities

$$EI_j = (EI_U)_j (1 + \eta_j), \qquad j = 1, \ldots, n \qquad (2)$$

are then used to compute the complete stiffness matrix $\mathbf{K}$.

(7) Repeat step 3 to step 6 for all time windows considered. The severity of the damage in each storey is finally given by the end result of η_j.

ADAPTIVE FILTER

In SI techniques employing the EKF, uncertainties in terms of variances of identified parameters are supposedly reflected in the error covariance matrix. The error covariance is dependent on the output noise covariance and the system noise covariance in the EKF algorithm. The variances of input and output noise can be estimated from resolution and accuracy of instruments and data acquisition system. The main problem is the difficulty in estimating the variance of system noise which includes modeling errors as well as input noise. In application of the EKF, the uncertainty in the system noise causes the divergence phenomenon, especially when the input noise is small in comparison with the modeling errors.

An adaptive filter was developed by Jazwinski (1969) as an algorithmic attempt to control divergence in Kalman filtering of orbit determination problems. In this paper, this adaptive filter is modified to suit SI problems for the purpose of obtaining statistically consistent variances of identified parameters.

Determination of System Error Covariance Q

Consider a time window beginning with k-th time step. The predicted residual vector at p steps later (i.e. time t_{k+p}) is defined as

$$\mathbf{r}_{k+p} = \mathbf{y}_{k+p} - \mathbf{H}(t_{k+p})\hat{\mathbf{x}}(t_{k+p}|t_k) \tag{3}$$

where $\mathbf{y}_{k+p}$ is an observation vector ($m\times 1$), $\hat{\mathbf{x}}(t_{k+p}|t_k)$ is an expected state vector ($n\times 1$), and $\mathbf{H}(t_{k+p})$ is an observation matrix ($m\times n$). The covariance of the predicted residual vector can be derived by means of the EKF algorithm as

$$E\{\mathbf{r}_{k+p}\mathbf{r}_{k+p}^T\} = \mathbf{H}(t_{k+p})\Phi(t_{k+p},t_k)\mathbf{P}(t_k|t_k)\Phi^T(t_{k+p},t_k)\mathbf{H}^T(t_{k+p}) + \mathbf{H}(t_{k+p})\left\{\sum_{i=1}^{p}\Phi(t_{k+p},t_{k+i})\mathbf{Q}(t_{k+i-1})\Phi^T(t_{k+p},t_{k+i})\right\}\mathbf{H}^T(t_{k+p}) + \mathbf{R}_{k+p} \tag{4}$$

where $E\{\cdot\}$ denotes expectation operator, Φ is a state transition matrix ($n\times n$), $\mathbf{P}$ is an error covariance matrix ($n\times n$), $\mathbf{Q}$ is a system noise covariance matrix ($n\times n$), and $\mathbf{R}$ is a measurement noise covariance matrix ($m\times m$). $\mathbf{Q}$ is determined by ensuring consistency between the residuals and their statistics such that

$$\frac{1}{p}\sum_{i=1}^{p}\mathbf{r}_{k+i}\mathbf{r}_{k+i}^T = E\{\mathbf{r}_{k+p}\mathbf{r}_{k+p}^T\} \tag{5}$$

Equation 4 can thus be written as

$$\mathbf{H}(t_{k+p})\left\{\sum_{i=1}^{p}\Phi(t_{k+p},t_{k+i})\mathbf{Q}(t_{k+i-1})\Phi^T(t_{k+p},t_{k+i})\right\}\mathbf{H}^T(t_{k+p}) = \frac{1}{p}\sum_{i=1}^{p}\mathbf{r}_{k+i}\mathbf{r}_{k+i}^T - E\{\mathbf{r}_{k+p}\mathbf{r}_{k+p}^T|\mathbf{Q}(t_{k+p})=0\} \tag{6a}$$

where

$$E\{\mathbf{r}_{k+p}\mathbf{r}_{k+p}^T|\mathbf{Q}(t_{k+p})=0\} = \mathbf{H}(t_{k+p})\Phi(t_{k+p},t_k)\mathbf{P}(t_k|t_k)\Phi^T(t_{k+p},t_k)\mathbf{H}^T(t_{k+p}) + \mathbf{R}_{k+p} \tag{6b}$$

In the present formulation, only diagonal elements of $\mathbf{r}_{k+p}\mathbf{r}_{k+p}^T$ are considered whereas all off-diagonal elements are assumed to be zero (i.e. no cross-correlation between residuals). Let $\mathbf{Q}(t_{k+p})$ equal to $\mathbf{G}_{k+p}\mathbf{Q}_{k+p}\mathbf{G}_{k+p}^T$ where $\mathbf{G}_{k+p}$ is a distribution matrix. The left hand side of Eq. 6(a) can now be expressed as $\mathbf{A}_{k+p}\text{diag}[\mathbf{Q}_{k+p}]$ where

$$\mathbf{A}_{k+p} = \sum_{i=1}^{p}\left[\mathbf{H}(t_{k+p})\Phi(t_{k+p},t_{k+i})\mathbf{G}_{k+i-1}\right]^2 \tag{7}$$

Hence, the diagonal terms of Eq. 6(a) can be obtained from

$$\mathbf{A}_{k+p}\text{diag}[\mathbf{Q}_{k+p}] = \varepsilon_{k+p} \tag{8a}$$

where

$$\varepsilon_{k+p} = \text{diag}\left[\frac{1}{p}\sum_{i=1}^{p}\mathbf{r}_{k+i}\mathbf{r}_{k+i}^T - E\{\mathbf{r}_{k+p}\mathbf{r}_{k+p}^T \mid \mathbf{Q}(t_{k+p})=0\}\right] \tag{8b}$$

It is reasonable to assume that $\mathbf{Q}$ remains constant in a time window of N sampling points, i.e. $\mathbf{Q}_k = \mathbf{Q}_{k+1} = \ldots = \mathbf{Q}_{k+N}$. The system noise covariance in this time window is given by

$$\text{diag}[\mathbf{Q}_{k,N}] = (\mathbf{A}_{k,N}^T \mathbf{A}_{k,N})^{-1}\mathbf{A}_{k,N}^T \varepsilon_{k,N} \tag{9a}$$

where $\mathbf{A}_{k,N}$ is an $Nm\times n$ matrix and $\varepsilon_{k,N}$ is an $Nm\times 1$ vector written as follows

$$\mathbf{A}_{k,N} = \{\mathbf{A}_k, \mathbf{A}_{k+1}, \ldots, \mathbf{A}_{k+N}\}^T, \qquad \varepsilon_{k,N} = \{\varepsilon_k, \varepsilon_{k+1}, \ldots, \varepsilon_{k+N}\}^T \tag{9b,c}$$

The main procedure of adaptive filter is schematically explained in Fig. 2. For purpose of discussion, we now let $\hat{\theta}$ denote a vector of parameters to be identified, such as unknown stiffnesses, and $\hat{\mathbf{x}}$ contains only response variables (displacements and velocities). Initially the EKF may be carried out once (not shown in Fig. 2) to obtain a better guess of $\hat{\theta}_0$. An adaptive filter cycle comprises two processes: (a) determination of $\mathbf{Q}$ by enforcing statistical consistency of residuals using N sampling points, and (b) determination of $\hat{\mathbf{x}}$, $\hat{\theta}$ and $\mathbf{P}$ by the EKF using M sampling points.

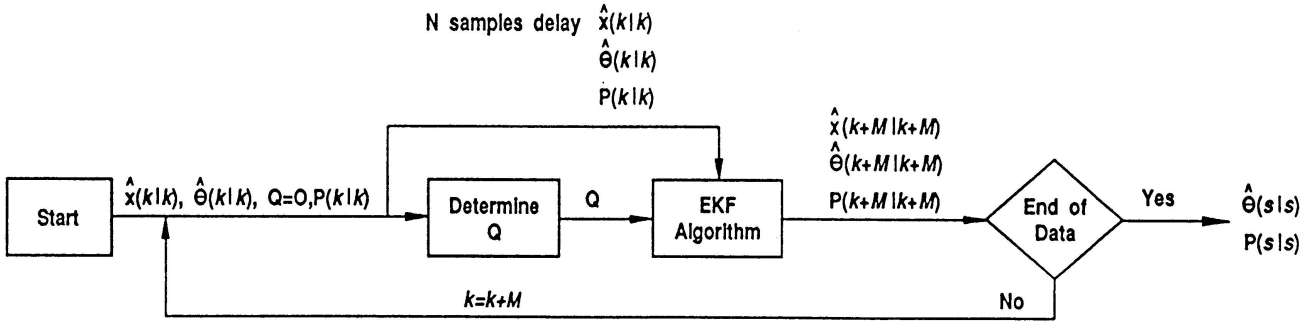

FIG. 2. The Adaptive Filter Procedure.

NUMERICAL EXAMPLES AND DISCUSSIONS

In our examples, the input is a force comprising several (five or more) harmonics of frequencies covering the first few significant vibration modes of the structure. Added to input and output time histories are independent Gaussian noises with zero mean and standard deviations equal to certain specified percentages of their respective unpolluted root-mean-square values.

Example 1 (ICM)

The procedure of ICM is illustrated by considering a 12-storey plane frame building. The "complete" plane frame model has a total of 36 DOFs (two joint rotations and one horizontal translation at each floor). The mass matrix and stiffness matrix for the undamaged building are derived from a small-scale steel laboratory model. The damping ratio is 0.5% as determined by free vibration tests of the laboratory model.

We now consider the building to be "damaged": the column stiffnesses in the first, fourth, eighth, ninth and eleventh storeys are reduced by 10, 15, 30, 20 and 25 per cents, respectively. An excitation force is applied at the top floor and horizontal responses at all floors are measured. Total observation time history of 2 s at a sampling rate of 0.0005 s is divided into 20 windows. All rotational DOFs are eliminated in the condensed model and the remedial model thus has 12 DOFs.

Following the procedure of the ICM described earlier, storey stiffnesses of the damaged building are identified without I/O noise and with different noise levels. The ratios of damaged storey stiffnesses to the corresponding values of the undamaged building are computed and summarized in Table 1. In the ideal case of zero I/O noise, the identified stiffnesses are almost exact (error < 1%) for all twelve storeys and the stiffness diffusion problem is negligibly small. In comparison, if the lumped mass model were used instead for the same conditions, the results (not shown in Table 1) would have been disastrous with error as high as 60% at some storeys. For an I/O noise level of 20% which is considerably high in practice, the identified results are remarkably good (with error ranging from 0.2% to 6% only) in view of the fairly large system for identification.

Story / I/O Noise	1st	2nd	3rd	4th	5th	6th	7th	8th	9th	10th	11th	12th
0%	90.0	99.6	100.5	85.0	99.9	99.8	100.0	70.1	80.3	99.9	75.0	99.6
10%	89.7	97.2	103.4	87.6	100.7	99.6	99.8	72.8	83.6	97.7	76.8	100.3
20%	90.9	97.1	95.8	86.9	100.2	101.9	100.7	74.1	83.4	97.1	76.0	101.2
20%*	88.5	120.8	126.0	91.0	92.9	115.1	140.0	79.7	78.6	97.8	79.4	76.9
20%*+	90.6	99.6	105.5	86.9	97.5	104.5	101.0	72.3	81.0	97.5	78.4	94.2
Exact	90.0	100.0	100.0	85.0	100.0	100.0	100.0	70.0	80.0	100.0	75.0	100.0

* Six horizontal response measurements at alternate floors.
\+ Averaged results based on twelve different time histories of excitation with same noise level

TABLE 1. Percentage Ratio of Damaged Storey Stiffness to Undamaged Storey Stiffness

In terms of computation time, the ICM requires only 20% more than the lumped mass approach in this example, whereas a complete structural identification with 36 DOFs would be very time consuming (easily ten times more) if convergence can be achieved at all. The ICM is hence a simple and yet effective approach to determine local structural changes with virtually no stiffness diffusion problem.

Example 2 (Adaptive Filter)

In this example, the adaptive filter procedure is applied to an 1-DOF system to obtain error variances of identified parameters under the influence of I/O noise. The mass is known and has a value of 1 whereas the stiffness (K) and damping coefficient (C) are to be identified. Assuming independent

system noises for all state variables, the distribution matrix G is simply a unit matrix. Initial conditions are: $x_1=y_0$, $x_2=\dot{y}_0$, $x_3=100$, $x_4=1$, $P_{3,3}=400$ and $P_{4,4}=0.1$. The sampling numbers are $N=20$ and $M=3$. Total observation time is 22.5 s at a sampling rate of 0.075 s.

To evaluate the statistical consistency of estimation error, the following performance index is defined:

$$\psi_\gamma = \left\{ \left[\frac{1}{k} \sum_{i=1}^{k} [x_\gamma(t_i) - \hat{x}_\gamma(t_i|t_i)]^2 \right] \Big/ \left[P_{\gamma,\gamma}(k|k) \right] \right\}^{\frac{1}{2}} \qquad (12)$$

where γ =1, 2, 3 and 4 denote displacement, velocity, stiffness and damping, respectively. Due to randomness, the performance index fluctuates with k and it would be desirable to have the index averaging about one.

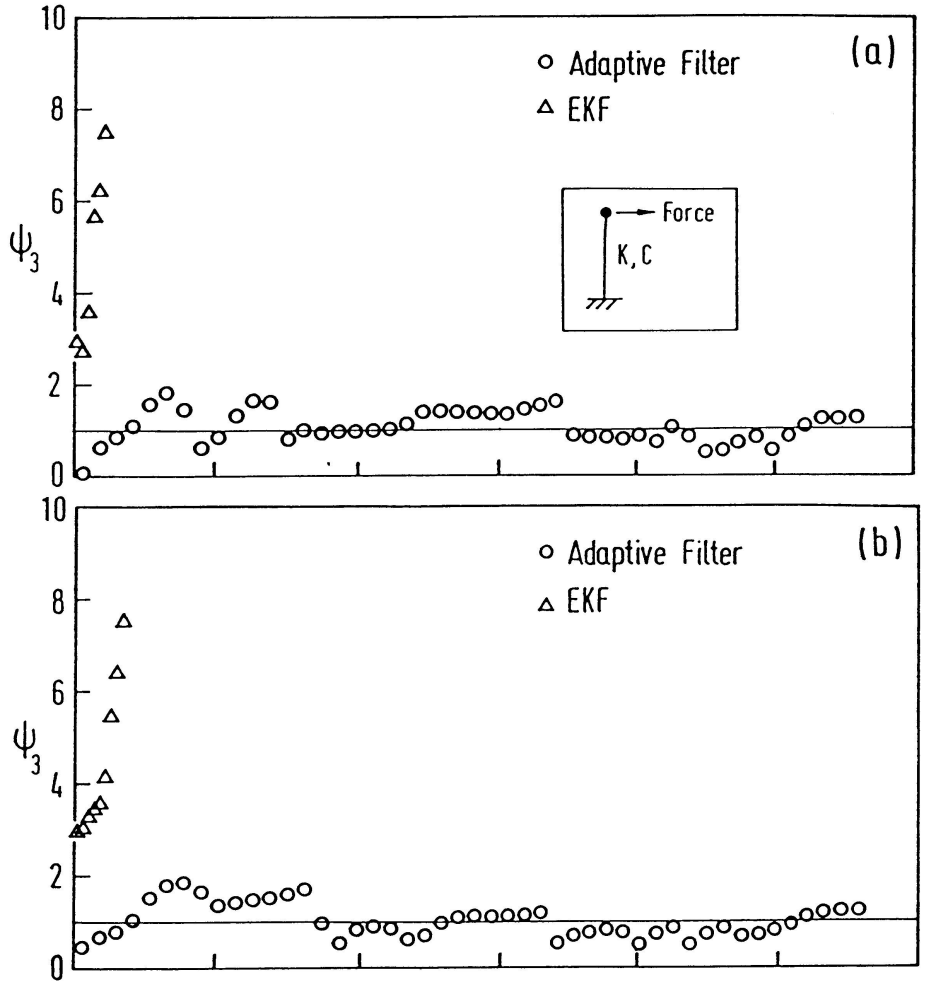

FIG. 3. Performance Indices for Stiffness (a) under 10% I/O Noise and (b) under 30% I/O Noise.

The performance of the adaptive filter is compared to that of the EKF with zero system noise(Q=0). The performance index for stiffness is shown in Fig. 3a for 10% I/O noise and in Fig. 3b for 30% I/O noise. It can be seen that the performance index diverges in the case of the EKF. This means that the error variance are statistically inconsistent and thus do not truly reflect the confidence level in the identified parameter. The performance indices in the case of the adaptive filter clusters around 1, which is an indication of good statistical consistency of error covariances determined in the SI process.

Example 3 (ICM with Adaptive Filter)

The last example demonstrates the combined application of the ICM and the adaptive filter for identification of local structural changes with confidence estimates of a three-storey plane frame building which has the same damping ratio, columns and beams as in Example 1. The excitation force is applied at the top floor and horizontal responses at all three floors are measured. Total observation time is 2 s at a sampling rate of 0.0005 s. In the application of the ICM, the observation time history is divided into 20 time windows.

For simulation of structural changes, we consider a damaged building with column stiffnesses at the first and third storeys reduced by 15% and 30%, respectively, and the second storey undamaged. These results in terms of percentage ratios relative to the "undamaged" values are summarized in Table 2. It can be seen that the effect of stiffness diffusion into the second storey is very small. Specifically, under a 0% noise level, the identified stiffness change of the supposedly undamaged second storey is only about 1%. The severity of damage in the first and third storeys is accurately reflected even for I/O noise level as high as 20%.

In the absence of I/O noise, the standard deviation of each identified stiffness ratio (in %) is about 0.8. The variability of identified results in this case is primarily attributed to the modeling errors. With 20% I/O noise, the standard deviation increases and thus the reliability of identified results is less. If randomness of an identified parameter is approximated by a Gaussian distribution, the reliability can be translated into a maximum likelihood range corresponding to a specified confidence level. As an illustration, 95% confidence ranges based on $\pm 1.96\sigma$ are presented in Table 3. Hence, with the determination of identified stiffnesses and their respective variances, the combined application of the ICM and the adaptive filter would be useful for the reliability analysis and safety evaluation of buildings.

I/O Noise	Storey	Stiffness Ratio	Standard Deviation	95% Confidence range
0%	1st	86.3	0.8	84.7 - 87.9
	2nd	101.2	0.8	99.6 - 102.8
	3rd	69.7	0.8	68.1 - 71.3
20%	1st	86.7	5.8	75.3 - 98.1
	2nd	95.1	5.8	83.7 - 106.5
	3rd	70.5	5.8	59.1 - 81.9
Exact	1st	85.0	-	-
	2nd	100.0	-	-
	3rd	70.0	-	-

TABLE 2. Percentage Ratio of Damaged Story Stiffness to Undamaged Storey stiffness and their Confidence Estimates

CONCLUSIONS

Two issues, namely (a) local damage detection and (b) confidence estimation of identified parameters, have been dealth with in this paper. Firstly, an "improved condensation" method is proposed to identify the locations and magnitudes of structural stiffness changes of buildings. Secondly, confidence levels in identified parameters are estimated by means of an adaptive filter which ensures statistical consistency of error covariances in the application of the EKF. The application of the proposed procedures to numerical examples have shown their potential as an effective tool to identify local structural changes of buildings with consistent confidence estimates.

APPENDIX I. REFERENCES

Agbabian, M. S., Masri, S. F., Miller, R. K., and Caughey, T. K., System identification approach to detection of structural changes. Journal of Engineering Mechanics, ASCE, 117(2), 370-390, 1991.

Jazwinski, A. H., Adaptive Filtering. Automatica, 5, 475-485, 1969.

Kalman, R. E., and Bucy R. S., New results in linear filtering and prediction theory. Journal of Basic Engineering, ASME, 83, 95-108, 1961.

Natke, H. G., and Yao, J. T. P., System identification approaches in structural safety evaluation. Structural Safety Evaluation Based on System Identification Approaches, Proceedings of Workshop at Lambrecht/Pfatz, 29 June to 1 July 1987, Natke and Yao, eds., Frieder Vieweg and Sohn, Braunschweig, Germany, 460-473, 1987.

Planes of Weakness in Finite Element Analysis

Surfaces de rupture en analyses aux éléments finis

Versagensflächen in Finite-Element-Berechnungen

Jörg-Martin HOHBERG
Dr. Eng.
IUB Engineering Ltd
Berne, Switzerland

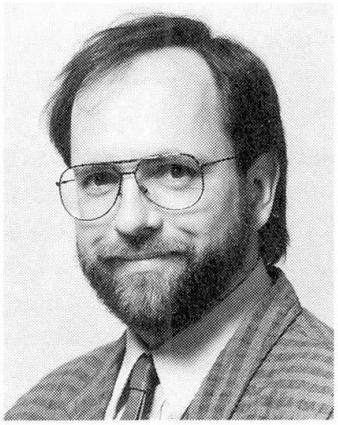

Jörg-Martin Hohberg (born 1953) studied structural engineering at TU Berlin, Imperial College London and ETH Zürich. After two years with Dyckerhoff & Widmann in Munich on p/c LNG storage tanks, and research in nonlinear seismic arch dam analysis at ETH, he is presently engaged in numerical rock analysis and design of underground structures.

SUMMARY

Interface elements enable the modelling of existing cracks as well as potential failure mechanisms within conventional FEM computations. If used to investigate limit equilibrium states without knowing the cracking process in detail, several tacit assumptions are made as to the load redistribution capacity of the structure. This bears a certain similarity to plastic limit analysis, which also features kinematical discontinuities, albeit with more idealized constitutive models. The discussion is followed by two simple applications involving a voussoir arch and a beam.

RÉSUMÉ

Les éléments joints permettent la modélisation des fissures existantes aussi bien que des mécanismes de rupture potentiels dans la méthode des éléments finis (FEM) conventionelle. Dans le cas où on les utilise dans la recherche des états limites d'équilibre sans connaître le processus de fissuration en détail, certaines hypothèses tacites sont faites concernant la capacité de la structure à redistribuer les charges. On retrouve ainsi certains aspects de la méthode de la charge ultime de plasticité, qui elle aussi, considère des discontinuités cinématiques, avec toutefois des modèles constitutifs plus idéalisés. La discussion est suivie par deux applications simples aux arcs et poutres en voussoirs.

ZUSAMMENFASSUNG

Trennflächenelemente gestatten die Modellierung bereits existierender Risse wie auch möglicher Versagensmechanismen innerhalb der herkömmlichen Finite-Element-Methode (FEM). Falls mit ihrer Hilfe Grenzgleichgewichtszustände ohne genaue Kenntnis des Rissprozesses untersucht werden, unterliegen sie einigen stillschweigenden Annahmen hinsichtlich der Fähigkeit des Tragwerks zur Kraftumlagerung. Darin ähnelt die Methode dem plastischen Traglastverfahren, das ebenfalls kinematische Diskontinuitätslinien kennt, allerdings mit weitergehender Idealisierung des Trennflächenverhaltens. Auf die Diskussion folgen als einfache Anwendungsbeispiele ein Bogen und ein Balken in Blockkonstruktion.

1. INTRODUCTION

The finite element method (FEM) is widely used for the assessment of material damage by following the gradual development of deterioration in structures in a step-by-step procedure. Usual material models are based on incremental plasticity, damage theory or smeared cracking, where for monotonic loading the anisotropy of damage is often neglected to avoid overstiff numerical results; such overstiff behaviour is absent in *discrete* crack models [1]. Apart from distributed ageing phenomena as continuum deterioration, the inspection of deficient structures may reveal a number of existing fractures, which are possibly oriented oblique to the present stress regime and need be modelled as to their effect on the stress redistribution and the failure mode of the cracked structure.

Through the joining of finite elements at their common nodes, the conventional FEM is basically a continuum method. At least with nodal displacements as primary variables, equilibrium is only satisfied in an integral sense: Although the displacement fields are compatible along the element sides, the stress fields exhibit finite jumps at interelement boundaries, thus precluding the computation of strict lower bound limit loads [2]. However, lines or planes of displacement discontinuity can be introduced via double nodes with suitable constraint conditions and used to investigate the ultimate bearing capacity of structures by means of *postulated* failure planes, a concept which is akin to the kinematic approach of limit analysis in that one looks for the mechanism giving the smallest failure load as *upper* bound to the true limit load.[1] The presence of an elastic compliance below the onset of plastic deformation does not invalidate the limit analysis theorems as long as displacements remain small [4]. It is rather the behaviour of the weak planes which infringes on certain vital hypotheses.

2. KINEMATICAL DISCONTINUITIES

2.1 The Concept in Limit Analysis

The general idea is that arbitrary velocity fields can be introduced, which do not need to satisfy equilibrium and may be discontinuous as long as they are kinematically compatible. For instance it is permissible to assume that large parts of the structure move as rigid blocks, separated by narrow plastic regions of thickness t. These are characterized by a high homogenous strain rate, which is the relative velocity between blocks per thickness, $\dot{\delta}/t$. The discontinuities are supposed to consist of a thin layer of material, which obeys a modified Mohr-Coulomb yield criterion (with associated flow rule) and behaves just like a solid, except that the in-plane 'stretching' strain rate $\dot{\varepsilon}_{ss}$ is zero because of the adjacent rigid bodies. Computing principal strain rates with $\dot{\varepsilon}_{ns} = \frac{1}{2}\dot{\gamma}_{ns}$ (Fig. 1),

$$\dot{\varepsilon}_{1,2} = \tfrac{1}{2}\dot{\varepsilon}_{nn} \pm \tfrac{1}{2}\sqrt{\dot{\varepsilon}_{nn} + \dot{\gamma}_{ns}} = \frac{\dot{\delta}}{2\,t}\,(\sin\alpha \pm 1) \tag{1}$$

their directions are found to bisect the angle between the n-direction and the velocity vector, resp. between the s-direction and the normal to the velocity. While $\dot{\varepsilon}_1$ denotes a volume increase due to shear dilatancy or opening, $\dot{\varepsilon}_2$ corresponds to a compression field in the adjacent block [5]. The latter would only disappear for a pure cleavage at $\alpha = 90°$, i.e. if the discontinuity were to coincide with a mode-I crack ($\dot{\varepsilon}_1 \geq \dot{\varepsilon}_2 = 0$). Principal directions at $45° \pm \frac{\alpha}{2}$ (with respect to s) characterize slip lines in a state of pure shear.

The internally dissipated work per unit area is that of a ductile homogenous material, the band thickness droping out during integration:

$$\dot{W}_l\,(\sigma_1\dot{\varepsilon}_1 + \sigma_2\dot{\varepsilon}_2)\;t = \tfrac{1}{2}\dot{\delta}\,\sigma_1\,(\sin\alpha + 1) + \tfrac{1}{2}\dot{\delta}\,\sigma_2\,(\sin\alpha - 1) \tag{2}$$

For a general α one obtains [6]

$$\dot{W}_l = \dot{\delta}\left[f_c\,\frac{1-\sin\alpha}{2} + f_t\,\frac{\sin\alpha - \sin\phi}{1-\sin\phi}\right] \tag{3}$$

[1] As stated in [3]: "The structure will collapse if there is any compatible pattern of plastic deformation for which the rate of work of the external loads exceeds the rate of internal dissipation."

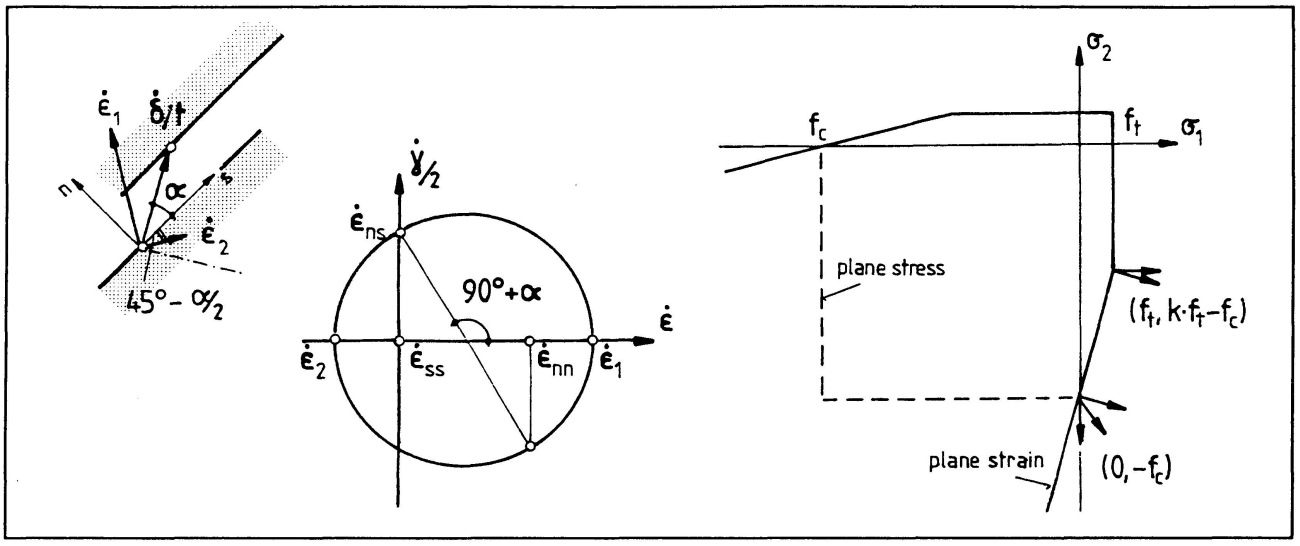

Figure 1: Strain rates and failure surface in band discontinuity

with the pure failure modi of shear and opening, using $k = (1 + \sin\phi)/(1 - \sin\phi)$:

$$\text{shear}\,(\alpha = \phi): \quad \dot W_l = \tfrac{1}{2}\dot\delta\, f_c\,(1 - \sin\phi) \equiv \dot\delta\, c\cos\phi \quad , \qquad \text{opening}\,(\alpha = \tfrac{\pi}{2}): \quad \dot W_l = \dot\delta\, f_t \tag{4}$$

From letting $t \to 0$ in eq. (1) – for which $\dot\varepsilon_{1,2}$ grows to $\pm$ infinity – it is concluded that the joint material needs to be formulated for plane-strain conditions [7]. Together with the associated flow rule arising from von-Mises' postulate of maximum dissipation, this implies that $\alpha < \phi$ is not permitted by this kind of model; it would become feasible only in *plane stress* where another corner stress state allows for simultaneous shear and compression failure [8].

2.2 Interface Element Formulations

The FEM knows a similar concept of degenerating a solid to a layer of finite thickness t, assuming a strain-formulated layer material model for a constant strain gradient across the thickness [9]:

$$\{d\sigma\} = [\mathbf{D}^e - \mathbf{D}^p]\,\frac{1}{t}\,\{d\delta\} \tag{5}$$

The stretching strain component ε_{ss} is again assumed to vanish, because of the assumption $t \ll L$, the length of the layer element [10]. In view of the fact that also $\frac{1}{t}\mathbf{D}^e$ grows to infinity with $t \to 0$, a very thin layer would infact behave rigid-plastic if $\mathbf{D}^e$ were not corrected for the layer element aspect ratio t/L [11]. With nodal displacements as primary unknowns, this is required by the finite-precision arithmetic of the equation solver. Note that only the plastic strain components correspond to the 'kinematic strains' in limit analysis and dissipate energy on the stress state.

For a vanishing layer thickness the interface can directly be formulated in relative displacements $d\delta = d\delta^e + d\delta^p$. The elastic stiffness of the bonded state is given by local penalty parameters $\kappa_s = G/t$ and $\kappa_n = E/t$, and the stress-strain constitutive model is just converted into a relationship between tractions and relative displacements, the factor $1/t$ being virtually incorporated into $\mathbf{D}^e$ and $\mathbf{D}^p$. Because of the traction formulation plain-stress and plane-strain states can no longer be distinguished in the joint. Whether or not a thin-layer element approaches indeed the slip behaviour of a zero-thickness interface, depends on the form of stress evaluation: Unless the information of the interface orientation is passed on to the constitutive routine, an ordinary principal stress criterion will result in premature failure of the interface compared to Coulomb friction, because the shear planes in the layer material are predicted according to eq. 1 as being inclined relative to the interface orientation [12].

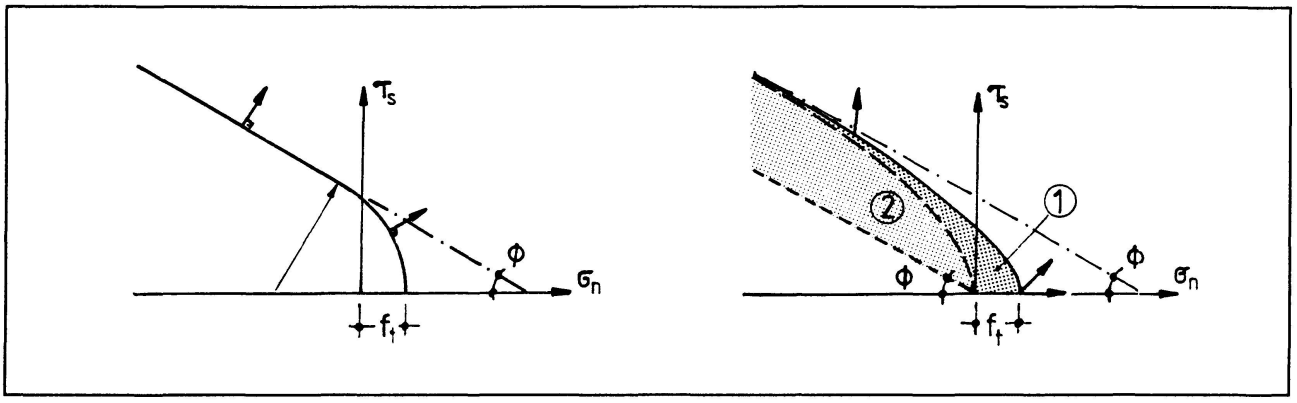

Figure 2: Modified Coulomb models in strains and relative displacements

A popular failure surface for combined slip and opening is the hyperboloid, which differs not too much from the cone with spherical cusp in limit analysis (Fig. 2). The continuous curvature simulates the added geometrical strength component resulting from the inclination of asperities with a mean roughness angle ψ, which are overridden under small compression and become progressively sheared off under high compression. With increasing $|\sigma_n|$ the surface approaches the asymptotic friction cone of a plane interface with a 'basic' friction angle ϕ_μ and zero dilatancy. Since the 'mobilised' angle of friction is of the form $\phi_{mob} = \phi_\mu + \psi(\sigma_n, \delta_s)$, the flow (or slip) rule can *never be associated* [13]. For a rough surface the truncated friction cone is but a linearization, where the geometric stiffness component is simplified to an apparent cohesion intercept.

Angles of δ^p larger than ψ must contain an opening component. There is no reason why the flow potential should display a smooth transition from shear to opening. More likely, the potential surface for shear dilatancy forms a corner singularity with the n-axis. This allows to distinguish irreversible opening due to override in shear from reversible gap displacements. If the interface is initially cemented, a retractable tension cap extends into the tension/shear domain, furnishing a tensile strength and a true cohesion. Both quantitites are destroyed together in any arbitrary combination of tension and shear (area '1' in Fig. 2 right) [14]. The roughness or apparent cohesion is treated separately: As continued override wears the asperities down, the failure surface will shrink in function of the accumulated sliding distance δ_s or, alternatively, of the plastic slip work W_s^p (softening of area '2').

3. LIMIT ANALYSIS VS. LIMIT EQUILIBRIUM METHODS

The theorems of limit analysis offer the great avantage that neither the initial conditions in the structure nor the exact load path to failure need be known, provided the material is sufficiently ductile and stable in Drucker's sense. Concrete departs from the assumption of unlimited deformability already in compression, such that a hypothetical plateau need be fitted at a reduced average stress over a particular strain range [3], this reduction being commonly termed the 'effectiveness factor' [15]. Since the strain history differs for each particular problem setting (bending, shear, etc.), this factor varies and accounts for different influences in a global manner. To confuse the matter further, also the effect of construction joints is sometimes subsumed in there [8] even though it could be accounted for by reduced material parameters in an explicitely modelled weak plane.

The definition of kinematical discontinuities ignores any dependence of the ductility on the angle α, which would be valid only for the assumption of 'unlimited ductility' at *zero* tensile strength. Even then a strain-capacity problem is present in the crack width across which shear stresses can still be carried by aggregate interlock. Because the kinematical discontinuities are usually not identified with cracks – except for socalled collapse cracks in pure tension [5] – plasticity theory tacitly assumes that the compression struts ($\dot{\varepsilon}_2$ in Fig. 1) are not restrained by the crack pattern in their ability to

For a joint inclined under the angle β to the horizontal, the external work due to a uniaxial compressive stress σ_y is given (per width B and unit thickness of the specimen) by

$$\dot{W}_E = \dot{\delta}\,\sigma_y \sin(\beta - \alpha)\,B$$

and the internal plastic work in the line of discontinuity

$$\dot{W}_I = \dot{\delta}\,f_c \frac{(1 - \sin\alpha)\,B}{2\cos\beta}$$

Equating external and internal work and minimizing with respect to β, one finds simply $\sigma_{y,min} = f_c$, just as for the associated case of $\alpha = \phi$ [8], only at a different critical orientation $\beta = \pi/4 + \alpha/2$.

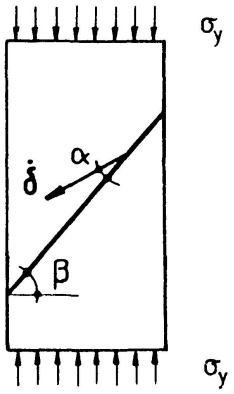

Figure 3: Analysis of a prism test with construction joint

adapt themselves to principal stress rotations during loading, cf. [16]. Interestingly, FEM interface models may be liable to the same pitfall if the limitation of dilatancy by the height of asperities is not incorporated in the constitutive model. This information need be supplied explicitely to force the stress point during continued plastic shear flow to the apex of the failure surface (Fig. 2), where alone subsequent gap can take place [17].

Neglecting the cementitious cohesion, the nonassociated slip rule and shear softening still violate the assumptions of limit analysis [13]. Only in statical determinate situations, where the amount of dilatancy does not play a role, certain limit load formulae remain valid (Fig. 3); but for highly confined situations as typical in geotechnics the limit load decreases substantially with $\psi < \phi$ [18]. Limit load theorems in their classical sense – i.e. the maximum lower bound and the minimum upper bound converging to a unique value – are no longer valid but need be recast in a weak form furnishing 'safer' lower and higher upper bound values [19,20]. On the basis of associated flow, solutions with finite element interfaces can still be obtained by optimization methods [21].

With the exception of blast loading and other energy-based design cases, upper-bound solutions are of little value in civil engineering practise anyhow. Through the prudent choice of material parameters one strives rather at obtaining conservative limit loads in spite of an underlying mechanism concept. Very good results have been obtained with interface elements for difficult limit load problems [22]. Pre-inserting planes of discontinuity without tracking their formation (i.e. strain localisation) means that part of the stress history is neglected in favour of a *limit equilibrium* analysis for a mechanism which is not necessarily the one that would actually develop. As with plastic limit theory one must therefore check also the yield criterion in the solid domains between the planes of weakness and the strain limits and transient strength components, which – depending on the unknown stress history – may undermine the full mobilisation of the mechanism's resistance [23]. It seems thus very helpful if interface element constitutive models dispose of an initial cementitious strength with the capability for mixed-mode decohesion, so that they can be inserted in a mesh as 'sleeping discontinuities' in the sense of Hillerborg's fictitious cracks.

4. EXAMPLES OF VOUSSOIR ARCHES AND BEAMS

To conclude this contribution, two simple applications to arches are given, which are either supposed to be constructed from independent blocks or to be radially cracked. Such voussoir arches are a classical application of rigid-plastic limit analysis even though the modification of the plastic-hinge concept to accommodate no-tension gaps between blocks seems rather bold [24]. The simplicity lies in the fact that slipping of blocks is excluded from the catalogue of allowable mechanisms – postulating a sufficiently steep orientation of the force resultant with respect to the interfaces –, that the stress range is supposed to be low enough to avoid crushing of edges and that the joints have no tensile strength. Therefore no energy will be dissipated in the mechanism, and the energy balance must be

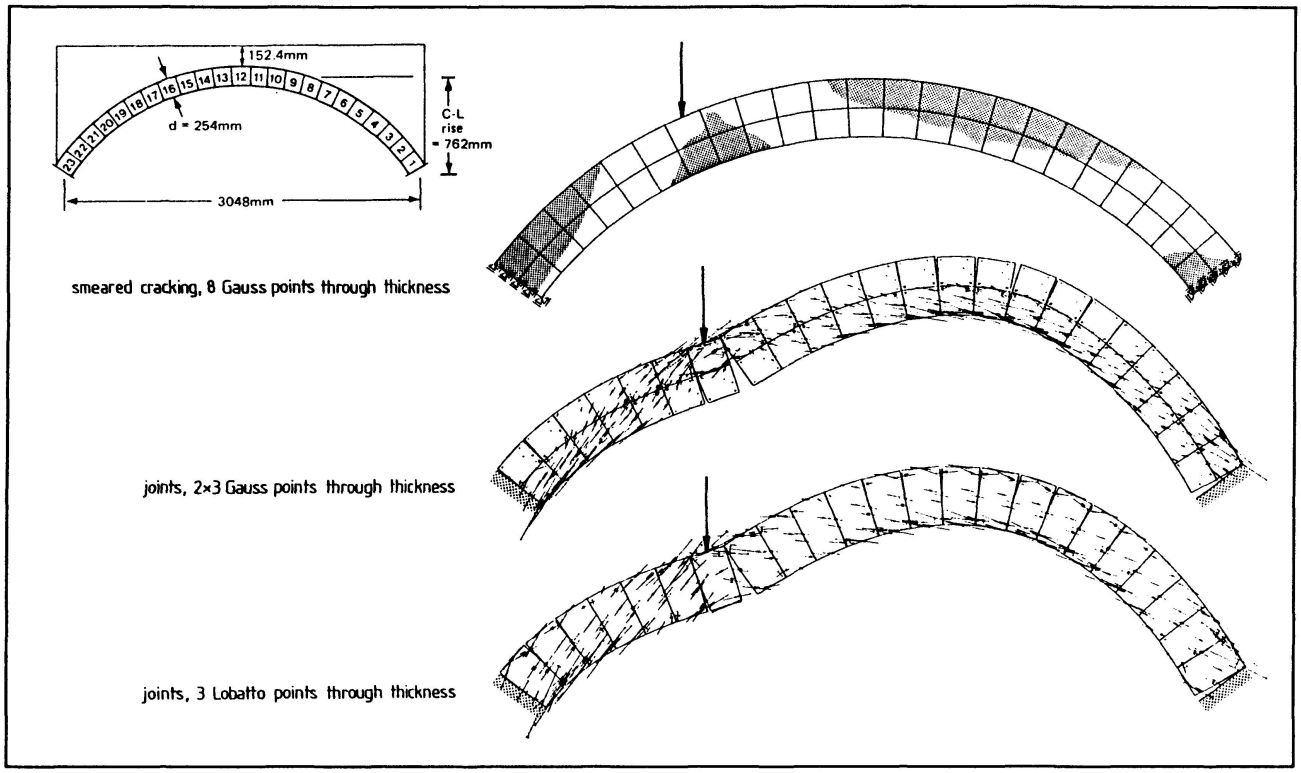

Figure 4: Discrete joint model of a circular arch

maintained by passive external work of parts of the structure moving against the direction of loading. According to limit analysis theory, any feasible thrust line which lies fully inside the arch would thus give a lower-bound limit load, whereas any collapse mechanisms would give an upper-bound limit load [25]. The added advantage of the FEM discretization of the joints is that the no-slip assumption is checked automatically, i.e. La Hire's vision of 1695 of arches as an assembly of wedges (viz. [26]) is 300 years later turned into a practical method.

The example in Fig. 4 shows a circular arch, which was tested in 1951 by Pippard & Chitty and previously analysed by mechanism and continuum FE methods [27]. Modelling every segment as a finite element separated by interfaces, it can be seen that the computed extent of joint opening – shortly before the fourth mechanism is formed – corresponds quite well to the prediction by the smared-crack model. This may surprise as it is often anticipated that the discrete model will automatically lead to a concentrated mechanism, but it finds an explanation in the tangential orientation of the thrust line and indicates that not all the joints would have to be included to catch the failure mechanism [25]. Observe also that the distance between the two outermost integration points determines the eccentricity of the pivot and hence the effective depth of the section in which the thrust line must reside. Other integration schemes – among them a socalled floating point scheme, which contracts the integration points into the remaining compression zone – have been tested [28], but the results for only one joint element across the thickness are seen to be rather satisfactory if a 3-pt. Lobatto rule (nodal integration) is used. Note also that the solids between partly open joints still exhibit tensile stresses, due to the coupling of equivalent nodal forces through the shape functions; this emphasizes once more the advantage of stress evaluation in discrete mechanisms.

The second case concerns the rather common problem of estimating the load carrying capacity of an unreinforced concrete beam by considering a hidden arch, even though in this particular case the 'beam' is a horizontal slice through a large concrete gravity dam under reservoir pressure [29]. According to the *lower*-bound theorem, any permissible stress field – i.e. not violating the yield limits of the material anywhere – would give a safe estimate of the load carrying capacity, irrespective of the

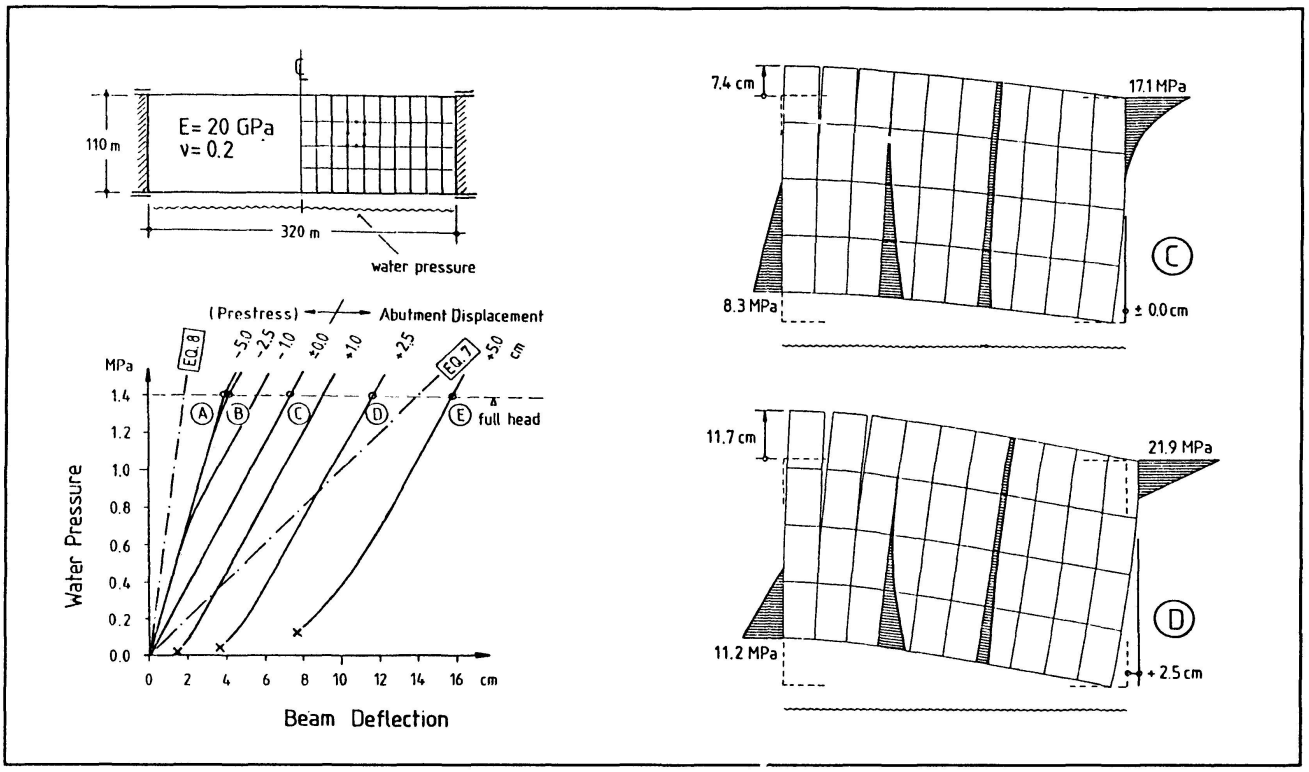

Figure 5: Hidden horizontal arch in a 'tension-free' beam

strain compatibility [3]. The maximum load will thus result from the arch with the largest camber, so that paradoxically the (elastic) beam seems the stiffer the deeper it is cracked in flexure. In terms of stress resultants, the arch is only stable if the bending moment does not exceed the normal force times half the depth of the cross-section, as otherwise the thrust line would pass outside the structure [25]. The problem with this particular loading is that the bending moment is already active *before* a sufficient normal force can build up. It would not arise if the segments were wedges [30], but as the joints are oriented parallel to the direction of loading, the thrust requires prying action in bending which is unstable under small pressure (points 'x' in the graph). If one does not count on residual prestress from joint grouting or cementitious cohesion – but takes rather some foregoing joint opening due to shrinkage or cold temperature into account –, the only way how such a voussoir beam could work without shear keys would be by means of considerable dilatancy developing during the relative slip between blocks [31]. Even then an absolute limit would be given by the height of asperities as previously mentioned.

5. CLOSING REMARKS

Interface elements to model weak planes or existing discontinuities are a very useful tool for limit equilibrium calculations. The conceptual similarity to upper-bound limit analysis lies in the need to perturbate prospective mechanisms for finding the most critical one, but fortunately there are many situations (like well-shaped arches) which are rather insensitive to the assumed location of discontinuities. However, phenomena of limited strain capacity and transient strength components need be regarded if they are not to defy the analysis results. The influence of more realistic interface constitutive models in the FEM may also be elucidating to limit analysis practise.

REFERENCES

1. ROTS J.G. and BLAAUWENDRAAD J., Crack models of concrete: discrete or smeared? fixed, multi-directional or rotating? *Heron* **34** (1), 1989.

2. PIAN T.H.H. and TONG P., Basis of the finite element method for solid continua. *Int. J. Num. Meth. Eng.* **1**, 1969, pp. 3-28.
3. DRUCKER D.C., On structural concrete and the theorems of limit analysis. *IABSE Mémoires* **21**, 1961, pp. 49-59.
4. SALENÇON J., *Calcul à la rupture et analyse limite.* Presses ENPC, Paris 1983.
5. MÜLLER P., *Plastische Berechnung von Stahlbetonscheiben und -balken.* ETH Zurich IBK Rep. 83, Basle 1978.
6. CHEN W.-F. and DRUCKER D.C., Bearing capacity of concrete blocks or rock. *J. Eng. Mech. Div. ASCE* **95** (4), 1969, pp. 955-978.
7. MARTI P., Plastic analysis of reinforced concrete shear walls. IABSE Coll. *Plasticity of Reinforced Concrete*, Copenhagen 1979. Introd. Rep. AK-28, pp. 51-69.
8. JENSEN B.C., Lines of discontinuity for displacements in the theory of plasticity of plain and reinforced concrete. *Mag. Concrete Res.* **27** (92), 1975, pp. 143-150.
9. DESAI C.S., ZAMAN M.M. et al., Thin-layer element for interfaces and joints. *Int. J. Num. Anal. Meth. Geomech.* **8** (1), 1984, pp. 19-43.
10. HOHBERG J.-M., discussion of 'Modeling of cyclic normal and shear behavior of interfaces' (by C.S. Desai and B.K. Nagaraj). *J. Eng. Mech. ASCE* **116** (8), 1990, pp. 1870-1880.
11. HOHBERG J.-M. and SCHWEIGER H.F., On the penalty behaviour of thin-layer elements. *NUMOG IV*, Swansea 1992 (in print).
12. HOHBERG J.-M., A review of joint constitutive models. *2nd NUMEG*, Prague 1992 (in print).
13. DRUCKER D.C., Coulomb friction, plasticity and limit loads. *J. Appl. Mech. ASME* **21** (1), 1954, pp. 71-74.
14. HOHBERG J.-M., Multimechanism plasticity with coupled damage in tension and shear. *COMPLAS III*, Barcelona 1992. Proc. 2, pp. 1503-1514.
15. EXNER H., On the effectiveness factor in plastic analysis of concrete. IABSE Coll. *Plasticity in Reinforced Concrete*, Copenhagen 1979. Final Rep. AK-29, pp. 35-42 + disc. pp. 67, 132/133, 349, 353.
16. KUPFER H. and BULICEK H., Comparison of fixed and rotating crack models in shear design of slender concrete beams. Int. Workshop *Progress in Structural Engineering*, Brescia 1991 (typescript 10 p.)
17. HOHBERG J.-M, *A joint element for the nonlinear dynamic analysis of arch dams.* ETH Zurich IBK Rep. 186, Basle 1992.
18. DE BORST R. and VERMEER P.A., Possibilities and limitations of finite elements for limit analysis. *Géotechnique* **34** (2), 1984, pp. 199-210 + disc. **35** (1), 1985, pp. 90-94.
19. DE JOSSELIN DE JONG G., Lower bound collapse theorem and lack of normality of strain rate to yield surface for soils. IUTAM Symp. *Role of Plasticity in Soil Mechanics*, Grenoble 1964. Proc. (1966), pp. 69-75 + disc. pp. 75-78.
20. COLLINS I.F., The upper bound theorem for rigid/plastic solids generalised to include Coulomb friction. *J. Mech. Phys. Solids* **17**, 1969, pp. 323-338.
21. SLOAN S.W., Upper bound limit analysis using finite elements and linear programming. *Int. J. Num. Anal. Meth. Geomech.* **13** (3), 1989, pp. 263-282.
22. VAN LANGEN H. and VERMEER P.A., Interface elements for singular plasticity points. *Int. J. Num. Anal. Meth. Geomech.* **15** (5), 1991, pp. 301-315.
23. MANFREDINI G., MARTINETTI S. and RIBACCHI R., Inadequacy of limiting equilibrium methods for rock slope design. *16th US Symp. Rock Mechanics*, Minneapolis/MN 1975. Proc. (1977), pp. 35-43.
24. KOOHARIAN A., Limit analysis of voussoir (segmental) and concrete arches. *ACI Journal* **49**, 1952, pp. 317-328 + disc. pp. 328/1-4.
25. HEYMAN J., The stone skeleton. *Int. J. Solids Struct.* **2** (2), 1966, pp. 249-279.
26. KURRER K.-E., Zur Entstehung der Stützlinientheorie. *Bautechnik* **68** (4), 1991, pp. 109-117.
27. CRISFIELD M.A., *Finite element and mechanism methods for the analysis of masonry and brickwork arches.* TRRL Res. Rep. 19, Crowthorne 1985.
28. HOHBERG J.-M. and BACHMANN H., A macro joint element for nonlinear arch dam analysis. *6th ICONMIG*, Innsbruck 1988. Proc. 2, pp. 829-834.
29. HOHBERG J.-M., discussion of 'Spatial action of straight gravity dams in narrow valleys' (by M.A. Herzog). *J. Struct. Eng. ASCE* **117** (2), 1991, pp. 637-641.
30. LIVISLEY R.K., Limit analysis of structures formed from rigid blocks. *Int. J. Num. Meth. Eng.* **12** (12), 1978, pp. 1853-1871.
31. PENDER M.J., Prefailure joint dilatancy and the behaviour of a beam with vertical joints. *Rock Mech. Rock Eng.* **18** (4), 1985, pp. 253-266.

Remaining Structural Capacity of Power Plant Frame
Capacité portante résiduelle d'une fondation sous portiques de turbines
Resttragfåahigkeit eines Turbinen-Rahmenfundaments

Jana MARGOLDOVÁ
Dr. Eng.
Czech Techn. Univ.
Prague, Czech Rep.

J. Margoldová received her Pd.D. degree in 1987 from the Czech Technical University in Prague. She works as a research engineer at the Klokner Institute of the Czech Technical University.

Radomír PUKL
Dr. Eng.
Czech Techn. Univ.
Prague, Czech Rep.

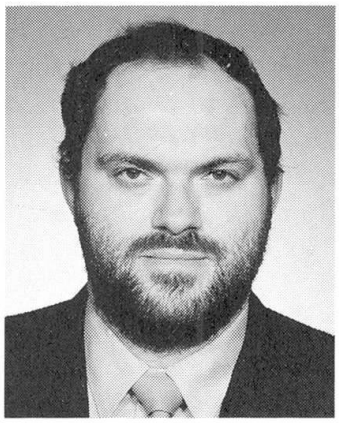

R. Pukl received his Ph.D. degree in 1985 from the Czech Technical University in Prague. He works in the field of computational mechanics at the Czech Technical University in Prague and at the Stuttgart University.

Vladimír ĆERVENKA
Consult. Engineer
Cervenka Consulting
Prague, Czech Rep.

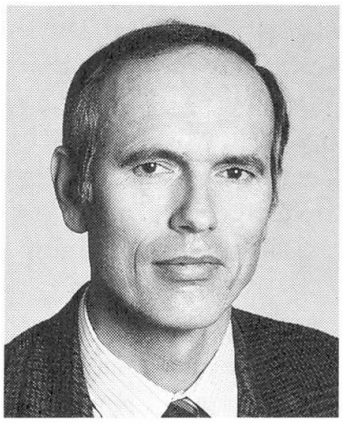

V. Cervenka received his Ph.D. degree in 1970 from the University of Colorado in Boulder. He is active in research and consulting of reinforced concrete structures and in software development.

SUMMARY
Remaining structural capacity of the turbine foundation frame in an old power station was assessed by means of the nonlinear finite element analysis performed by a computer programme. The effects of the quality of filler concrete of joints and of the boundary conditions were studied parametrically.

RÉSUMÉ
L'article traite de la détermination de la capacité portante résiduelle d'une fondation sous portiques, prévue pour des turbines dans une ancienne centrale électrique, au moyen de calcul par éléments finis non linéaires. Les vérifications ont porté sur l'influence de la qualité du béton des noeuds des portiques et des conditions aux limites.

ZUSAMMENFASSUNG
Die Resttragfähigkeit von Rahmenfundamenten für Turbinen in einem alten Kraftwerk ist mittels einer nichtlinearen Finite-Element-Analyse bestimmt worden. Die Einflüsse der Betonqualität in Rahmenknoten und der Randbedingungen sind untersucht worden.

INTRODUCTION

Heavy prefabricated reinforced concrete frames were typically used for construction of large thermal electric power plants in Czechoslovakia in the 50s and 60s within an extensive energy-production plan. These power plants burn low-quality brown coal and are the main source of energy in Czechoslovakia. In the course of time number of problems have emerged in connection with the servise of these plants. To mention only the most serious ones: uncontrolled environmental polution and structural damages due to heavy service loading. The most exposed structures are the reinforced concrete foundation frames of turbines. They are subjected to large static and dynamic loadings, chemical and thermal effects. Today in many cases these structures are also at the end of their designed life time. This life time is about half of that of similar unexpposed structures. It is in the interest of the electric power industry to extend the life service of these structures and thus to avoid building new plants. This tendency is also evident world-wide. In this context the technical diagnostic is becoming the important engineering branche. It is expoliting the reliability theory, the structural modeling and on site investigations. The last two mentioned categories were used in the present report for the diagnostic of the remaining structural capacity.

The concerned power plant is located in the North-West Bohemia and has been under reconstruction. It had been subjected to the long term monitoring to determine the extent of wearing after twenty years of service. In order to asses the remaining structural capacity of the turbine foundation the structure was analyzed by the finite element program SBETA. The damage and failure states of the structure were simulated. The goal of this analysis was to simulate the effects of the poorly manufactured joints of the precast members on the load carying capacity. The results served to design the measures for the necessary reconstruction.

2. PROGRAM SBETA

Program SBETA was recently developed at the Institute of Material Science of the University of Stuttgart in cooperation with the Klokner Institute of the Czech Technical University in Prague. It is a commercial program designed for the analysis of reinforced concrete structures in the plane stress state. It can predict the response of complex concrete structures, with or without reinforcement, in all stages of loading, including failure and post-failure. It can be used to analyze the remaining structural capacity of existing structures. Details about the program and its constitutive model can be found in papers [5,6] and documentation [8]. Here only a brief description is given. The other applications of the program are reported in ref. [2,3,4,7]

The constitutive model in SBETA is based on the smeared material approach with isotropic damage model in uncracked concrete and orthotropic damage after cracking. The behavior of concrete is described by the stress-strain diagram, which is composed of the four branches: nonlinear loading in compression, linear loading in tension, and linear softening in both, tension and compression. The parameters of this diagram are adjusted according to the plane stress state using the biaxial failure function of Kupfer for compression. The mechanics of cracked reinforced concrete, which is relevant to this study case, includes: (a) reduction of compressive strength in direction parallel with cracks; (b) variable shear retention factor; (c) tension stiffening. All these properties are controlled by the tensile strain, which reflects the crack opening. The nonlinear fracture mechanics is introduced by means of the Bažant's crack band theory [1]. The tension softening modulus is adjusted for each element according to the fracture enegry. Both, fixed and rotated crack models are implemented. Reinforcement behavior is bi-linear.

A four-node quadrilateral finite element is used for the concrete. The reinforcement can be included either in a smeared form, as a part of the concrete element, or discrete, as a bar element passing through the quadrilateral element. The updated Lagrangean formulation is adopted allowing the modeling of a second order geometry effect. The non-linear solution is performed by means of a step-wise loading and by an equilibrium iteration within a load step. Newton-Raphson and arc-length methods are the options for the solution strategy in the equilibrium iteration.

The program system SBETA includes a pre-processor, a solution program, and an efficient post-processor. The finite element analysis can be interactively controlled and runs in several levels of real-time graphics. Thus, the solution process can be observed and solution parameters can be adjusted by a user if necessary. A restart option is available. The post-processor generates automatically deformed shapes and images of stress, strain and damage fields (cracking, crushing). All results of the analysis presented in this paper are produced by the SBETA post-processors.

3. ANALYSIS OF DAMAGED POWER PLANT FRAME

3.1 Girder Joint in Precast Foundation Frame

The schematic plan view of the frame is in Fig.1. The precast reinforced concrete girders A and B are supported by column. Each girder is formed by a couple of two identical girders, A_1, A_2 and B_1, B_2. The interaction of the coupling girders is assured by the slab, which is casted over the girders. The joint of girdes is located above the column. During the construction a space of 350 mm had been left between the vertical end faces of adjacent girders, the reinforcement was welded and the space was filled by concrete. The location of the joint is denoted in Fig.1. There were doubts about the quality and correct casting of the filler concrete and about full interaction of parallel longitudinal girders. The diagnosis of the frame was done by means of nondestructive testing methods combined with visual investigations supported by endoscop. However, a detailed investigation of this joint was impossible because of technological obstructions. The main purpose of the structural analysis was to make an estimate of the function of the joint under various assumptions of quality of the filler concrete.

3.2 Finite Element Model

In the linear analysis of the whole space frame, which was performed also for other purposes, the function of the structural detail of joint in the global structural system was studied. On the basis of this global analysis the region of damaged joint was identified. From the complex structure of the frame only a section adjacent to the joint was modeled. The surrounding structure was approximated by appropriate boundary conditions and artificial springs.

The analytical model, its geometry, boundary conditions and reinforcing are shown in Fig.2. The finite element mesh is shown in Fig.3. It has 387 quadrilateral elements. The vertical stirrups were modeled by smeared reinforcement and all main horizontal and inclined bars were modeled by discrete reinforcement. The concrete quality of girders identified from core-drilled samples was 28 MPA. The nominal quality of filler concrete in the joint was 34 MPA. However, there were doubts about the quality of its casting and its actual state could not be reliably verified. Therefore, variable properties of the filler concrete were considered in this study by

values of 1%, 10%, 60% and 100% of its nominal value.

Two alternatives of boundary conditions were considered for the modelling of the surrounding structure. In the first one the column under the joint of the longitudinal girders was modeled by springs and the continuity of the structure was modeled by conditions of the symetry in the middle of the girders. In the second case the support on the column was rigid and the continuity of the girders was modeled by the springs. This enabled the approximate simulation of the axial displacements of girders due to flexibility of the frame structure.

The loading is due to technological forces which are trasfered through numerous fastenings as indicated by vertical arrows in Fig.2. The force in the load-displacement diagram refers to the sum of the technological forces. Two loading cases were considered. In the first loading case the full interaction of girders A_1, A_2 and B_1, B_2 was assumed and the girders were loaded by the half of the total technological load. (The structure was designed under this assumption.) The second loading case assumed no interaction between the girders and the full technological loading was applied on the internal girders. In both cases the dead load of girders was included.

The study was performed on the personal computer 286 under MS-DOS operating system. Solution of one case on this computer took about 10 hours of computer time. (Of course in case of PC486 the time would be much shorter.) In addition to the ultimate load capacity each analysis provided ample of informations on stress and strain state, crack patterns and failure mode. The fixed crack approach has been used in all cases.

3.3 Discussion of Results

The behavior of analyzed system is illustrated in Fig.4., which shows the crack patterns in three load stages and the failure state with cracks, crushing and amplified deformations. The load displacement diagram with the load levels corresponding to the stages in Fig.4 is shown in Fig.5. The yielding of reinforcement is also graphically indicated (but apparent only from coloured output). Strong shear behavior is evident from inclined cracking. The failure mode was dependent on the degree of lateral constraint and the quality of the filler concrete in the joint. In case of a high lateral constraint and the 100% quality of the filler concrete the maximum load was 4.75 times of the admissible loading. The failure mode is of the concrete arch-type, with crushing of the cracked concrete in the web and in the bending compression zone.

The effect of the filler concrete quality on the frame behavior can be seen from the comparison of Figures 4(c) and 6. The load level is 2 times of the admissible load. The quality of the filler concrete described by the compressive strength was 100% in Fig.4(c), 60% in Fig.6(a) and 10% in Fig.6(b). In case of the lowest quality, Fig.6(b), the filler concrete in the joint fails in compression and after that the behavior is fairly ductile with all major reinforcement yielding. The ultimate load factor, (related to the admissible load) is in this case 3.5. The reduction of load capacity was also caused by partially releasing the lateral constraint. In the most unfavorable case, with the elastic springs modeling the lateral constraint and 1% of filler concrete quality the ultimate load was almost equal to the admissible load with no marginal safety.

The results of the numerical analysis were used to support the design of measures for extending the service life of the frame, which were based on the restoring the full interaction of girders and strengthening the space frame. They were also utilized in a reliability analysis. It was a valuable contribution to the safety and economy of the engineering solutuion.

4. CONCLUSIONS

The computer program SBETA was succesfully applied to the assesment of the remaining structural capacity of the turbine foundation frame. The nonlinear finite element analysis proved to be a rational method for determination of ultimate load capacity of this statically indetermined structure, whose behavior significantly deviates from the simple design models based on cross-sectional analysis. The FE analysis was used to design the economical and rational repair measures .

REFERENCES

[1] BAŽANT, Z.P., OH, B.H. - Crack Band Theory for Fracture of Concrete. Mater. Struct. RILEM, Paris, France, 16, 1983, pp. 155-177

[2] ČERVENKA, V., PUKL, R., ELIGEHAUSEN, R. - Computer Simulation of Anchoring Technique in Reinforced Concrete Beams. Computer Aided Analysis and Design of Concrete Structures, Proceedings 2nd SCI-C International Conference, Eds. N. Bicanic, H. Mang, Zell am See, Austria, April 1990, Pineridge Press, Swabsea, U.K. 1990, ISBN 0-906674-74-3, pp. 1-20

[3] ČERVENKA, V., PUKL, R., ELIGEHAUSEN, R. - FEM Simulation of Concrete Fracture. ECF 8 Fracture Behavior and Design of Materials and Structures, Preprints of the 8th Biennial European Conference on Fracture, Torino, Italy, October 1990, pp. 728-733

[4] ČERVENKA, V., ELIGEHAUSEN, R., PUKL, R. - SBETA Computer Program for Nonlinear Finite Element Analysis of Reinforced Concrete Structures. IWB Mitteilungen 1990/1, Stuttgart University, ISSN 0932-5921, ISBN 3-9801833-6-X

[5] ČERVENKA, V., ELIGEHAUSEN, R., PUKL, R. - Computer Models Of Concrete Structures. IABSE Colloquium "Structural Concrete", Stuttgart, Germany, April 1991, ISBN 3-85748-063-7, pp. 311-320

[6] ČERVENKA, V., PUKL, R. - Computer Models Of Concrete Structures. Structural Engineering Int., Vol. 2, No. 2, May 1992, IABSE Zurich, Switzerland, ISSN 1016-8664, pp. 103-107

[7] ČERVENKA, V., PUKL, R., ELIGEHAUSEN, R. - Fracture Analysis of Concrete Plane Stress Pull-Out Tests. Fracture Processes in Concrete, Rock and Ceramics, Noordwijk, Netherlands, June 1991, pp. 899-908

[8] SBETA – Nonlinear Finite Element Analysis of Reinforced Concrete Structures, Software and Documentation, Peekel Instruments, Industrieweg 161, 3044 AS Rotterdam, The Netherland.

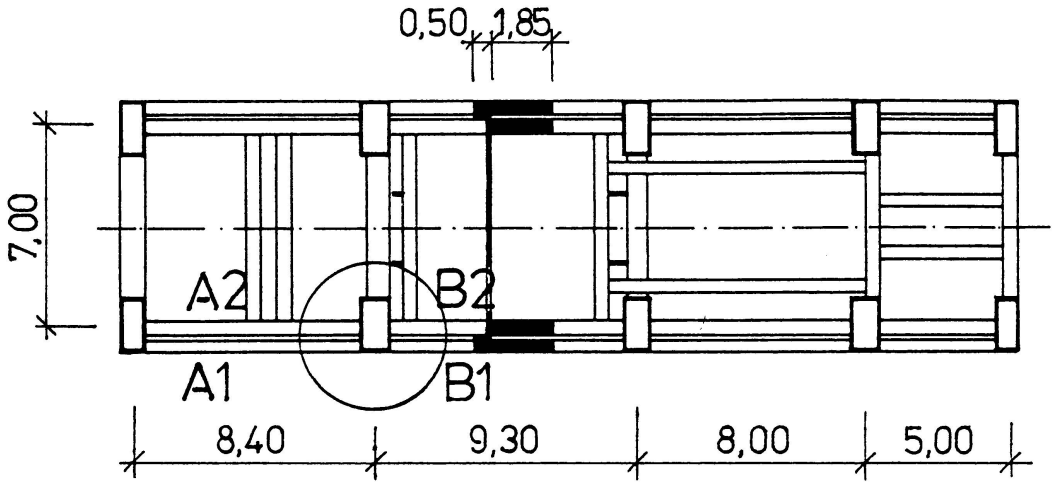

Fig.1 Power station turbine frame: schematic plan view (dim. in meters).

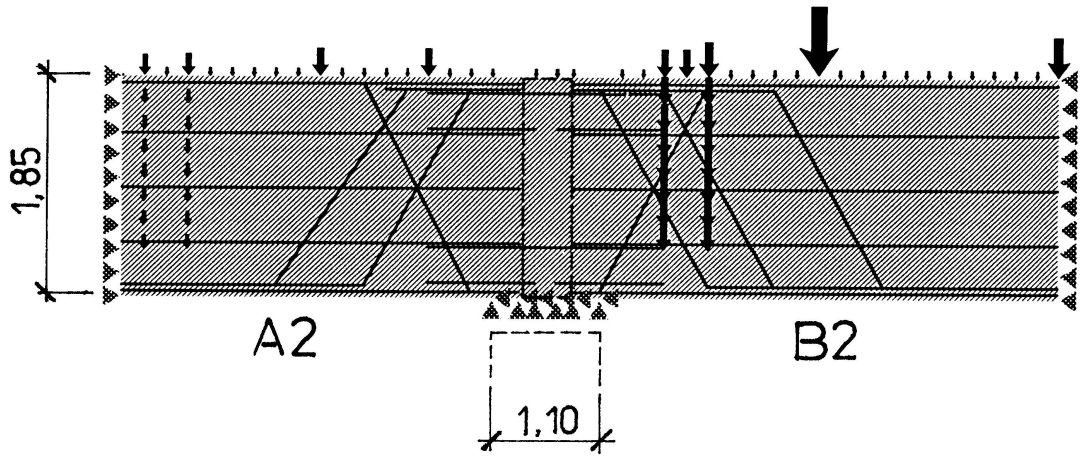

Fig.2 Structural model of a detail with reinforcement, loading and boundary conditions.

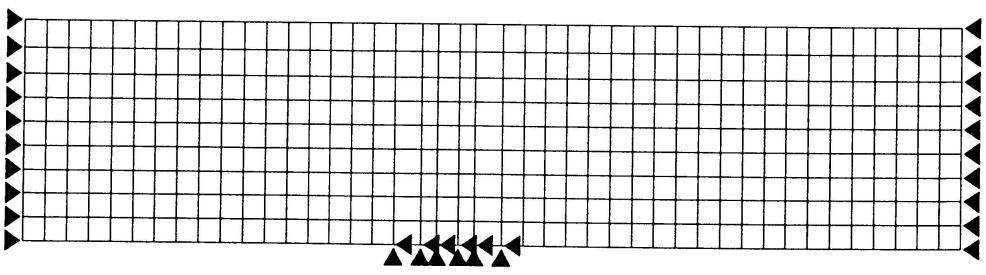

Fig.3 Finite element mesh of the structural model.

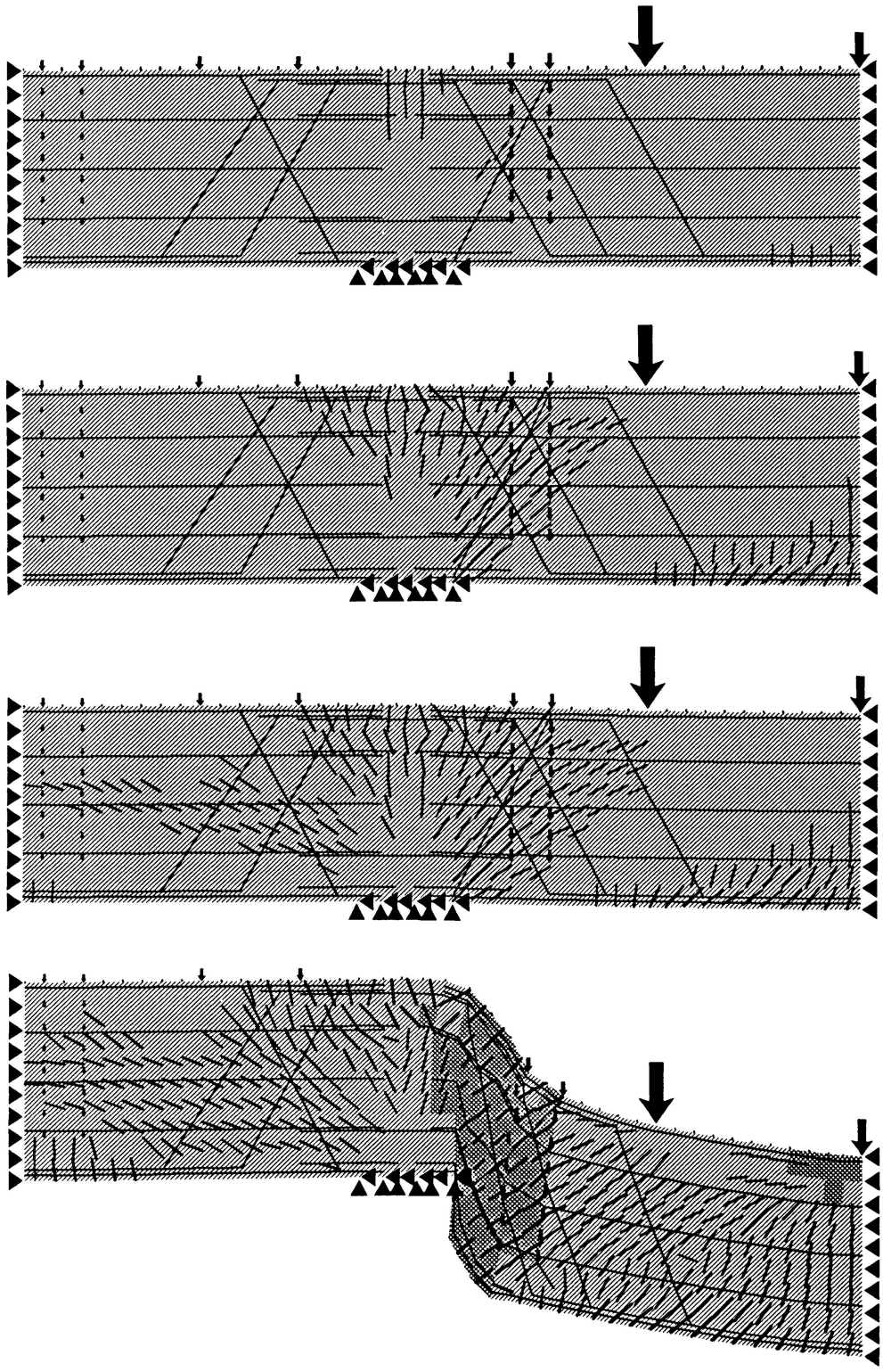

Fig.4 Sequence of crack patterns.

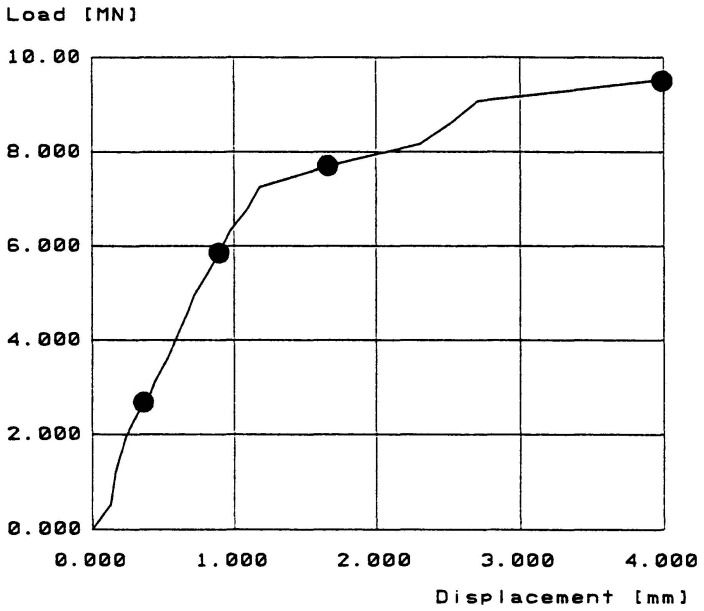

Fig.5 Load-displacement diagram.

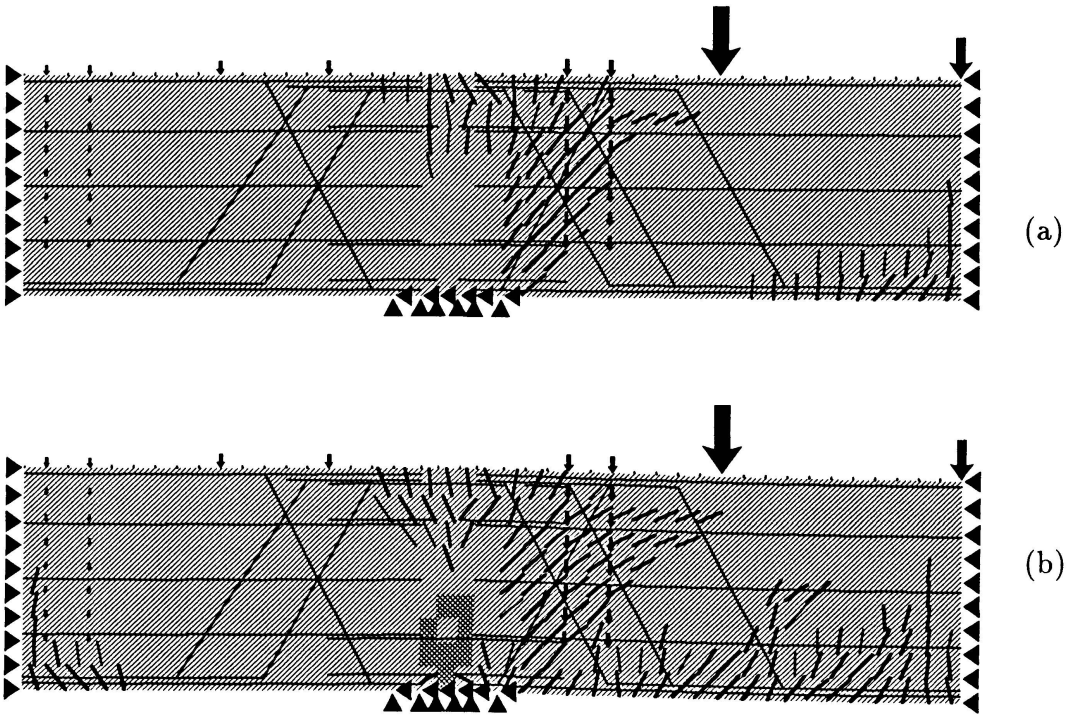

Fig.6 Comparison of damage states for cases of different joint concrete qualities. Load factor = 2.

Analytical Models for Strength and Stiffness Evaluation of Concrete Structures

Modèles pour l'évaluation de la résistance et la rigidité des structures en béton

Modelle für die Berechnung von Tragfähigkeit und Steifigkeit von Betontragwerken

Filip C. FILIPPOU
Associate Professor
University of California
Berkeley, CA, USA

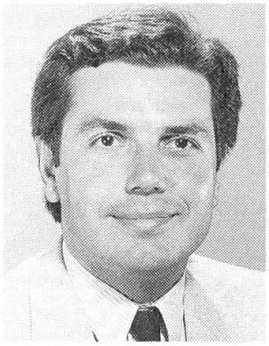

Filip C. Filippou, born 1955, received his civil engineering degrees at TU München and at the University of California, Berkeley. Since 1983 he is on the faculty at the University of California, Berkeley with main field of interest the design and analysis of concrete structures.

Fabio F. TAUCER
Junior Researcher
University of California
Berkeley, CA, USA

Fabio F. Taucer, born 1966, received his civil engineering degrees at the Universidad Central de Venezuela, Caracas and at the University of California, Berkeley. He is involved in modeling the nonlinear behavior of reinforced concrete structures.

Enrico SPACONE
Doctoral Student
University of California,
Berkeley, CA, USA

Enrico Spacone, born 1961, received his civil engineering degrees at the University "La Sapienza", Rome, Italy and at the University of California, Berkeley. He worked for two years at the EPF in Lausanne, Switzerland. He is currently working on his doctoral dissertation.

SUMMARY

The development of rational measures for strengthening and retrofitting of existing concrete structures depends on advanced methods of assessing their strength and stiffness. These methods should be capable of predicting the future behavior of the entire structure based on information about the original design and the current state of the structure. This paper presents a general frame member model based on the fiber concept and capable of simulating the hysteretic behavior of concrete members under arbitrary histories of biaxial moment and axial force.

RÉSUMÉ

Les moyens de renforcement et de remise en état de structures en béton se basent sur des méthodes avancées pour établir la résistance et la rigidité de ces structures. Ces méthodes devraient être capables de prévoir le comportement de toute la structure à partir d'informations tirées du projet original et de l'état actuel de la structure. Le présent article propose un modèle général pour l'étude de cadres. Ce modèle repose sur le concept de fibre et peut reproduire le comportement histérétique d'éléments en béton sous l'action d'une flexion biaxiale et d'une force axiale arbitraires dans le temps.

ZUSAMMENFASSUNG

Die Entwicklung rationaler Methoden für die Verstärkung und Instandsetzung von gebauten Betontragwerken hängt von Modellen ab, die imstande sind, die Tragfähigkeit und Steifigkeit ihrer Tragelemente vorauszusagen. Diese Methoden sollten imstande sein, ausgehend von Information über den Anfangs- und jetzigen Zustand des Tragwerks, das zukünftige Verhalten vorauszusagen. Diese Arbeit stellt ein allgemeines Model für Rahmenelemente unter allgemeiner Belastungsgeschichte von zweiachsiger Biegung und Normalkraft vor.

1. INTRODUCTION

The development of rational measures for strengthening and retrofitting of existing concrete structures depends on advanced methods of assessing their strength and stiffness. These methods should be capable of predicting the future behavior of the entire structure based on information about the original design and the current state of the structure. The latter can be usually approximated from current measurements of material and structural properties using system identification methods. In regions of high seismic risk the difficulty of the problem is compounded by the complex loading history of existing structures, which might have experienced several small and moderate earthquake excitations in their service life.

The evaluation of the future behavior of existing concrete structures depends on the development of advanced analytical models, which describe the time and load dependent nonlinear behavior of the structural members. These models should satisfy two basic requirements: (a) they should be reliable, robust and computationally efficient and (b) they should be of variable complexity depending on the degree of detail required from the analysis: while individual critical members of the structure can be evaluated with sophisticated finite element models, the behavior of multistory buildings and multiple span freeway structures can be described with sufficient accuracy with member models. In fact, the ability to mix finite element models of critical regions of the structure with nonlinear or even linear member models of the rest of the structure should be an important consideration in the development of such models.

In the following, a new fiber beam-column finite element for the analysis of reinforced concrete structures is presented. Contrary to most existing beam finite elements which are based on the definition of displacement shape functions, the element described herein assumes a constant axial force and linear bending moment diagrams inside the element, thus assuming force shape functions. A general overview of the element formulation and of the element nonlinear iteration scheme needed for the element state determination is first presented, followed by the description of a few numerical examples in which the element response is compared with experimental results

2. ELEMENT FORMULATION

The beam-column element is shown in the local reference system x,y,z in Fig. 1. The element is represented without rigid-body modes, thus forces and deformations are measured with respect to the cord connecting the two end nodes. Forces and displacements are grouped in the following vectors:

$$\text{Element force vector} \qquad \mathbf{Q} = \{Q_1 \quad Q_2 \quad Q_3 \quad Q_4 \quad Q_5\}^T \tag{1}$$

$$\text{Element displacement vector} \qquad \mathbf{q} = \{q_1 \quad q_2 \quad q_3 \quad q_4 \quad q_5\}^T \tag{2}$$

Similarly, section forces and deformations can be grouped in the vectors:

$$\text{Section force vector} \qquad \mathbf{D}(x) = \{M_1(x) \quad M_2(x) \quad N(x)\}^T \tag{3}$$

$$\text{Section deformation vector} \qquad \mathbf{d}(x) = \{\chi_1(x) \quad \chi_2(x) \quad \bar{\varepsilon}(x)\}^T \tag{4}$$

The element is composed of a finite number of longitudinal fibers Each cross section is therefore described by the number of fibers, their area, location and force-deformation relations. Since the element has been developed for the analysis of reinforced concrete structures, concrete and steel constitutive models have been used [1]. Small kinematics are postulated and plane sections are

assumed to remain plane and normal to the longitudinal axis. Consequently, the effects of shear and bond-slip are neglected in the present model. The nonlinear nature of the problem depends entirely on the nonlinear fiber force-deformation relations. The element formulation is based on the assumption that the axial force is constant and the bending moment diagram is linear inside the element. In symbols this translates to a simple relation between section and element forces:

$$\mathbf{D}(x)=\mathbf{b}(x)\cdot\mathbf{Q} \qquad \text{and} \qquad \Delta\mathbf{D}(x)=\mathbf{b}(x)\cdot\Delta\mathbf{Q} \tag{5}$$

where Δ denotes increments and $\mathbf{b}(x)$ is defined by:

$$\mathbf{b}(x)=\begin{bmatrix} \left(\frac{x}{L}-1\right) & \left(\frac{x}{L}\right) & 0 & 0 & 0 \\ 0 & 0 & \left(\frac{x}{L}-1\right) & \left(\frac{x}{L}\right) & 0 \\ 0 & 0 & 0 & 0 & 1 \end{bmatrix} \tag{6}$$

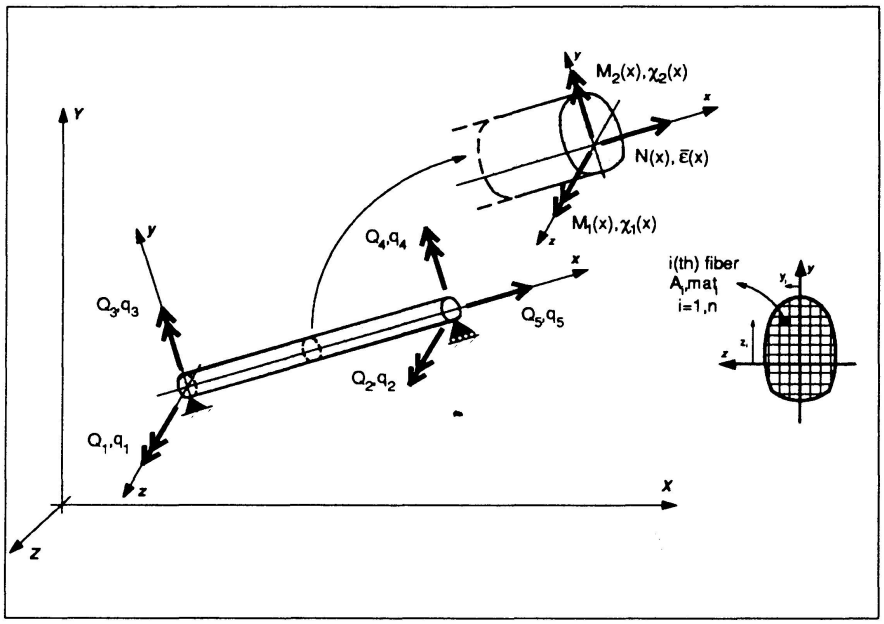

FIGURE 1 - BEAM ELEMENT FORCES AND DISPLACEMENTS WITHOUT RIGID BODY MODES IN LOCAL REFERENCE SYSTEM: FIBER DISCRETIZATION OF CROSS SECTIONS

The force field, as defined by (5), is exact as long as only nodal forces act on the element. Loads acting inside the element can be easily introduced using the procedure described in [1].

The element is formulated using the flexibility method rather than the classical stiffness method, because of the advantage of defining an "exact" force field inside the element. Calling **P-Q** the element unbalanced forces (difference between applied and resisting forces **P** and **Q** respectively) and $\Delta\mathbf{q}$ the element deformation increments, the nonlinear system of equations at the element level is written:

$$[\mathbf{F}]^{-1}\cdot\Delta\mathbf{q}=(\mathbf{P}-\mathbf{Q}) \tag{7}$$

In Eq. 7 the element stiffness appears as the inverse of the element flexibility to indicate that the element is flexibility-based. The element flexibility matrix is determined integrating the section flexibilities according to:

$$\mathbf{F}=\left[\int_0^L \mathbf{b}^T(x)\cdot\mathbf{f}(x)\cdot\mathbf{b}(x)\cdot dx\right] \tag{8}$$

Section flexibility is obtained by inverting the section stiffness. The element is implemented in a stand alone program organized along the lines of a typical finite element code. Loads are applied on the structure and the program computes the corresponding displacements. The nonlinear solution procedure is organized as follows:

Load increments $\Delta \mathbf{P}$ are applied to the structure and a Newton-Raphson scheme is used to compute the corresponding structure displacement increments. At every Newton-Raphson iteration it is necessary to determine the element resisting forces corresponding to the updated element displacements. This is a challenging task when working with a flexibility-based element, because force and not displacement shape functions must be used. A new scheme has been developed for the proposed element, based on residual section and element deformations. Given the updated element displacements, the following steps are performed:

1) Compute the element linearized force increments using the last computed element tangent stiffness, and update the element forces;
2) Compute the section force increment using (5);
3) Compute the section deformation increment using the last computed section flexibility;
4) From the new section deformations, using the hypothesis that plane sections remain plane and normal to the longitudinal axis, compute the new fiber strains;
5) Compute fiber stresses and tangent moduli using the fiber force-deformation relations;
6) Compute the new section tangent stiffness, the section resisting forces and the section unbalanced forces, difference between applied and resisting forces;
7) Transform the section unbalanced forces into section residual deformations using the section flexibility;
8) Integrate the section residual deformations to compute the element residual deformations;
9) Compute the element flexibility using (8);
10) Compute the new element force increments;

Step 10) is needed because the element residual deformations can not be applied to the element alone, otherwise node compatibility would be violated. Forces based on the new element stiffness are applied to the element in order to yield element displacements equal and opposite to the element residual deformations. Correspondingly, force and deformation increments are applied to all sections: these increments are computed repeating steps 3) through 9) until convergence is achieved. The element converges when the unbalanced forces at all sections are sufficiently small. Element convergence implies that the element resisting forces corresponding to the applied displacements have been computed and the following Newton-Raphson iteration can be performed.

The new element convergence scheme is based on the equilibrium conditions (5). It can be shown that during the iterations equilibrium and convergence inside the element is respected, and section force-deformation relations are satisfied, at least within a certain tolerance, when convergence is reached. More details on the approach and a thorough description of the iteration scheme are presented in [1].

3. EXAMPLES

A series of comparisons between analytical and experimental results are used to study the element performance. Four examples are illustrated in this section: these refer to three reinforced concrete cantilevers discretized with a single beam-column element. Displacement control techniques have

been used to match experimental and analytically imposed displacements: a very strong linear elastic spring has been positioned at free end of the cantilever to control the tip displacements.

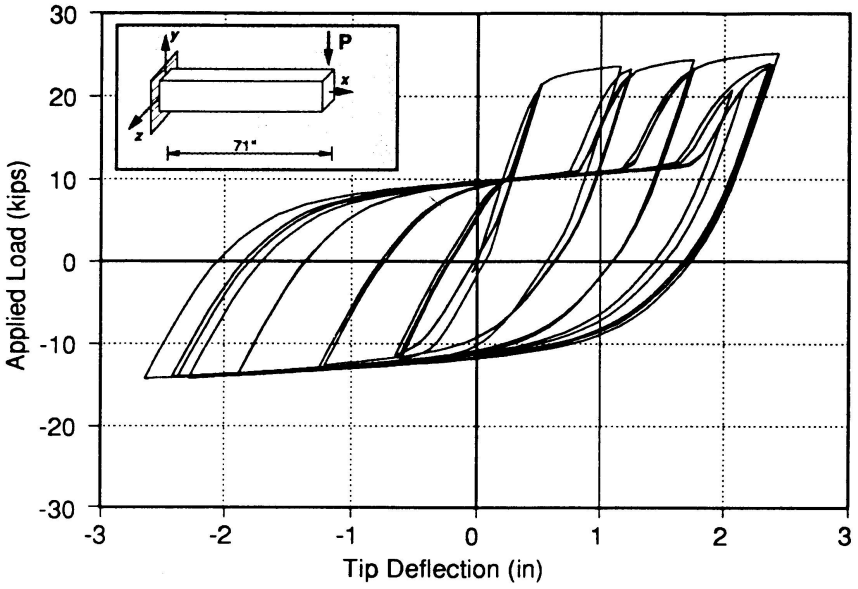

FIGURE 2 - TIP LOAD-DISPLACEMENT RESPONSE OF CANTILEVER BEAM UNDER CYCLIC UNIAXIAL BENDING

The first example shows the uniaxial bending of a cantilever beam R1 with a rectangular cross section tested in [2]. The simulation of the tip displacement response in the strong direction y is shown in Fig. 2. Analytical and experimental results agree well, especially for displacements up to yielding of the built-in end. At this point bond-slip and shear deformations become important and since the element does not include such effects, the analytical and experimental results show some discrepancy.

The remaining examples refer to the bending behavior of a cantilever under a compressive axial load and biaxial or uniaxial bending moments, which was tested in [3]. Fig. 3 illustrates the uniaxial case in which a constant axial force and a cyclic force along the weak axis z are applied at the tip of the cantilever. Displacement control was not used in this example. Numerical and experimental results are very similar and show a stiffer fiber model behavior, especially for low levels of lateral force at which "pinching" is evident in the experimental results.

The same cantilever is studied under biaxial bending conditions. Two cyclic transverse loads are applied at the free end of the cantilever. Displacement control is used in this example. Fig. 4 shows the tip response in the strong direction y. The correlation between analytical and experimental results is very good both for small and large displacements. When the concrete is fully cracked at the built-in section, bond-slip effects appear in the experimental data, but their contribution to the tip displacements is small.

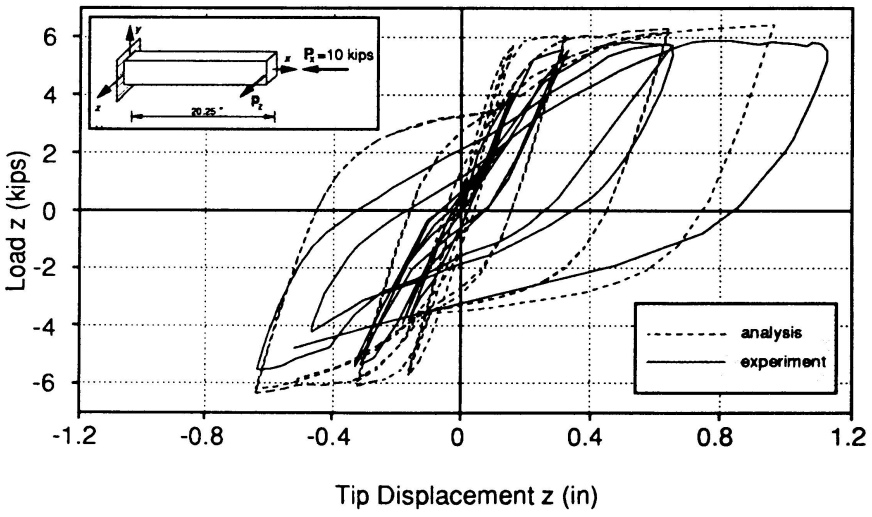

FIGURE 3 - TIP LOAD-DISPLACEMENT RESPONSE OF CANTILEVER UNDER CONSTANT AXIAL LOAD AND CYCLIC UNIAXIAL BENDING: NUMERICAL AND EXPERIMENTAL RESULTS

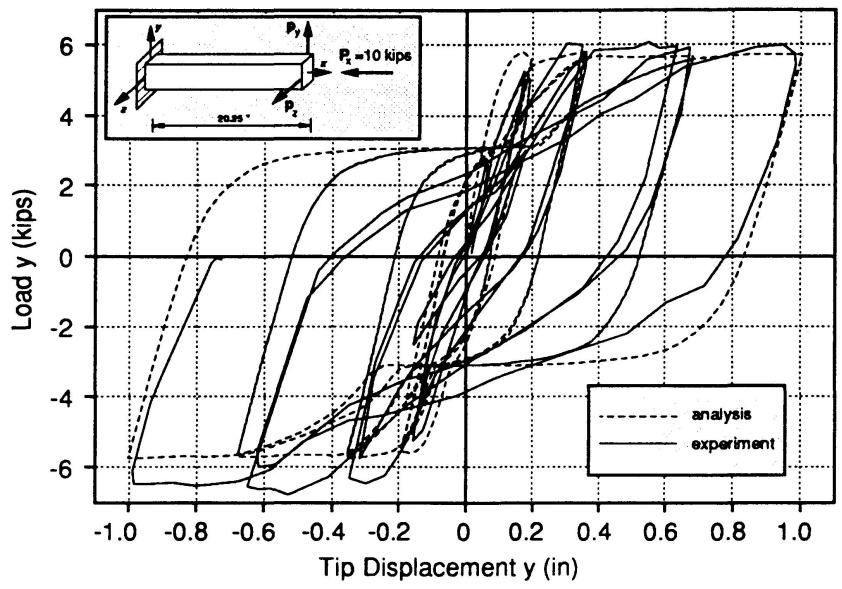

FIGURE 4 - TIP LOAD-DISPLACEMENT RESPONSE IN THE STRONG DIRECTION y OF A CANTILEVER BEAM UNDER CONSTANT AXIAL LOAD AND CYCLIC BIAXIAL BENDING: NUMERICAL AND EXPERIMENTAL RESULTS.

Finally, the same cantilever beam is studied under both cyclic bending and cyclic axial force. According to the notation of Fig. 5, the following load and displacement histories have been imposed:

$$\mathbf{P}_x = -75 \pm 30 kips$$

$$\mathbf{p}_y = \pm 0.96 in$$

$$\mathbf{p}_z = \pm 0.96 in$$

Load and deformation increments are applied so that cycles are simultaneous: all three quantities reach their maximum and minimum values at the same time. This example is particularly important to show the capability of the proposed element to represent softening and stiffness degradation without any computational difficulties. This is due to the fact that force equilibrium is always maintained along the element. When softening initiates at the built-in section, the whole beam unloads respecting the prescribed linear bending moment diagrams. All sections unload elastically except for the built-in section, which softens. Correspondingly, the end curvature increases while curvatures at all other sections decrease.

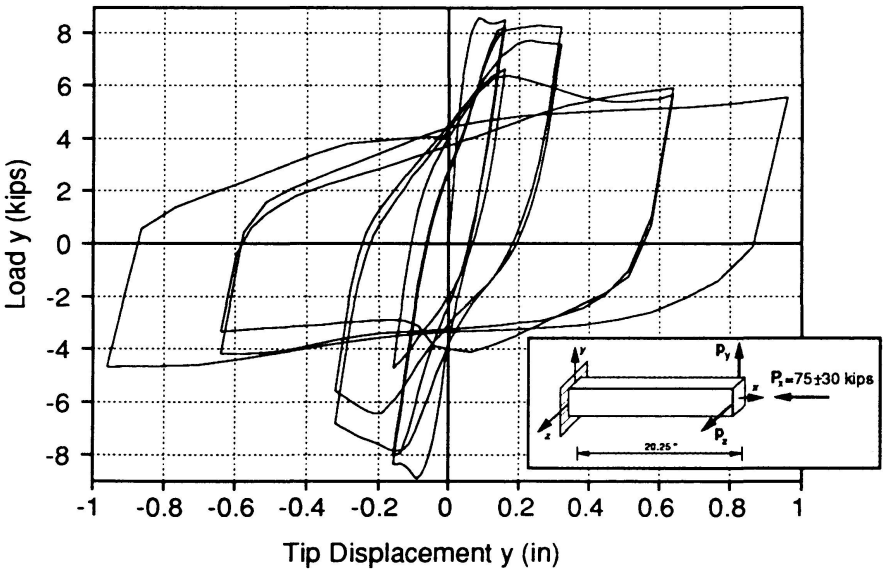

FIGURE 5 - TIP LOAD-DISPLACEMENT RESPONSE IN STRONG DIRECTION y OF CANTILEVER UNDER CYCLIC AXIAL LOAD AND CYCLIC BIAXIAL BENDING

4. CONCLUSIONS

To predict the response of existing reinforced concrete structures to strong ground motions and to develop better strengthening and retrofit measures for structures in zones of high seismic risk integrated experimental and analytical studies are very important. The beam-column fiber element presented in this paper is part of an ongoing effort to develop reliable computational tools of different levels of complexity and, thus, reliability, for modeling reinforced concrete structures. Most two-node reinforced concrete finite elements are based on the stiffness approach which postulates linear curvatures and constant axial strain along the element. These deformation distributions do not represent the physical behavior

when sections start yielding. The proposed finite element is based on the assumption of linear bending moment diagram and constant axial force along the element. This hypothesis is exact when no load is applied inside the element. The computational cost for each element is higher when a flexibility based element is used, because of the iteration scheme necessary to compute the element resisting forces corresponding to the applied displacements. However, fewer elements are needed to discretize the structure, thus requiring a smaller number of total degrees of freedom. Further refinements of the element are needed to include bond-slip and second order effects.

5. REFERENCES

1. TAUCER F.F., SPACONE E. and FILIPPOU F.C., A Fiber Beam-Column Element for Seismic Response Analysis of Reinforced Concrete Structures. UCB/EERC–91/17, Earthquake Engineering Research Center, University of California, Berkeley, 1992.
2. MA S.M., BERTERO V.V. and POPOV E.P., Experimental and Analytical Studies on the Hysteretic Behavior of Reinforced Concrete Rectangular and T-Beams. Report UCB/EERC-76/2, Earthquake Engineering Research Center, University of California, Berkeley, 1976.
3. LOW S.S. and MOEHLE J.P., Experimental Study of Reinforced Concrete Columns Subjected to Multi-Axial Cyclic Loading. *Report UCB/EERC-87/14*, Earthquake Engineering Research Center, University of California, Berkeley, 1987.